Electrostatic Charge Generation and Wall Fouling in a High-Pressure Gas-Solid Fluidized Bed: Implementation and Preliminary Testing of a Measurement Technique

Fawzi Salama

Thesis submitted to the
Faculty of Graduate and Postdoctoral Studies
In partial fulfillment of the requirements
For the M.A.Sc. degree in Chemical Engineering

Department of Chemical and Biological Engineering
Faculty of Engineering
University of Ottawa

Abstract

Due to the nature of gas-solid fluidized beds, providing continuous contacts between fluidizing particles and between particles and the reactor wall, the occurrence of electrostatic charges is unavoidable. In the polyethylene industry, electrostatics is a major problem. Large amounts of electrostatic charges are generated causing polyethylene and catalyst particles to adhere to the reactor wall, forming sheets. Particle sheets can break off and block the distributor plate, causing long shutdown periods for clean-up which result in economic loss due to decreased production and higher maintenance costs. The overall purpose of the project of which this thesis is part of is to help industry in minimizing this problem by examining the mechanisms underlying this phenomenon.

Towards this goal, an experimental technique for the measurement of the degree of wall fouling and its charge distribution was previously developed and implemented in an atmospheric system with a column of 0.102 m in diameter. This technique was extended in this thesis to a pilot-scale unit (0.154 m in diameter) designed to be capable of operating at pressures and temperatures up to 2 600 kPa and 100°C respectively and gas velocities up to 1 m/s, which are operating conditions of industrial polyethylene reactors. Preliminary experiments showed that increasing the operating pressure from 101 kPa to 401 kPa almost doubled the amount of polyethylene wall fouling due to the higher bubble rise velocity at this pressure, enhancing charge generation within the fluidized bed. Changing the particle size distribution by removing particles smaller than 250 μm had no significant effect on the extent of the wall fouling. Increasing the column diameter from 0.102 m to 0.154 m decreased wall fouling due to the lower column wall area per mass of particles. Overall, particle-particle contacts generated positively and negatively charged particles, but did not produce a net charge in the bed due to the negligible elutriation. However, particle-wall contacts produced a net charge. The formation of the wall layer was due to the image force created by the net charge and the layering effect created by the attraction between oppositely charged particles.

Résumé

En raison de la nature des lits fluidisés gaz-solide, où le contact des particules fluidisées et des particules sur la paroi du réacteur est persistant, la génération de charge électrostatique est inévitable. En effet, dans l'industrie de production de polyéthylène, l'électrostatique est un problème majeur. Ces grandes quantités de charges électrostatiques conduisent à l'adhérence des particules de polyéthylène et du catalyseur sur le mur du réacteur, formant ainsi de l'encrassement. Ces couches peuvent se briser et bloquer la plaque de distribution résultant en de longues périodes de fermeture et nettoyage qui portent à des pertes économiques en raison des coûts d'entretien plus élevés et de la diminution de production. L'objectif global du projet dont cette thèse fait partie est d'aider l'industrie à minimiser ce problème en examinant les mécanismes qui produisent ce phénomène.

Afin d'atteindre cet objectif, une technique expérimentale pour la mesure du degré d'encrassement sur la paroi du réacteur a été développée et mise en œuvre sur un système atmosphérique utilisant une colonne de 0.102 m en diamètre. De plus, la technique a été étendue pour utiliser une colonne à échelle pilote (0.154 m de diamètre) conçue pour opérer à des pressions et températures pouvant atteindre 2 600 kPa et 100°C, respectivement, et des vitesses de gaz de 1 m/s; des conditions d'opération équivalentes aux réacteurs industriels. Des expériences préliminaires ont démontré que l'augmentation de la pression de 101 kPa à 401 kPa a presque doublé le niveau d'encrassement dû à une vitesse de montée des bulles supérieure qui augmente la génération de charge dans le lit fluidisé. Par contre, l'augmentation du diamètre de la colonne de 0.102 m à 0.154 m a réduit l'encrassement en raison d'une surface de contact inférieure par rapport à la masse de particules fluidisées. Une modification de la distribution de la taille des particules en éliminant les particules inférieures à 250 µm n'a eu aucun effet significatif sur le degré d'encrassement des murs. En général, le contact entre particules ont chargé certaines particules positivement et d'autre négativement, mais il n'y a pas eu de charge nette dans le lit en raison d'entraînement de particules. Par contre, les contacts entre particules et paroi ont produit une charge nette. La formation de la couche sur la paroi est produite en raison de la force image créée par la charge nette et par l'encrassement produit par l'attraction entre les particules de charges opposées.

Table of Contents

List of Tables

List of Figures

Nomenclature

Symbol	Meaning	Units
$\boldsymbol{C_0}$	Capacitance between contacting surfaces	C/V
$\boldsymbol{D}$	Bed diameter	m
$\boldsymbol{d_b}$	Bubble diameter	m
$\boldsymbol{d_p}$	Particle diameter	m
$\boldsymbol{d_{pN}}$	Normalized mean particle diameter	μm
$\boldsymbol{e}$	Charge of a single electron (constant)	C
$\boldsymbol{\vec{E}}$	Electric field	V/m
$\boldsymbol{F}$	Force	N
$\boldsymbol{g}$	Gravitational constant	m/s^2
$\boldsymbol{H}$	Bed height	m
$\boldsymbol{K}$	Bubble velocity coefficient	–
$\boldsymbol{m}\%$	Particles mass percentage of the initial particles	%
$\boldsymbol{n}$	Zaki-Richardson exponent	–
$\boldsymbol{q}$	Electrostatic charge	C
$\boldsymbol{q/m}$	Specific charge	$\mu C/kg$
$\boldsymbol{r}$	Distance between two point charges	–
$\boldsymbol{Re}$	Reynolds number	–

$\boldsymbol{Re_{mf}}$	Reynolds number at minimum fluidization	$-$
$\boldsymbol{u}$	Fluid superficial velocity	m/s
$\boldsymbol{u_b}$	Bubble rise velocity	m/s
$\boldsymbol{u_e}$	Velocity of dynamic wave	m/s
$\boldsymbol{u_{mf}}$	Minimum fluidization velocity	m/s
$\boldsymbol{u_t}$	Particle terminal velocity	m/s
$\boldsymbol{u_\epsilon}$	Velocity of kinematic wave	m/s
$\boldsymbol{V_c}$	Contact potential	V
$\boldsymbol{\epsilon}$	Bed void fraction or porosity	$-$
$\boldsymbol{\epsilon_0}$	Permittivity of vacuum (constant)	F/m
$\boldsymbol{\rho}$	Charge density	C/m^3
$\boldsymbol{\rho_f}$	Fluid density	kg/m^3
$\boldsymbol{\rho_p}$	Particle density	kg/m^3
$\boldsymbol{\phi}$	Work function	eV
$\boldsymbol{\phi_s}$	Particle sphericity	$-$

Acknowledgements

I would like to convey my sincere thanks to my supervisor Dr. Poupak Mehrani for the privilege of being part of her research group. Her extraordinary support and guidance made this project possible.

I would like to thank Dr. Michael Muhle and Dr. F. David Hussein from Univation Technologies, LLC (USA) for their comments and recommendations. Additionally, thanks to Univation Technologies for providing funding and all the polyethylene resins used in this work.

I would also like to thank fellow graduate students Di Song and Ye Tian for helping perform the experiments. I would like to thank Andrew Sowinski who was instrumental in the design and assembly of the experimental unit.

I would like to acknowledge the technical support staff of the Chemical Engineering Department at the University of Ottawa: Louis Tremblay, Franco Ziroldo and Gérard Nina. This project would not have been possible without their help and expertise.

Finally, I would like to thank NSERC and OGS for their financial contributions.

Chapter 1. Introduction

Gas-solid fluidization is a process whereby a bed of solid particles is transformed by the upward flow of gas across it into a suspended state. Fluidization occurs when the velocity of the gas exerts a sufficient drag force on the particles to counteract the weight of the particles. Fluidization technology is widely used in the chemical, petrochemical, and food industries, among others. An example application of this technology is the catalytic polymerization of ethylene to produce polyethylene.

A major nuisance in some gas-solid fluidized beds is the generation of electrostatic charges due to the continuous contacts amongst the particles and between the particles and the column wall. The generated charges might cause particle agglomeration causing deviation from the desired particle properties, large electrostatic discharge endangering operators and equipment, and the adhesion of particles to the reactor wall and other surfaces necessitating regular shutdown for clean-up.

The presence of electrostatic charges in gas-solid fluidized beds have been reported for many decades (Lewis et al., 1949) and there have been studies attempting to study this phenomenon for almost as long (Ciborowski & Wlodarski, 1962). But although there has been some progress in the understanding of electrostatic charging in fluidized beds and several proposed solutions, the problem persists. The fundamental mechanisms of charge generation and dissipation in gas-solid fluidized beds are poorly understood, particularly when the fluidized particles are insulating such as polyethylene. This is partly due to complex nature of the fluidization process, the complex nature of the electrostatic phenomenon, and the current lack of understanding of the fundamental processes underlying electrostatic charging in insulators.

The overall goal of this thesis is to generally inquire into the mechanisms of electrostatic charging in polyethylene fluidized beds and particularly to study the effects operating pressure, particle size distribution and column diameter on electrostatics. Before further discussion of electrostatics in gas-solid fluidized beds, relevant topics in fluidization and electrostatics are briefly reviewed.

1.1 Gas-Solid Fluidization

When a gas is passed upward through a bed of particles at a superficial velocity lower than the minimum fluidization velocity, the gas simply percolates through the bed. The pressure drop experienced by the gas is well-modelled by the semi-empirical Ergun equation. At the velocity of minimum fluidization, the apparent weight of the bed is supported by the drag force exerted by the upward flowing gas. At or above the minimum fluidization velocity, the bed acquires the characteristics of a fluid: objects denser than the bed sink and lighter objects float; the bed takes the shape of the container; and the bed is uniform and well-mixed. Because of these properties, fluidized beds have a significant number of commercial applications (Kunii & Levenspiel, 1991).

As the superficial gas velocity is increased above minimum fluidization, the bed experiences increasingly vigorous fluidization regimes as depicted in Figure 1.1. A higher velocity, called the minimum bubbling velocity, is required for gas bubbles to rise through the bed. If the bed is sufficiently narrow, the bubble diameters can approach or equal that of the fluidization column resulting in a phenomenon called slugging. At higher gas velocities, bubbles become more frequent and the bed level becomes indistinguishable. This regime is called turbulent fluidization. At even higher gas velocities, the particles are partially entrained by the gas. This regime, called fast fluidization, requires the recycling of entrained particles because the bed is quickly depleted by entrainment.

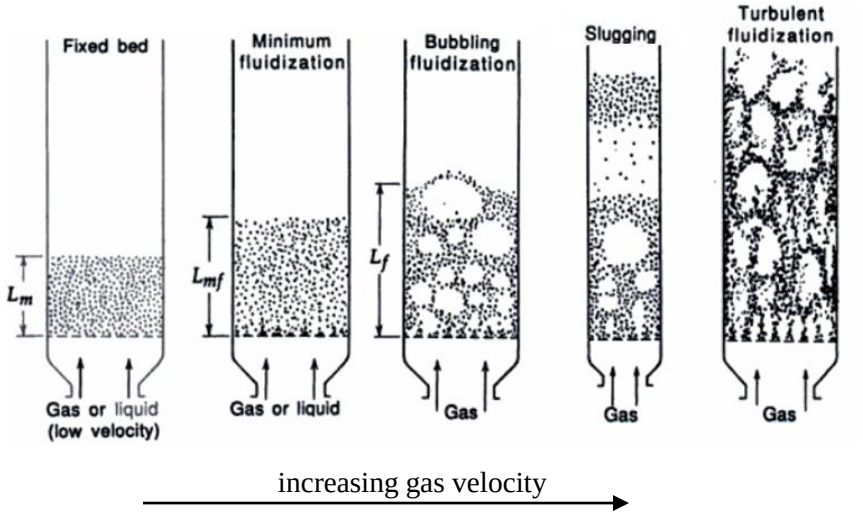

Figure 1.1: Fluidization flow regimes, adapted from Kunii & Levenspiel (1991).

Different particles exhibit distinct fluidization behaviours due to their differing densities and mean diameters. Geldart (1973) classified particles into four categories as shown in Figure 1.2. Type C particles, such as flour, have very small diameters. They exhibit high cohesive forces due to large specific surface area and low masses, making them difficult to fluidize. Channels might form, allowing the gas to bypass fluidizing these particles. Type A particles, such as catalysts, are larger and denser. They are aeratable and exhibit homogenous fluidization at the minimum fluidization velocity and bubbling fluidization at gas velocities at a higher velocity called the minimum bubbling velocity. Type B particles, such as sand, have diameters above 150 µm. They experience no homogenous bed expansion but bubble readily at the minimum fluidization velocity. Type D particles, such as wheat, are very large and coarse. They are difficult to fluidize because of the predominance of jets.

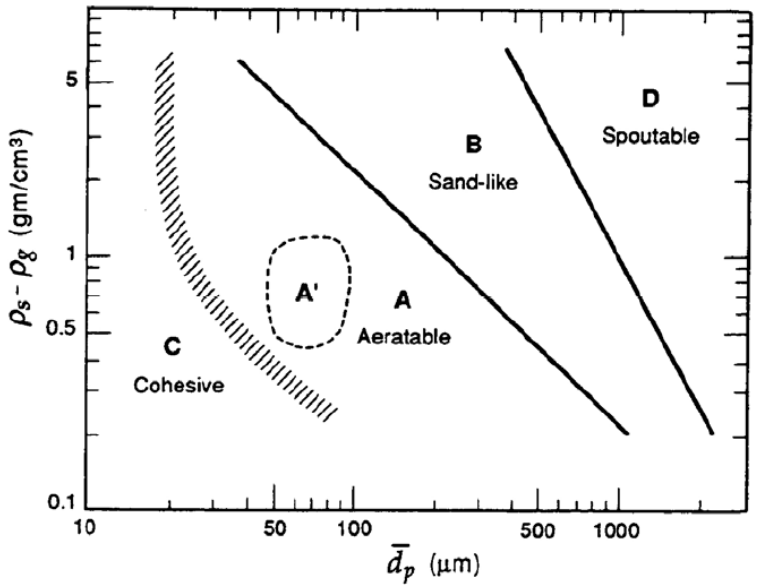

Figure 1.2: Geldart particle classification (Kunii & Levenspiel, 1991).

1.1.1 Polyethylene Production using the Unipol Process

One of the processes implementing fluidization technology is the catalytic polymerization of ethylene to produce polyethylene. In the Unipol process shown in Figure 1.3 (Fulks et al., 1985), the fluidizing ethylene gas is fed from the bottom of the reactor (20) where it is evenly

distributed by the distributor plate (22). The catalyst (whether Ziegler-Natta, metallocene, or other types) is introduced at the middle of the bed. An expanded portion of the column reduces the gas velocity and reduces the entrainment of bed particles. Exiting unreacted ethylene gas is recycled after being compressed (24) and then cooled in a heat exchanger (26). Heat removal is necessary because the polymerization reaction is highly exothermic with an adiabatic reaction temperature of almost 1500°C. The gas is then recycled to the inlet of reactor along with the unreacted catalyst. To remove the product (34), valve (36) is opened allowing the product to fill segregation zone (40). Then valve (36) is closed and valve (38) is opened to allow the discharge of the product into an external recovery zone. Such reactors are usually operated at pressures and temperatures of up to 30 atm and 110°C, respectively (Mun, 2005).

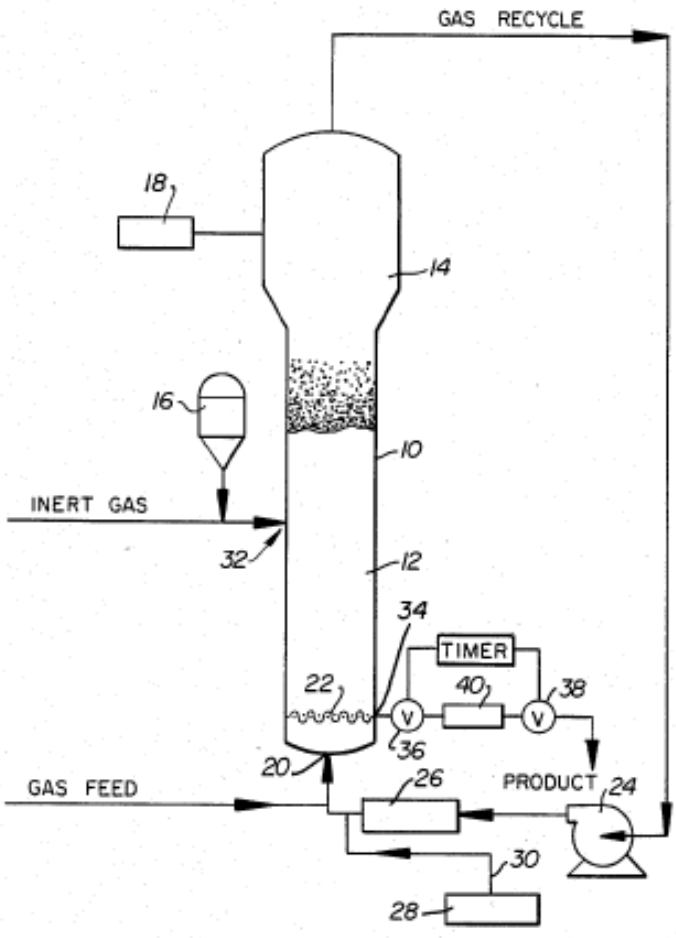

Figure 1.3: Unipol polyethylene fluidized bed process, adapted from Fulks et al. (1985).

1.1.2 The Effect of Pressure on Fluidized Bed Hydrodynamics

One of the operating conditions that influences fluidized bed hydrodynamics is the operating pressure. Pressure affects hydrodynamics mainly by modifying fluidizing gas properties particularly gas density. Because of the significant effect of fluid density on fluidized bed hydrodynamics, the operating pressure indirectly affects almost all bed properties, of which the minimum fluidization velocity, the minimum bubbling velocity, and bubble hydrodynamics are the most significant. In addition, it affects the bed void fraction, regime transitions, heat transfer, sintering, agglomeration, elutriation, particle attrition, and jetting (Yates, 1996).

For laminar flow ($Re_{mf} < 0.5$), the minimum fluidization velocity (u_{mf}) is independent of pressure while for turbulent flow ($Re_{mf} > 500$) it is inversely proportional to the square root of pressure (Yates, 1996).

The occurrence of bubbling flow can be predicted by the two-fluid model. This model predicts the existence of a stable and an unstable region of bed operation. Voidage propagates through the bed in the form or either dynamic of kinematic waves which velocities are predicted respectively by the following two equations:

$$u_e = \sqrt{3.2\ g\ d_P(1-\epsilon)(\rho_p - \rho_f)/\rho_p} \qquad (1)$$

$$u_\epsilon = n\ u_t(1-\epsilon)\epsilon^{n-1} \qquad (2)$$

The symbols used are defined in the nomenclature section. If the velocity of the dynamic wave exceeds that of the kinematic wave, bubbles cannot form and the bed will expand homogenously. Increasing the pressure extends the stable (bubble-less) region, possibly making a bed of group B particles behave like group A (i.e., homogenous fluidization at the minimum fluidization velocity and the incipience of bubbles at a higher minimum bubbling velocity) (Yates, 1996).

Of particular importance to this thesis is the effect of pressure on the frequency and nature of particle-particle and particle-wall contacts since these contacts are the primary mechanisms of electrostatic charge generation in fluidized beds, as will be discussed in more detail later. General particle mixing within the fluidized bed is also significant. It is well known that mixing

within a fluidized bed is primarily due to the rise of bubbles. The bubble rise velocity can be calculated from the following equation:

$$u_b = K\left(\frac{1}{2} g d_b\right)^{1/2} \quad (3)$$

From this equation is it possible to conclude that the rise velocity of a bubble is proportional to its diameter (d_b).

The effect of pressure on bed hydrodynamics has been better studied in Group A particles. Bubbles of Geldart group A decrease in size with increasing pressure. This might be due to either (a) an increase in gas flow through the emulsion phase due to an increase of emulsion phase voidage at higher pressure, or (b) a decrease in bubble stability (Yates, 1996). Bubble stability is hypothesized to be limited by either the terminal velocity of particles in the wake or particle fingering at the roof the bubble. The first hypothesis states that if the bubble rise velocity exceeds the particle terminal velocity, particles in the wake will be drawn into the bubble breaking it up into smaller bubbles. Since terminal velocity decreases with pressure, this explains the decreased stability at higher pressure. The second hypothesis states that bubble stability is limited by the apparent viscosity of the dense phase. At higher pressures, dense phase voidage increases resulting in lower viscosity and therefore less stable bubbles.

Results from studies of the fluidization of group B particles are not as clear. Hoffman and Yates (1986) reported that bubble size increased up to 6-11 bar, depending on the excess gas velocity, and decreased thereafter. The extent of these effects depended on the height above the distributor plate at which the observation was made. The bubble velocity coefficient K (shown in equation 3) was found to increase at pressures in excess of 20 bar. This resulted in an increase of bubble rise velocity despite a decrease in bubble size, the opposite of the trend observed at atmospheric pressures. It was also found that at elevated pressures, bubbles were increasingly concentrated at the center of the bed possibly due to increase bubble coalescence. Olowson and Almstedt (1990) found that increasing pressure up to 6 bar increased bubble frequency, rise velocity and volume fraction. They also observed increasing gas throughflow at higher pressure which might account for decreased bubble stability. Finally, Brouwer et al. (2012) found that increasing pressure up to 5 bar increases bubble size at equivalent gas superficial velocities.

1.2 Electrostatics

Electrostatic phenomena have been observed for millennia (Iversen & Lacks, 2012). Although mostly a nuisance, electrostatics has several useful applications including in laser printers, spray coating, and electrostatic precipitators (Cross, 1987).

In the following sections fundamental concepts in electrostatics are discussed, the mechanisms underlying electrostatic phenomena in conductors and insulators are examined, and finally a review of electrostatics in particulates is presented.

1.2.1 Electrostatic Fundamentals

Electrostatic charge arises from a deficit or surplus of electrons causing the object in question to be positively or negatively charged, respectively. The force acting between any two point charges can be described by Coulomb's law:

$$F = \frac{1}{4\pi\epsilon_0}\frac{q_1 q_2}{r^2} \tag{4}$$

Where F is the electrostatic force, ϵ_0 is the permittivity of free space (a universal constant), q_1 and q_2 are the two charges and r is the distance between the points. This law can be applied to non-point charges, such as for a sphere with a uniform surface charge, if the distance is sufficiently large. In this case, the total charge of the sphere can be assumed to reside at its center-point for the purpose of the calculation. Coulomb's law as written above considers only two charges. The force acting on a charge due to multiple surrounding charges can be simply calculated by the summation of the forces acting on the charge due to each of the charges.

Another important law in electrostatics is Gauss's law which describes the relationship between an electric field and the resulting charge distribution. The differential form of Gauss's law can be written as:

$$\nabla \cdot \vec{E} = \frac{\rho}{\epsilon_0} \tag{5}$$

Where $\vec{E}$ is the electric field, ρ is the charge density and ϵ_0 is the permittivity of free space. One implication of this law is the concept of the Faraday cage which can be demonstrated in the

following way. Take a volume fully enclosed by a conductive shell and choose the control volume such that it dissects the walls of the shell. At electrical equilibrium, there can be no potential gradient within the wall of the conductor since if there was a gradient, electrons will flow within the conductor until the gradient nullified. Since there is no potential gradient, there can be no current and no electric field within the walls of the conductor. Since the control volume was chosen to be dissecting the wall, there is no electric field across the control volume. Therefore, the left-hand term in Gauss's law equals zero and so does the right-hand term. Therefore, the charge density within the control volume is zero, meaning it encloses zero net charge. Now suppose that the shell encloses a charged object. The implication of the above reasoning is that the inner wall of the shell must possess an equal and opposite charge to the charged object. This effect is called a Faraday cage. Faraday cages can be used to electrically shield objects from background electric fields in the environment.

Electrostatic charge can be generated by simple contact between any two materials as illustrated in Figure 1.4(a). The exchange of charge between the surfaces occurs due to the difference in the surface energies. This is known as contact charging. More energetic contact generating friction between the surfaces increases the amount of charge exchanged. This is known as frictional charging, shown in Figure 1.4(b). Practically, it is often not possible to separate these two methods of charging. Therefore contact and frictional charging are grouped together and termed triboelectric charging.

Triboelectric charging is the primary method of charging in insulators. In conductors, induction charging, illustrated in Figure 1.4(c), can also occur. If a charged object which in this case is positively charged approaches a conductor, it attracts electrons within the conductors such that the side nearer to the object becomes negatively charged and the side further becomes positively charged. This is known as image charging because the charged object creates an oppositely charged “image” of itself on the conductor. The force of attraction between the object and this image is referred to as the image force. If the further side of the conductor is grounded[1], charge on that side will dissipate to ground. After the charged object is removed, a net negative charge remains on the conductor.

[1] Grounding or earthing refers to connecting a conductor to an electric sink. If the conductor was not polarized by an external electric field, it would be discharged. In this case, the further side of the conductor is discharged.

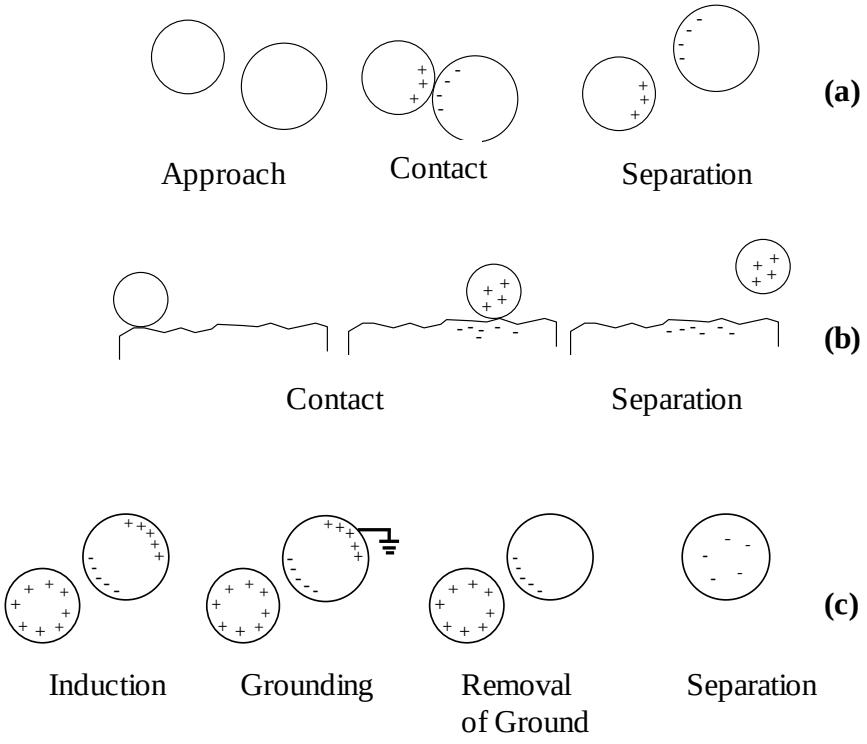

Figure 1.4: Electrostatic charge generation mechanisms: (a) contact, (b) frictional, and (c) induction charging.

Materials can be arranged according to their charging tendency in a triboelectric series such as the one presented in Figure 1.5. Materials with the most tendency to charge positively are located at the top of the series and materials with the tendency to charge negatively are located at the bottom. Contacts between two materials, one higher up and the other lower down the series, would cause the higher-up material to charge positively and the lower-down material negatively.

Triboelectric series are completely experimental and are generally only roughly reproducible. The irreproducibility is due to slight differences of the properties of the materials and differences of experimental conditions used when producing the series. This is partly due to the lack of understanding of the fundamental mechanism underlying triboelectric charging.

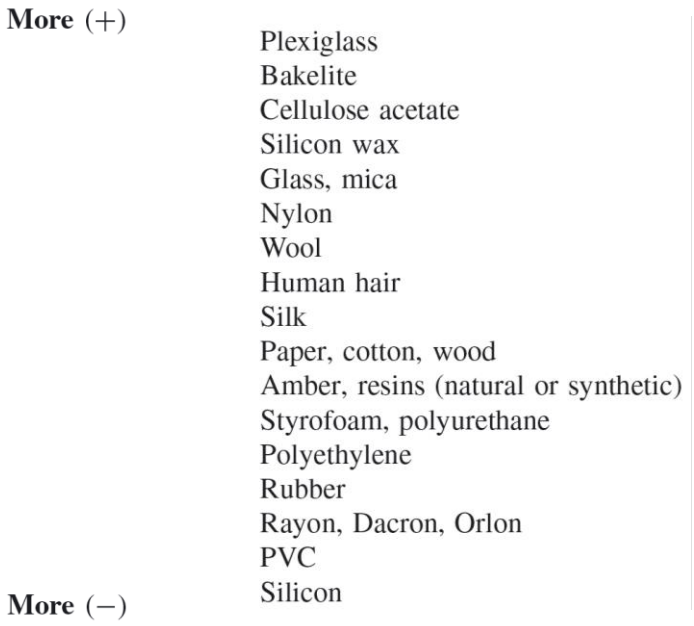

Figure 1.5: A triboelectric series, adapted from Mardiguian (2005).

Concepts presented in this section were mostly developed as a result of earlier experiments with electrostatics and present a macroscopic view of electrostatic phenomena. Research on the underlying microscopic processing is presented in the next two sections for conductors and insulators, respectively. Electrostatic phenomena are well understood for conductor-conductor contacts but are poorly understood for conductor-insulator or insulator-insulator contacts. This thesis is concerned with the latter two types of contact. However, models developed for conductor-conductor contacts form the basis of later models pertaining to the other two categories. Therefore, a brief overview of the electrostatics in conductors is presented first.

1.2.2 Electrostatics in Conductors

Contact between two conductor surfaces causes electrons to flow across the interface until thermodynamic equilibrium is reached (Lowell & Rose-Innes, 1980). The amount of charge transferred depends on the work functions of the two surfaces in contact. The work function, an inherent property of the material, is the amount of work required to remove an electron from the Fermi level, which is the highest occupied molecular level at equilibrium, to just outside the metal. In this case the contact potential between the two surfaces would be:

$$V_c = \frac{(\phi_B - \phi_A)}{e} \quad (6)$$

Where V_c is the contact potential between the surfaces, ϕ_B and ϕ_A are the surface work functions, and e is the electric charge of an electron (-1.602x10^{-19} C).

As the surfaces in contact are separated, electrons will tunnel across the interface, reducing the final charge left on the surfaces. Harper (1967) experimentally found that the final charge can be predicted from the contact potential using the relation:

$$q = C_0 V_c \quad (7)$$

Where q is the final charge and C_0 is the capacitance between the surfaces.

The capacitance was found to correspond to a separation on the order of 100 nm, much higher than the 1 nm predicted by the tunneling model (Lowell & Rose-Innes, 1980). This discrepancy was explained by the surface roughness since the presence of protuberances prevents the intimate contact of the surfaces assumed in the original model. The metal-metal contact charging process is illustrated in Figure 1.6. As two metal surfaces are brought into contact, the metal with the lower work function has electrons at higher energy levels and therefore some of its valence electrons transfer to the other metal. This results in a positive charge on the first and a negative charge on the second metal.

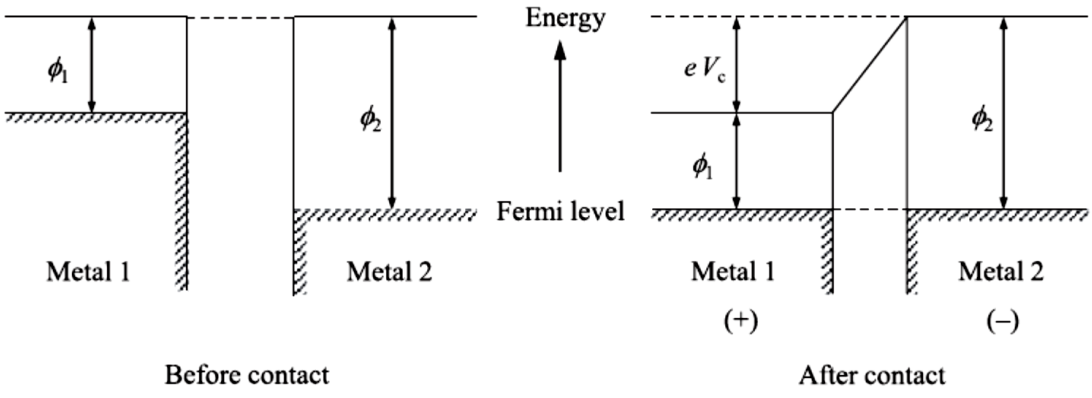

Figure 1.6: Electron potential energy for metal-metal contacts, adapted from Matsusakaa et al. (2010).

1.2.3 Electrostatics in Insulators

The study of contact charging involving insulators is more complex than pure conductor-conductor charging. Low charge mobility makes the assumption of thermodynamic equilibrium inapplicable and renders contact charging a local phenomenon dependent on the microscopic properties of the surfaces. Experimentally measured macroscopic charge is therefore a net value with significant underlying local variation. The local nature of contact charging in insulators, such as polymers, makes it susceptible to minor variations on the contact surface such as the presence of impurities, chain ends or side groups. These reasons, among others, have led some researchers to conclude that "electrostatic charging [in insulators] may never be predictable" (Lacks, 2012).

Many models have been proposed to explain electrostatic charging in insulators. They can be classified into two broad categories based on the proposed charge carriers: electronic and ionic models.

1.2.3.1 Electronic Models

Earlier works emphasized the analogy between conductors and insulators. Many models based on the assumption of electron transfer have been developed and extended. Lowell and Rose-Innes (1980) reviewed the relevant literature.

Metal-insulator contact charge was found to vary linearly with the work function of the metal, reminiscent of metal-metal contacts. Contact charging was determined by the difference between the metal Fermi level and an "effective" Fermi level characteristic of the insulator. The Fermi-level of metals is about 4 to 5 eV which is much lower than the conduction band and much higher than the valence band of a typical polymer, e.g. polyethylene. Therefore, electrons transfer to or from the valence and conduction bands is not possible and cannot account for contact charging. Studies with pure samples of crystalline insulators showed that they did not charge when contacted by metals. The fact that contact charging does occur in less pure samples indicates that impurity states, such as side groups, surface impurities, ends of molecular chains and cross-linking sites, account for contact charging. Effective work functions for most polymers were found to be in the range of 4.08-4.85 eV, based on metal-polymer contacts. While

electronic models were developed based on experiments with metal-insulator charging, the derived effective work functions could roughly predict insulator-insulator contact charging.

Although decades has elapsed since major work on electronic models has been performed, convincing proof of their validity is yet to be presented (Williams, 2012).

1.2.3.2 Ionic Models

Recent works emphasized the heterogeneity of insulator surfaces. Rejecting electrons as the charge carriers, most have concluded that contact electrification is driven by ion or material transfer between the contacting surfaces.

Apodaca et al. (2010) observed that essentially identical pieces of the same material can acquire charge when contacted suggesting that microscopic variations in the surface composition can cause macroscopic changes in charging properties.

Baytekin et al. (2011) showed that surfaces of charged insulators are composed of random "mosaics" of positively and negatively charged nanoscopic regions. Surface charge in individual regions was much larger than the net, macroscopic charge. It was also noted that charge transfer was accompanied with material transfer and changes in the surface composition. However, the relationship between material and charge transfer was not clear. They concluded that contact electrification is a complex process involving "bond cleavage, chemical changes, and material transfer occurring within distinct patches of nanoscopic dimensions."

Baytekin et al. (2012) observed that after repeated contact between PTFE (Polytetrafluoroethylene) and PS (Polystyrene), the charge on the particles reverse. This suggested that the nature of the surfaces in contact changed due to material exchange between the surfaces. The charge reversal was related to the relative softness/hardness of the surfaces in contact, which controls material transfer. This conclusion also was shown to be true for other pairs of materials. Confirming this conclusion, Sow et al. (2012; 2013) found that macroscopic strain affects the amount and direction of charge transfer.

Burgo et al. (2012) observed the formation of macroscopic regions of opposite charge on the surfaces of PTFE and PE (Polyethylene) following their contact. Analysis of the regions showed that the positively charged region on PTFE was formed by species derived from PE and that the

negatively charged region on PE was formed by species derived from PTFE. This indicated that charge transfer is related to material transfer. It was hypothesized that charge transfer is caused by the following tribochemical processes. As the two surfaces are brought into contact, mechanical shear is concentrated in a fraction of the surfaces causing temperature peaks in some zones. Extensive chain breakdown occurs in these zones causing the formation of radical species. Electrons transfer from the hydrocarbon to the fluorocarbon due to the high electronegativity of the fluorine atoms, forming hydrocarbon cations and fluorocarbon anions. These species, according to Burgo et al, are the charge carriers.

McCarty and Whitesides (2008) proposed that contact electrification in insulators is due to the partition of ions between the surfaces in contact. In the case of insulators with mobile ions, these ions are the charge carriers. For other insulators, the partitioning of hydroxide ions in the adsorbed surface water layer drives contact electrification. Observing that in many published triboelectric series polar materials charge positively and nonpolar materials negatively and noting some experimental results indicating that hydrophobic materials accumulate hydroxide ions, it was concluded that hydroxide partitioning explains the observed results.

Overall it can be concluded that ion and material transfer in insulators tribocharging is still an area of ongoing research.

1.2.4 Electrostatics in Particulates

The study of electrostatics in systems of particles presents additional challenges. It is often not possible to measure the charge on an individual particle or to control the charging process as it is in discrete objects. Moreover, due to the uncertainty about the fundamental mechanism of electrostatic charging, progress on understanding charging in particulates has been limited.

Two models have been proposed to account for charging in particulates: the condenser model and the charge relaxation model (Matsusakaa et al., 2010). The condenser model is an extension of the effective work function model presented in equations (6) and (7). As discussed above, such a model assumes that electrons are the transferred species in insulators and requires the knowledge of an "effective" work function. The charge relaxation model assumes that the charge transferred causes a potential difference between the surfaces in contact in excess of the breakdown potential of the atmosphere, which for air is approximately 3.0×10^6 V/m (Cross,

1987). In such a case, the final charge on the particle is only a function of the breakdown potential and the particle diameter. The two models have been successfully applied for pneumatic transport of powders in metal pipes. They are yet to be applied for more complex systems such as dust devils, sand storms, powder flow in insulating tubes, or fluidization.

1.2.4.1 Bipolar Charging

One peculiar phenomenon in particulate charging is bipolar charging. Many studies have noted a size-dependence of charge polarity of particles of the same material with smaller particles charging negatively and larger particles positively (Ali et al., 1998; Forward et al., 2009; Cartwright et al., 1985; Zhao et al., 2003), or the reverse (Liu et al., 2010; Giffin and Mehrani, 2010; Mehrani et al., 2005; Sowinski et al., 2010, Sowinski et al., 2012). Zhao et al. (2003) proposed that bipolar charging can be due to differences in the (a) inherent work functions, (b) microscopic surface structures, (c) specific areas and consequently contaminant absorption, or (d) surface energies. There is little experimental evidence to confirm or deny any of the explanations.

Kok and Lacks (2009) used the high energy state electron theory of Lowell and Truscott (1986) to develop a model for contact charging between larger and smaller particles. It was assumed that electron transfer from donor to accepter states is non-reversible within the process time-frame. The simulation resulted in smaller particles accumulating electrons and charging negatively. This was attributed to their higher specific surface area. Interestingly, Cai (2013), using a similar model, showed that there exists an upper limit of charge in the bed whereby particles reach charge saturation simply due to the dynamics of the process, independent of the air breakdown potential.

1.3 Electrostatics in Fluidized Beds

The continuous contacts between particles and other particles and between particles and the column wall in a fluidized bed generate a significant amount of electrostatic charges which is a major nuisance in some industrial operations.

The generated charges could cause particle agglomeration causing deviation from the desired particle properties such as particle size. Large electrostatic discharges could endanger operators and equipment. The adhesion of particles to the reactor wall and other surfaces requires regular shutdown for clean-up, which is a major problem in industrial operations such as polyethylene production.

1.3.1 Electrostatics in Polyethylene Reactors

The generation of electrostatic charges in polyethylene reactors such as the one described in section 1.1.1 is a major nuisance primarily due to a problem known as "sheeting".

Charged fluidizing particles (polyethylene resin and catalyst particles) adhere to, or foul, the walls of the fluidized bed. Particles create an image charge of opposite polarity on the conductive reactor walls and the force of attraction between the particles and their image causes the particles to adhere to the walls. Particle wall fouling occurs at zones shown in Figure 1.7 where the drag force is minimum. The sheets formed on the reactor wall have thicknesses of approximately 0.00635 to 0.0127 m (¼ to ½ inches), heights of inches to several feet and widths in the range of 0.0762- 0.4572 m (3-18 inches) (Hendrickson, 2006). The exothermic polymerization reaction in these zones causes spikes of the local temperature causing the sheets to melt. When these sheets become sufficiently large, they detach from the reactor wall and fall into the distributor plate partially blocking it. The detachment of the sheets generates further electrostatic charges which cause further sheeting. Sheets can also block the product discharge valve. Industrially, a reactor might operate for only a few hours before sheeting necessitates its shutdown for clean-up (Fulks et al., 1985). Depending on the severity of the problem, reactor shutdown and clean-up may take from two to three days and in some cases to even more than a month. Sheeting has been observed to be most prominent in processes utilizing Ziegler-Natta catalysts Type III and Type IV, some bimodal catalyst systems and particularly metallocene catalysts (Hagerty et al., 2005).

The economic cost of this problem is considerable. There are about 100 plants worldwide utilizing the gas-phase process to produce polyethylene, with an average production capacity of about 200 million metric tonnes of polyethylene per year. The marginal cost per day of shutdown for an average plant is a minimum of $1 million. Assuming average shutdown of 3 days per year, the total marginal loss to industry is about $330 million annually.

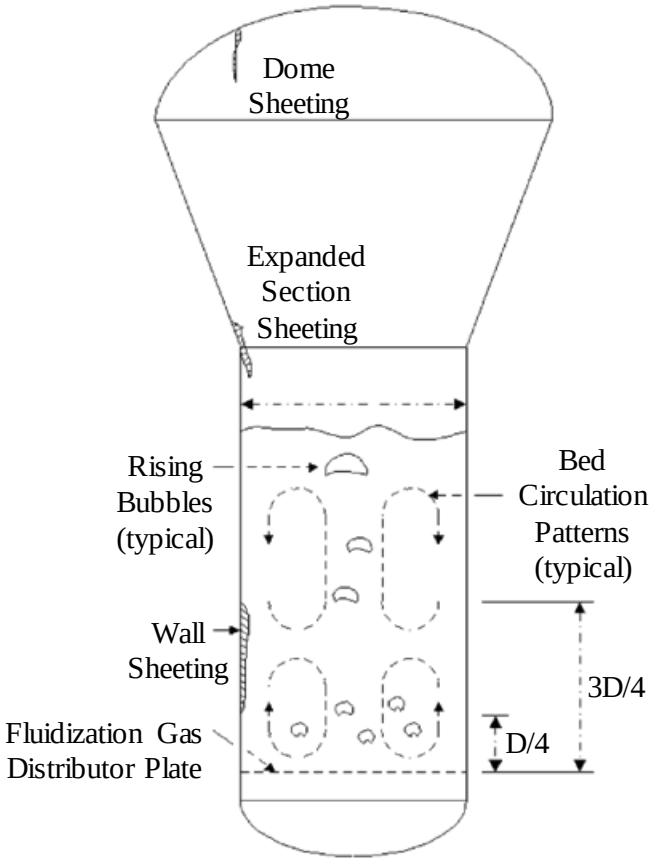

Figure 1.7: Wall fouling or "sheeting" in polyethylene production fluidized beds, adapted from Hendrickson (2006).

1.3.2 Electrostatic Charge Measurement Techniques

The two most common measurement techniques for electrostatic charges in fluidized beds are the Faraday cup and the electrostatic probe.

1.3.2.1 Faraday Cup Technique

The Faraday cup technique consists of two concentric copper cups, illustrated in Figure 1.8, electrically isolated from each other with a piece of insulating material. The outer cup, which is connected to ground, shields the inner cup from background electric fields. A charged object is inserted into the inner cup. The object charge induces an equal and opposite charge on the cup in accordance with Gauss's law as previously mentioned in section 1.2.1. Although in practice the cup does not fully enclose the object and therefore does not constitute a true Faraday cage, the charged object is generally sufficiently deep inside the cup to make the difference immaterial (Cross, 1987). The cup is connected to an electrometer to measure the charge.

Several implementations of Faraday cups in fluidized beds are found. In most cases, a sample of the particles is removed from the fluidized bed for measurement in an external Faraday cup such as using a vacuum pump (Fasso et al., 1982; Mountain et al., 2001), placing a sampling tube inside the bed (Fujino et al., 1985; Zhao et al., 2003), sampling ports with lock and gate mechanisms along the column wall (Moughrabiah et al., 2009; Tardos & Pfeffer, 1980) or manually removing wall deposits with a scoop after fluidization is complete (Ali et al., 1998). There are two difficulties with such techniques. First, the removal of particles requires handling them which can alter their charge or introduce additional charges before they are placed inside a Faraday cup. Second, a single sample cannot be representative of the whole bed since several regions of differing charge density and even polarity exist in a fluidized bed as will be described in later sections. Mehrani et al. (2005) configured the experimental system such that the fluidization column is the inner Faraday cup. However, this method was limited to only measuring the charge of entrained fines. Sowinski et al. (2010) developed a measurement technique to sample all particles in a fluidized bed. This method will be described in section 1.3.4.

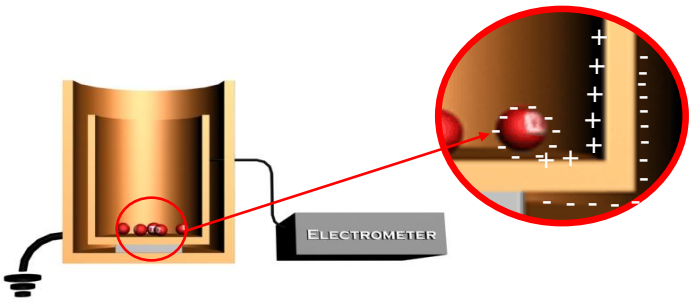

Figure 1.8: Faraday cup technique.

1.3.2.2 Electrostatic Probe Technique

The electrostatic probes technique is depicted in Figure 1.9. The probe consists of a conductive bar or wire enveloped by an insulating layer, and an outer conductive grounded layer. The charged object is brought to the proximity of one end of the probe, inducing a charge on the probe. The other end of the probe is connected to an electrometer to measure this induced charge. In fluidized beds, a wide variety of electrostatic probe setups have been utilized to characterize electrostatics. The probe can be located at the wall of the column, near the center of the bed or at the distributor plate; it can be located at below or above bed-level. The measured signal can be electric potential, field, current, charge or capacitance. In most cases, probes were located at the wall of the column and measured potential or current. An electric charge signal is an integral of the current and therefore these two measurements are inter-changeable. Designs for potential and current probes are very different and the two types cannot be easily inter-changed.

Conventionally, industrial polyethylene beds utilized current probes consisting of a semi-spherical tip assembled such that only the tip is inside the column and located at a height of approximately half of the reactor diameter above the distributor plate (Hagerty et al., 2005). The probe signal is continuously monitored during operation. Deviation from the baseline steady-state is considered an indication of the inception of sheeting. However, as a method to detect sheeting, conventional probes are not particularly reliable. Moreover, the mechanisms contributing to the measured signal in a freely bubbling bed of insulating particles, such as polyethylene, are poorly characterized. For these reasons, industry also uses other styles of probes in addition to conventional probes including probes at the exit of the column measuring static from elutriated fines, probes at the overhead of the bed and distributor plate probes. However, conventional probes continue to be widely used.

Potential and current probes measure slightly different phenomena. Potential probes measure the potential induced on the electrostatic probe by the electric field surrounding it. A sufficiently small probe does not affect the potential distribution within the bed. Therefore, the results produced would be a true characterization of electrostatic potential in the bed.

Current probes measure both the charge induced on the probe and the charge transferred to it. The tip of the probe inserted into the bed effectively represents a piece of the reactor wall instrumented to measure charge flow (Hagerty et al., 2005). In the present research, bench-scale

tests of an electrostatic probe contacted with polyethylene particles showed that charge generation due to contact between the probe and particles dominates the resulting measured charge (Appendix 3). Therefore, current probes do not accurately measure the net charge accumulated within the bed but represent a sample of the charge generated due to particle-wall contacts. The probe in this case essentially represents a sample of the column wall. Moreover, the results obtained would be affected by the fouling of the probe tip with a layer of particles. A fouling layer would limit further particle-probe contacts, of which the resulting electrostatic charge generated is the primary contributor to the obtained signal as mentioned. For these reasons, electrostatic probes measuring current do not reliably measure electrostatic charge in fluidized beds.

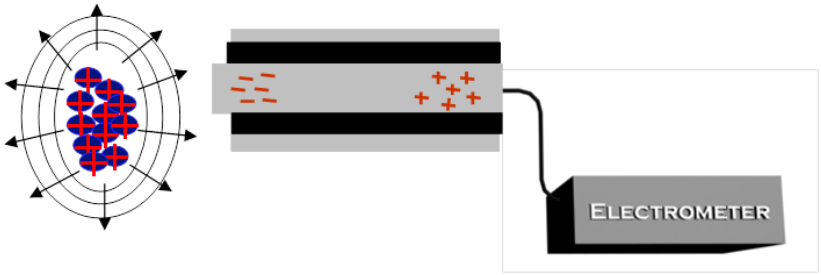

Figure 1.9: Electrostatic probe technique.

1.3.3 Previous Works on Electrostatics in Gas-Solid Fluidized Beds

Many studies have been reported in literature aimed at better understanding of electrostatic phenomena in fluidized beds. A brief review of this literature is presented below. The experimental setups utilized are presented followed by the obtained results.

1.3.3.1 Experimental Setups

Most studies utilized 3D columns although 2D columns were used in some cases. Column materials included steel, glass, Perspex, Plexiglas and PVC. Three-dimensional column diameters ranged from 0.02 to 0.25 m, two-dimensional column widths were up to 0.5 m, and static bed heights ranged from 0.005 m to 0.60 m.

The two most common particles used were glass beads and polyethylene resin, although some studies used acrylic resin, polystyrene, polyamide or others. In most cases, the particles used were of Geldart group B (with diameters of a few hundred microns) although a number of studies used Geldart group A particles (<100μm).

The majority of works were conducted at room temperature and pressure, using air or nitrogen as the fluidizing gases and operating in the bubbling regime. Fluidizing gas relative humidity was varied in a number of cases. Fluidization time was typically in minutes or hours.

The two most common measurement techniques were Faraday cups and electrostatic probes, previously described in section 1.3.2.

The experimental setups of the reviewed studies are summarized in Appendix 1, Table A1.1.

1.3.3.2 Results

The experimental techniques reviewed above were utilized to study charge distribution within fluidized beds, the time required for charge saturation and bipolar charging as well as the effects of gas relative humidity, gas velocity, particle size, particle material and column material on electrostatics. The effects of operating pressure and column diameter are presented in more detail in subsequent sections due to their particular importance to this thesis.

Many studies have observed a stabilization of charge after a period of time, ranging from 2 minutes (Murtomaa et al., 2003) to 60 minutes (Fujino et al., 1985; Giffin & Mehrani, 2010). Charge could continue to increase after that period but much more slowly (Bafrnec & Bena, 1972). Giffin and Mehrani (2010) reported that charge saturation was much faster in the slugging than the bubbling fluidization regime.

Most studies noted opposite polarities of charge below and above the bed level, suggesting that the bulk of the bed and the entrained fines were oppositely charged, and that charge at about bed level was minimal (Giffin & Mehrani, 2010; Moughrabiah et al., 2009; Murtomaa et al., 2003; Sowinski et al., 2010; Wang et al., 2008; Yu et al., 2010). Differing results were also reported. Liu et al. (2010) observed that within the fluidized bed, the upper part of the bed had an opposite polarity to the bottom. Fujino et al. (1985) observed that the potential was maximum at about the bed level.

Bipolar charging, where smaller particles acquired a charge of opposite polarity to larger particles have been observed in many cases. As noted above, entrained fines can have a charge opposite to the bed. In some cases, a correlation between the charge polarity and the particle size was observed (Ali et al., 1998; Forward et al., 2009; Giffin & Mehrani, 2010; Liu et al., 2010; Mehrani et al., 2005; Sowinski et al., 2010; Zhao et al., 2000) while in others there was minimal size dependence (Mountain et al., 2001).

Conflicting results on the effect of average bed particle size on electrostatics were reported. Boland and Geldart (1972) reported increasing electrification with increasing lead glass ballotini particle size in the range of 100-800 μm and Guardiola et al. (1996) reached a similar conclusion about increasing glass beads particle size in the range of 250-420 μm. Both studies attributed the results to the increasing particle-particle contact area with increasing size. Wang et al. (2008) reported increasing potential in a bed of polyethylene particles with decreasing particle size in the 185-1700 μm range and attributed this to a larger number of particles per unit area leading to more intensive electrification. Sowinski et al. (2012) reported that wall fouling due to electrostatic charge decreased significantly for polyethylene particles with diameters larger than 600 μm. Approximately 6% of the particles adhered to the wall for beds with average particle sizes below that threshold but only 1% of particles adhered when the diameter was above it.

The effect of fluidizing gas relative humidity (RH) on fluidization electrostatics is complex. In some cases, increasing RH increased electrification and in others reduced it or had a minimal effect (Bafrnec & Bena, 1972; Boland & Geldart, 1972; Ciborowski & Wlodarski, 1962; Guardiola et al., 1996; Ham et al., 1992; Tardos & Pfeffer, 1980; Yao et al., 2002;). Depending on the nature of the particles fluidized, the formation of a water layer on the surface of the particles was thought to affect both electrostatic charge generation and dissipation, respectively increasing and decreasing charge (Fujino et al., 1985). Giffin and Mehrani (2013) concluded that the influence of moisture is not only dependent on the nature of the fluidizing particles, being hydrophobic or hydrophilic, but also it is dependent on the column wall material. Minimal effect of relative humidity was observed for polyethylene particles fluidized in a stainless steel column.

Published studies have consistently reported an increase in electrostatics with an increased fluidizing gas velocity (Bafrnec & Bena, 1972; Ciborowski & Wlodarski, 1962; Fujino et al., 1985; Guardiola et al., 1996; Ham et al., 1992; Liu et al., 2010; Moughrabiah et al., 2009; Tardos

& Pfeffer, 1980; Yao et al., 2002). Sowinski et al. (2010) also observed an increase in wall fouling with increasing superficial velocity. However, at the transition to slugging flow a decrease in electrostatics (Guardiola et al., 1996; Sowinski et al., 2010) and wall fouling (Sowinski et al., 2010) was observed.

The materials of fluidizing particles and fluidization column wall are some of the most important factors because electrostatics is a surface phenomenon. Relatively more conductive particles such as glass beads generate significantly less charge and foul much less than more insulating particles such as polyethylene resin. Moreover, different resins of polyethylene have differing charging properties partly due to differing utilized catalysts (Hagerty et al., 2005). The fundamental reasons underlying these differences are not well understood. Similarly the degree of bed electrification is higher in columns made of insulating material such as Plexiglas than in metal columns. Therefore, in order to understand the electrostatic charging in industrial operations it is essential for investigations to be conducted in systems as closely related as possible to these operations.

1.3.3.3 The Effect of Operating Pressure

Although polyolefin production reactors, of the most significant applications for research on electrostatics in gas-solid fluidized beds, operate at high pressures of up to 3 000 kPa, the majority of studies found in open literature are performed at atmospheric conditions. The effect of the operating pressure on gas-solid fluidized bed electrostatics has been reported by only one research group (Moughrabiah et al., 2009; Liu et al., 2010).

Moughrabiah et al. (2009) utilized the apparatus shown in Figure 1.10. Four electrostatic probes were located at the center of the fluidized bed at various heights above the distributor plate, including one at above the bed level. Four corresponding probes were located at the same heights but near the wall of the column. The electrostatic charge generated on the probes during fluidization for only pressures up to 724 kPa was recorded for only 500 s and used as a measure of bed electrification. Utilizing glass beads as the fluidized particles, Moughrabiah et al. concluded that increasing operating pressure from 379 to 724 kPa increased bed electrification due to an increase in bubble rise velocity, frequency, and volume fraction.

Utilizing the same apparatus as Moughrabiah's, Liu et al. (2010) studied the effect of operating pressure on the fluidization of polyethylene resin. Various resins of polyethylene were used. In contrast to their first work (Moughrabiah et al., 2009), the authors concluded that it was difficult to predict the effect of operating pressure on electrostatics due to the complex influence of hydrodynamics and the effect of resin properties on electrification.

It is not possible to draw a clear conclusion on the effect of the operating pressure on electrostatics in polyethylene fluidized beds from these two studies. Also note that electrostatic probes utilized in the studies reviewed above, although convenient, have serious methodological issues as discussed in section 1.3.2.2.

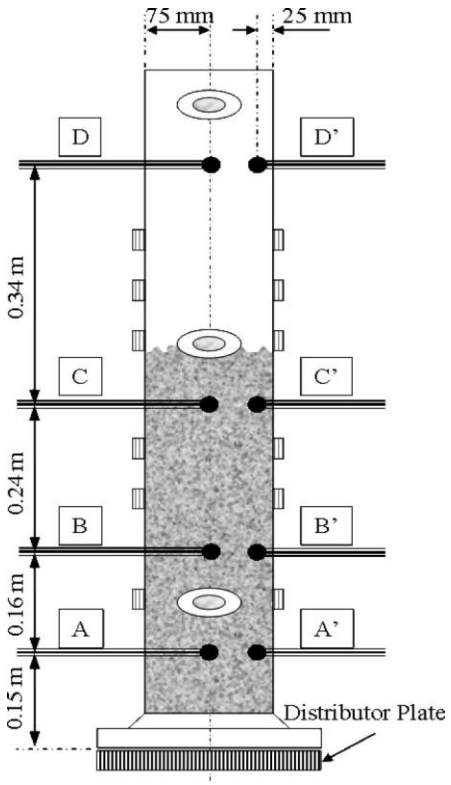

Figure 1.10: Schematic of measurement apparatus used by Moughrabiah et al. (2009). A-D and A'-D' refer to electrostatic probes with tips located at the center and the edge of the bed, respectively.

1.3.3.4 The Effect of Column Diameter

The effect of column diameter on electrostatics in fluidized beds has only been reported by Rojo et al. (1986) using a capacitance probe method shown in Figure 1.11. The method consisted of a

metal probe located at the top of the fluidized bed measuring the potential difference between the probe and the metallic distributor plate. Due to the simple geometric configuration of the apparatus, an expression for the capacitance of the bed relating the potential and the electric charge within the bed was possible to develop. This expression allowed for the calculation of the charge given the measured potential. Using this method, Rojo et al. studied the influence of the bed height to diameter (H/D) ratio and that of the column diameter. 350-420 μm glass ballotini particles were fluidized in Perspex columns with diameters of 0.035 to 0.054 m and H/D ratios in the range of 1 to 3 were used.

It was concluded that increasing the H/D ratio increased charging up to a ratio of 2 and decreased it thereafter. The increase was attributed to the greater velocities reached by bubbles with increasing bed height due to bubble agglomeration resulting in bubbles with larger diameters and therefore greater rise velocities as per equation (3). The greater velocities caused more vigorous motion of particles and therefore increased friction and electrostatic charge generation. The decrease after an H/D ratio of 2 was attributed to the onset of slugging. The authors explained that since slugs have lower rise velocities than free bubbles, less motion in the bed was produced and therefore there was less charge generation.

On the other hand, it was concluded that column diameter has no influence on charge generation if the H/D ratio was constant. This was because beds operating at the same H/D ratio were operating in the same fluidization regimes (bubbling or slugging). It is important to note that the column diameters studied (0.035-0.054 m) were quite small lab-scale units (i.e. mini-beds) and not necessarily comparable with pilot-scale operations.

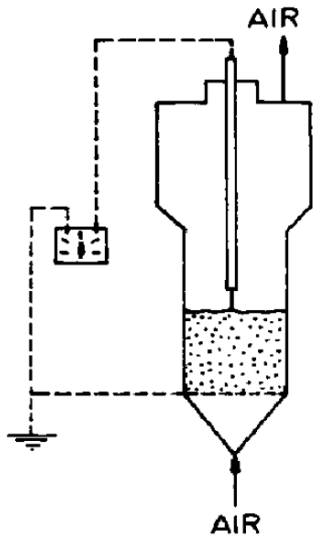

Figure 1.11: Experimental apparatus used by Rojo et al. (1986).

1.3.4 Works on Wall Fouling in Gas-Solid Fluidization Beds

Wall fouling due to electrostatic charging is a major industrial problem as described in section 1.3.1. Previous studies have only focused on the study of electrostatic charge to the exclusion of wall fouling. Therefore, it is difficult to apply the results of these studies to the problem of wall fouling and sheeting in the polyolefin industry.

To address this issue, a novel measurement technique was developed by Sowinski et al. (2009; 2010) shown in Figure 1.12, to not only characterize electrostatic charge but also to investigate the degree of wall fouling in fluidized beds. At the exit of the column, a filter bag was used to capture entrained fines. The bag was placed inside a Faraday cup for the charge of the fines to be measured cumulatively during the fluidization period. A modified knife-gate valve was used as the distributor plate and a Faraday cup was used as the column windbox. Once fluidization was complete, the knife-gate valve could be opened, allowing the majority of the bulk of particles to drop into the Faraday cup. If any particles were adhered to the wall of the column, they could be removed by tapping the column or by using compressed air passed through the column from the top to detach them from the wall. This method enabled the mass of the particles in various regions of the fluidized bed (i.e., entrained fines, bulk of the bed, and particles adhered to the column wall) to be measured, as well as their charge. The particles diameters were also measured in the three regions.

This technique was successfully implemented in an atmospheric, 0.102 m in diameter, fluidization column. Using this system, for the first time, the charge distribution in the fluidized bed and the magnitude of the particles reactor wall fouling was studied, as well as the effects of gas velocity and fluidization regime (Sowinski et al., 2010), particle size (Sowinski et al., 2012), column wall grounding (Sowinski et al., 2011), fluidization time (Giffin & Mehrani, 2010) and fluidizing gas relative humidity (Giffin & Mehrani, 2013) on wall fouling and electrostatics.

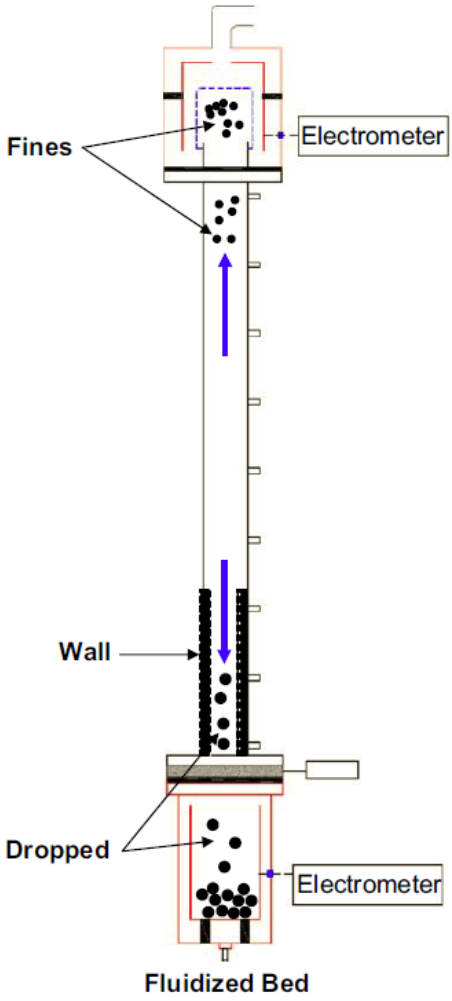

Figure 1.12: Electrostatic charge measurement technique, adapted from Sowinski et al. (2010).

1.4 Thesis Objectives

The ultimate goal of the research project, which this thesis is part of, is to help industry, particularly the polyolefin production industry, in minimizing or eliminating the negative impact of electrostatics in fluidized bed reactors on process operability. In order to achieve this, an understanding of the mechanisms of electrostatic charge generation in fluidized beds is required. In this regard, the measurement method described in section 1.3.4 was first developed that enabled the investigation of the electrostatic charge distribution as well as the degree of reactor wall fouling within a gas-solid fluidized bed. Studies concerning the effects of various experimental parameters on electrostatics were performed using this method in an atmospheric pilot-scale system. However, the industrial gas-solid fluidized beds, particularly those of polyethylene reactors, are operated at elevated pressures, temperatures as well as gas velocities in turbulent fluidization regime. Therefore, the current study was conducted in continuation of this project to apply the previously developed online charge measurement technique to a system capable of operating at conditions similar to industrial operations.

The specific objectives of this study were to:

- Scale up the measurement technique described above to a larger unit capable of operating at temperatures (up to 100°C), pressures (up to 2 600 kPa) and gas velocities (up to 1 m/s) similar to those used in industrial polyethylene production reactors. In addition, the unit had a larger column diameter equal to diameters of pilot-scale industrial reactors rendering the produced results more relevant to industry.
- Perform preliminary tests on the new system. The effect of operating pressure, varied from 101 kPa to 401 kPa, on electrostatic charge generation and wall fouling was studied.
- Briefly examine the effect of fluidizing particle size distribution.
- Examine the effect of column diameter by comparing results from the larger, newer unit, with the smaller, existing unit. Finally, propose possible mechanisms underlying the adherence of fluidization particles to the column wall.

1.5 Thesis Outline

The second chapter of this thesis describes the experimental apparatus and the measurement technique used in this research as well as the procedures followed and materials used. The basic idea underlying the measurement technique was previously developed by Sowinski et al. (2010). It was extended in this work to a larger unit.

The third chapter presents and analyzes the obtained results. In this chapter, the initial properties of the particles used for experiments are presented. Then the average results around which the obtained results vary are examined and analyzed. The mechanisms of charge generation and wall layer formation in fluidized beds are discussed. Finally, the effects of various parameters, specifically the operating pressure, particle size distribution and column diameter, on wall fouling and electrostatic charge generation are examined.

The final chapter presents the overall conclusions of this research and recommendations for future work. Additional experimental data and supporting information appear in the appendices.

Chapter 2. Materials and Methods

This chapter describes the materials utilized, the experimental apparatus used and the procedures followed to conduct two types of experiments: a) bubbling fluidization conducted in the new, larger, and the small fluidization columns; and b) bench-scale shaking tests.

2.1 Materials

2.1.1 Fluidizing Gas

This research involved only preliminary testing of the new high pressure column and thus experiments were performed with compressed building air as the fluidizing gas. On average, the relative humidity of the gas was 9.3% and the temperature was 21.0°C. Building air is supplied at a pressure of approximately 791 kPa.

2.1.2 Fluidizing Particles

Please change to read" Although the overall focus of this research was the investigation of electrostatic phenomenon in gas-solid fluidized beds in general, the experimental work was mainly focused on one application related to the polyethylene industry using metallocene based catalysts. Metallocene-based resin particles of linear low-density polyethylene (LLDPE) were used for all experiments, which were received courtesy of Univation Technologies, LLC (USA). Particle properties are summarized in Table 2.1.

Table 2.1: Properties of polyethylene particles used in this work.

Property	Units	Value
Physical Properties		
Particle density	kg/m^3	918
Static bed voidage		0.4
Sieving Mass Percentage		
1000 µm	%	8
500 µm	%	55
250 µm	%	34
< 250 µm	%	2
Particle Size Distribution	µm	20-1500
Mean Particle diameter	µm	573
Specific surface area	m^2/g	0.0120
Geldart Group		B
Minimum fluidization velocity (u_{mf})		
at 101 kPa	m/s	0.15
at 401 kPa	m/s	0.12
Surface Properties		
Scanning Electron Microscope (SEM) Image		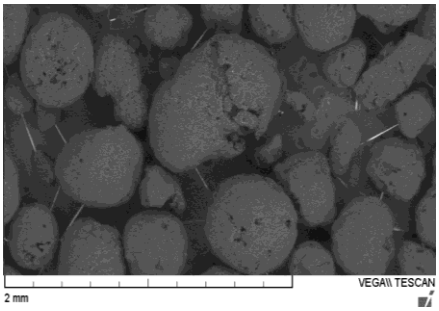
Sphericity		0.81
Morphology		Coarse
Chemical Properties		
Chemical Formula		$(C_2H_4)n$
Chemical Structure		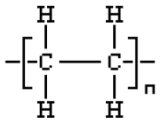
Catalyst		
Catalyst type		Metallocene
Catalyst Base elements		Si
Melt Index		1
Polar Molecule		No
Water adsorption		Hydrophobic
Electrical Properties		
Effective work function	eV	5.23

Particle Density

The particle density of 918 kg/m^3 was provided by Univation Technologies, LLC.

Static Bed Voidage

The static voidage was determined using a 25 mL pycnometer. A solution of 60% ethanol-40% water was used. The particles were gradually poured into the pycnometer along with the solution such that solution only wetted the particles and filled the gaps between them. The volume of solution added therefore approximated the voidage, which was calculated using the equation:

$$static\ bed\ voidage = \frac{volume\ of\ solution}{volume\ of\ particles + \ volume\ of\ solution} \qquad (8)$$

The mass of particles added was measured. The volume was calculated using the particle density.

Mean particle diameter and specific surface area

The Malvern Mastersizer 2000 with Hydro2000S sampler (Malvern Instruments Ltd, UK). was used to measure the particle size distributions. In addition, it provided the particles specific surface area.

Geldart Classification

The particles density was 918 kg/m^3 and their mean diameter (dp_{50}) was 573 µm. The fluidizing air density varied from 1.1 kg/m^3 at 101 kPa, and 4.3 kg/m^3 at 401 kPa. At the higher pressure, the difference between the particle and gas density is 915.3 kg/m^3, equivalent to 0.9153 g/cm^3. As Figure 1.2 shows, at a particle diameter of 573 µm and difference in density of 0.9153 g/cm^3, the particles are of class B. The particles are also of Geldart class B at atmospheric conditions.

Minimum fluidization velocity (u_{mf})

The minimum fluidization of the particles was determined by varying the superficial velocity of the gas and observing the pressure drop across the bed. Below the minimum fluidization velocity the pressure drop across the fixed bed varies linearly with the superficial gas velocity. Above the minimum fluidization velocity, the pressure drop across the fluidized bed is almost constant. The superficial gas velocity at the intersection of the linear best fit lines in the two regions, the fixed

and fluidized beds, is the minimum fluidization velocity. This was determined to be 0.15 m/s and 0.12 m/s for operating pressures of 101 kPa and 401 kPa, respectively. Increasing pressure decreases the minimum fluidization velocity in the turbulent flow regime but does not affect it in the laminar flow regime as discussed in section 1.1.2. For the conditions used in this study, neither rule is valid (Re_{mf} ~ 5) and the minimum fluidization velocity decreased slightly with increasing pressure.

Particle surface morphology and sphericity

Scanning electron microscopy (SEM) pictures of the polyethylene particles were taken, a sample of which is shown in Table 2.1, using a Tescan Vega-II XMU VPSEM allowing the calculation of circularity based on the projected area. Sphericity was assumed to be equal to the circularity. The sphericity of the particles was determined from these pictures. The circularity of the particles can be calculated from the equation:

$$circularity = 4\pi\left(\frac{area}{perimeter^2}\right) \quad (9)$$

Using the Photoshop software and the SEM pictures, the particles projected area and parameter were determined allowing the calculation of their circularity. The circularity of many particles was determined and the average was determined to be 0.81. The particles sphericity was assumed to be equal to their circularity.

Work function

The effective work function of polyethylene was determined to be 5.23 eV by Tanoue & Masuda (2006).

2.2 Fluidization Experiments

Fluidization experiments were performed in two systems:

a) a smaller 3-D fluidization system equipped with an online electrostatic charge measurement technique operated at atmospheric conditions. This system was previously developed by Sowinski et al. (2010); and

b) a larger 3-D fluidization system functional at higher pressures and temperatures utilizing the same electrostatic charge measurement method as the smaller unit. This system was designed and built in the present work.

2.2.1 Fluidization Columns and Measurement Technique

Particles were fluidized in either one of the two columns. The two columns nominal diameters were 0.102 m and 0.154 m. Since they were equivalent in design, the following description applies to both columns except when noted. Dimensions of the apparatus described below are shown in Table 2.2 for reference. Schematics of the two systems are shown in Figure 2.1 and Figure 2.2. Pictures of the two systems are compared in Figure 2.3, and more detailed pictures of the larger system are shown in Figure 2.4.

The measurement technique consisted of two Faraday cups, referred to as top and bottom Faraday cups, and the blade of a knife-gate valve acting as the distributor plate. The purpose of this measurement technique is to quantify the mass and the net charge of particles in several regions of the fluidized bed, particularly the layer of particles adhered to the wall.

At the top, the exit of the column was fitted with a filter bag located inside the Faraday cup to capture the entrained fines during fluidization. The cup consisted of an inner and outer Faraday cup. The inner Faraday cup was used to measure the net charge while the outer Faraday cup acted as an electric shield for the inner cup to protect it from interference of electric fields in the environment. The inner cup was made of copper for both the larger and smaller column. The outer cup was made of copper for the smaller column and of stainless steel for the larger column. The top Faraday cup was connected through a triaxial cable to a Keithley digital electrometer Model 6514 (Keithley Instruments, Inc., Ohio, USA) to continuously measure the net charge of the entrained particles during fluidization. The filter bag was made of cloth. It was attached to a

Teflon adapter which was in turn attached to the top of the column for three purposes. First, Teflon insulated the somewhat conductive filter bag from the column, preventing charge flow from the column to the filter bag and therefore preventing interference from the column's charge on the charge measurement apparatus. Second, it prevented the filter bag from being dislocated by the flowing gas. Third, it ensured that the fluidizing gas, and the particles it entrained, flowed through the middle of the filter bag and not through gaps between the bag and the top of column. Four layers of Dustlock filter supplied by BC Air Filter (BC, Canada) were inserted into the filter bag to capture the entrained particles. This filter contained an adhesive which entrapped the particles inside the filter bag.

The perforated distributor plate was the blade of a knife-gate valve and the column windbox was used as the outer cup of the bottom Faraday cup. After fluidization was complete, the distributor plate was opened, dropping the bulk of the particles into the bottom Faraday cup and allowing the measurement of their net charge. For the smaller column, the knife-gate valve was of Series G pneumatic knife gate valve supplied by the Red Valve Company Inc. (Pennsylvania, USA), while that of the larger column was a ORBINOX Series 50 pneumatic knife gate valve, shown in Figure 2.4(a), supplied by Meridian (Alberta, Canada). The valve blades, shown in Figure 2.4(b), consisted of two perforated stainless steel 316 plates and a metal screen sandwiched between them. The holes of the plates were in the hexagonal arrangement. The top plate hole diameter was smaller than the bottom's. The holes of the top and bottom plates were respectively 2 mm and 4 mm for the smaller column, and respectively 3 mm and 4 mm for the larger column. The metal screen had an average mesh size of 32 μm for both columns.

The bottom Faraday cup, similarly to the top cup, was made of an inner cup and an outer cup. The inner cups for both columns were made of copper, as was the outer cup for the smaller column. The outer cup of the larger column was made of stainless steel. The outer cups acted as windboxes. Air flowed in the outer cup and around the inner cup, evening its distribution before entering the bottom of the distributor plate. The Faraday cups were connected using a triaxial cable to a Keithley digital electrometer Model 6514 to measure the net particles charge.

Since it was desired to operate the larger column at high pressure but still conveniently access the inner Faraday cups, two manways were used to enclose the top and bottom Faraday cups as

shown in Figure 2.3 and Figure 2.4(c,d). The manways were GD Engineering 14" Class 300 Banklock 2 vertical quick opening closures supplied by SPX Flow Technology (TX, USA).

Numerous ports were located at regular intervals along the fluidization column allowing various measurement devices such as pressure transducers to be mounted along the column. A differential pressure transducer, measured the pressure drop between a port near the bottom of the bed and another port located above the static bed height. For the smaller and larger columns, the bottom ports were respectively 0.076 m and 0.165 m above the distributor plate, and the top ports were respectively 0.686 m and 0.775 m above the distributor plate. The smaller column differential pressure transducer was an Omega PX654 (Omega Engineering, Inc., Connecticut, USA) and the larger column's was an ABB 2600T (ABB Inc., Burlington, Ontario). An absolute pressure transducer, ABB 264HS (ABB Inc., Burlington, Ontario), was connected to a port at the top of the larger column to measure the absolute pressure within the column.

Since the smaller system was operated at atmospheric conditions, the exit of its fluidization column was open to the atmosphere. For the larger unit, in order to control the pressure within the system, the exit of the column was fitted with a Swagelok spring-loaded back-pressure regulator.

The flowrate of the gas was measured and controlled using mass flow controllers. A Brooks model SLAMf53S mass flow controller was used in the larger column system and an MKS Model 1559A in the smaller system.

A relative humidity meter, Vaisala temperature and humidity transmitter model HMT338, was connected to the inlet gas of the smaller column. It continuously measured the gas relative humidity and temperature. They were found to be relatively consistent averaging about 9.3% and 21.0°C. Since the same gas supply was used with the larger system as for the smaller system, these values were assumed to be true for the larger system as well. Therefore, no relative humidity meter was included in the larger system.

An electrostatic probe was located near the bottom of the bed, at 0.076 m and 0.165 m above the distributor plate for the smaller and larger columns, respectively. Electrostatic probes are not reliable measurements for electrostatics as discussed in section 1.3.2.2. Therefore, the results obtained from the electrostatic probes are not reported in this thesis.

A bench-scale Faraday cup consisting of two copper Faraday cups was used to measure the net charge of the particles before fluidization. The diameters of the inner and outer cups were 0.152 m and 0.203 m respectively, and their heights were respectively 0.254 m and 0.305 m. The Faraday cup was connected to a Keithley digital electrometer Model 6514 using alligator clips and a triaxial cable.

All measurement devices and controllers were connected to a PC, and all data was collected and recorded using the LabView software. Data was sampled at a frequency of 10 Hz with the exception for the minimum fluidization velocity measurements in which a frequency of 100 Hz was used.

Particle size distribution (PSD) measurements were performed in a Malvern Mastersizer model 2000 with Hydro2000S sampler (Malvern Instruments Ltd, UK). The particles were suspended in a solution of 60%-ethanol, 40%-water. The suspended particles were passed across a laser beam. The diffraction of the light is inversely proportional to the particles size. Detectors monitored the intensity of the light scattered and provided a particle size distribution.

Table 2.2: Dimensions and materials of the fluidization columns.

Section	**Feature**	**0.10 m Column**	**0.15 m Column**
Column	Inner diameter (m)	0.102	0.154
	Fluidization Height (m)	1.3	2.5
	Total Height (m)	2.4	4.5
Filter bag	Diameter (m)	0.102	0.178
	Height (m)	0.178	0.229
Distributor plate	Top plate hole diameter (mm)	2	3
	Bottom plate hole diameter (mm)	4	4
Bottom Faraday cup	Inner cup diameter (m)	0.152	0.254
	Inner cup height (m)	0.254	0.305
	Inner cup material	Copper	Copper
	Outer cup diameter (m)	0.254	0.356
	Outer cup height (m)	0.305	0.610
	Outer cup material	Copper	Stainless steel
Top Faraday cup	Inner cup diameter (m)	0.127	0.254
	Inner cup height (m)	0.330	0.305
	Inner cup material	Copper	Copper
	Outer cup diameter (m)	0.152	0.356
	Outer cup height (m)	0.406	0.610
	Outer cup material	Copper	Stainless steel
Differential pressure transducer	Bottom port height above the distributor plate (m)	0.076	0.165
	Top port height above the distributor plate (m)	0.686	0.775
Electrostatic probe	Height above the distributor plate (m)	0.076	0.165

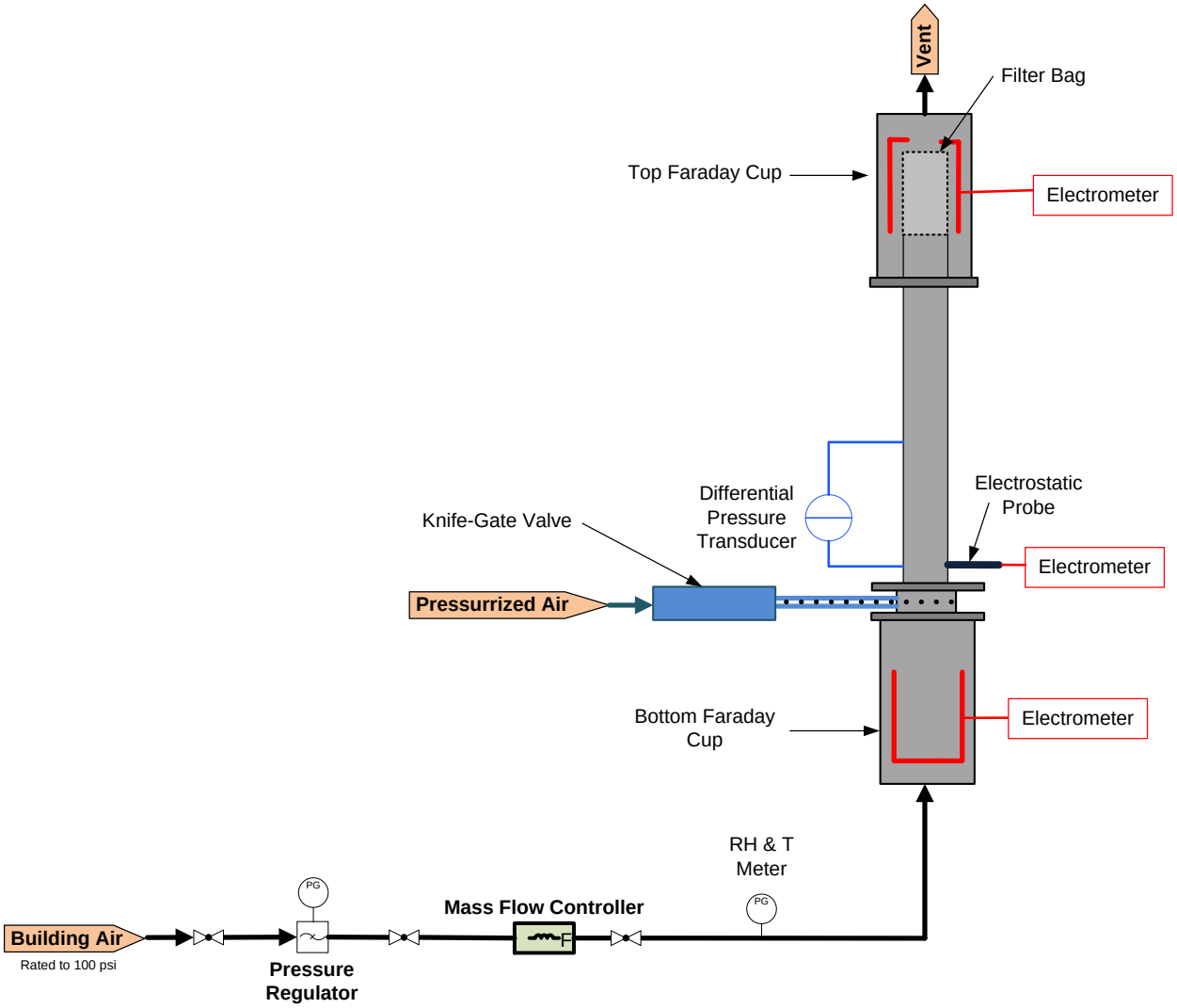

Figure 2.1: Schematic of the smaller atmospheric fluidization system.

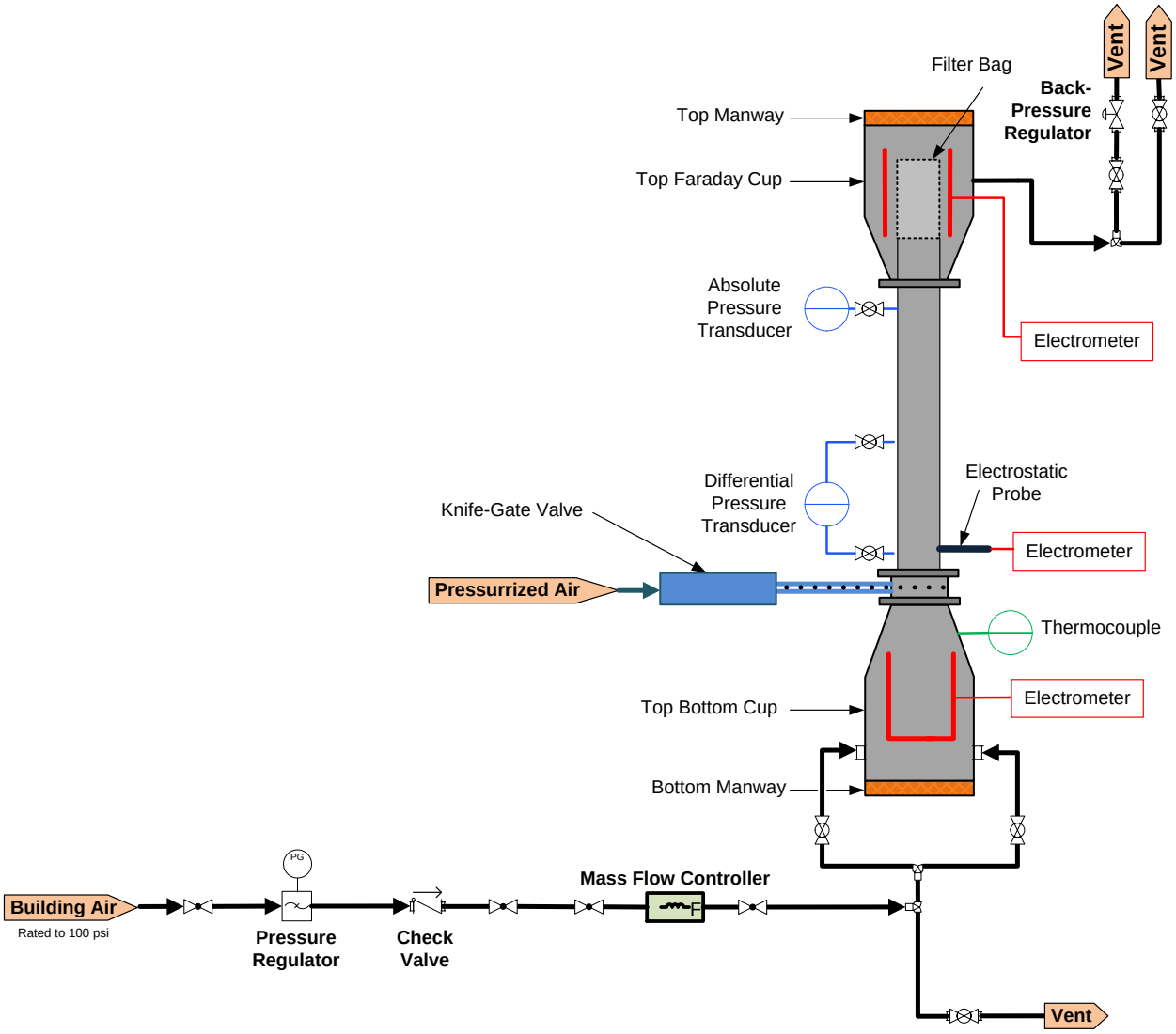

Figure 2.2: Schematic of the larger high-pressure fluidization system.

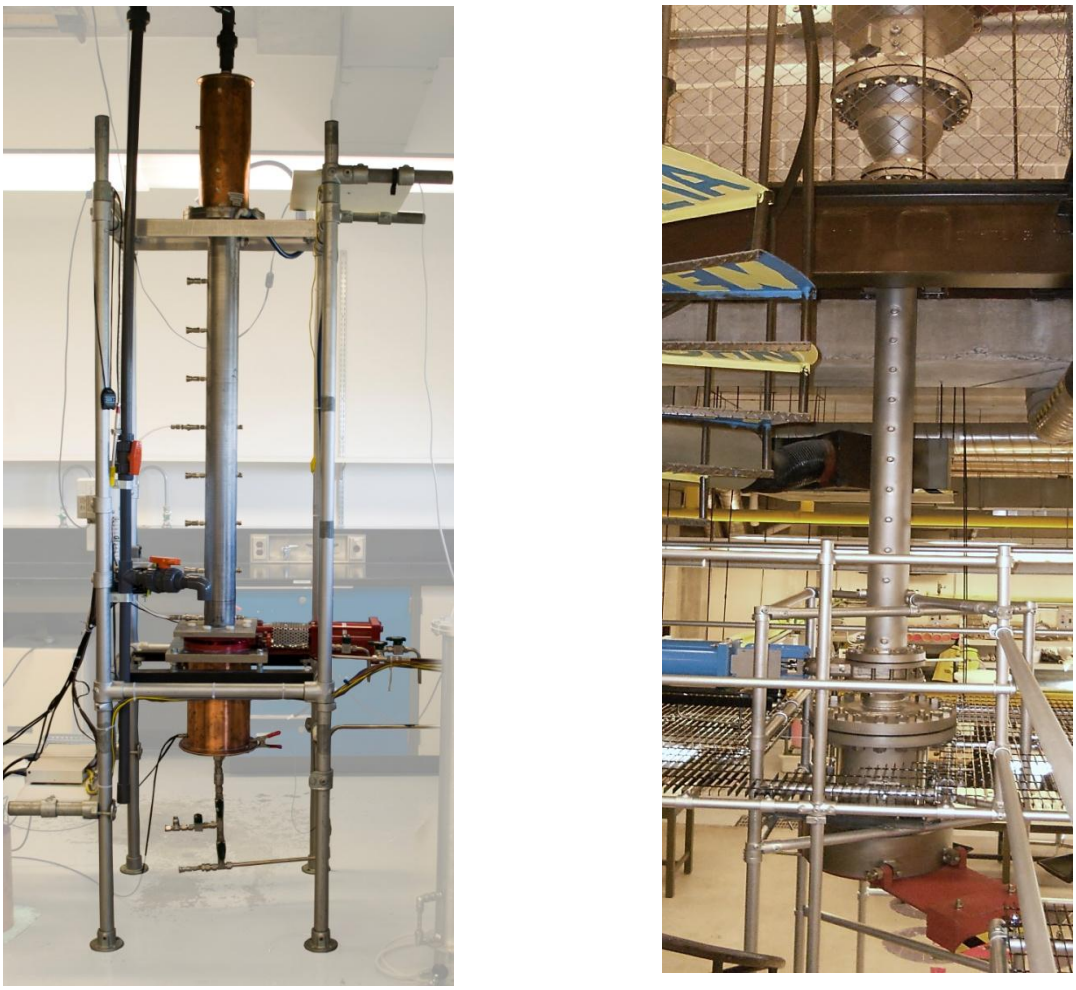

(a) (b)

Figure 2.3: Pictures of the fluidization systems: (a) smaller atmospheric unit and (b) larger high-pressure system.

(a)

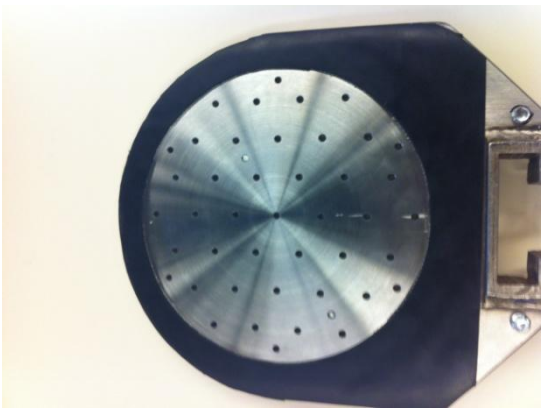

(b)

(c)

(d)

Figure 2.4: Detailed pictures of the larger system showing (a) the knife gate valve, (b) the knife-gate valve blade perforated to act as a distributor plate, (c) the bottom Faraday cup with the manway open while the inner Faraday cup is being removed, and (d) the top Faraday cup with the manway open.

2.2.2 Experimental Procedure

The desired mass of the particles to be fluidized was first measured in a stainless steel container. In addition, a sample of particles was taken for PSD analysis. A fresh batch of particles was used in each trial. The measured mass of particles was then poured into an external Faraday cup to measure their charge. A background reading of approximately half a minute was recorded prior to pouring the particles into the Faraday cup to ensure that the charge signal recorded by the electrometer was stable. After recording the charge, the particles were then poured from the Faraday cup into the fluidization column.

The filter bag was filled with four layers of Dustlock filters as described previously. The mass of the filter bag including the filters was measured. The filter bag was then attached to the Teflon adapter, using a metal clamp in the larger column and adhesive tape in the smaller column, and inserted at the top of the fluidization column. The top Faraday cup was then attached. In the case of the larger column, the top manway was closed. The top Faraday cup and the electrostatic probe were connected to two electrometers.

The gas flowrate was then started and increased within approximately half a minute to the desired value. In the case of experiments with above-atmospheric pressure in the larger column, a back pressure regulator was used to control the pressure within the fluidization column using the following procedure. First, all exit valves from the column were closed. Gas was introduced, at a velocity below the particles minimum fluidization velocity to avoid fluidization, but to only slowly pressurize the column. Once the pressure approached the desired pressure, the back-pressure regulator was slowly opened and adjusted until a stable pressure was reached concurrently with increasing the gas flowrate to the desired value. This procedure was completed within approximately 2 to 3 minutes.

Once the gas flowrate and desired pressure were stable, data were then recorded using the LabView software for 60 minutes. Recorded data included the entrained fines cumulative charge, the electrostatic probe measurements, bed pressure drop, column absolute pressure, gas flow rate, room temperature and relative humidity, gas temperature, and gas relative humidity (this last value was measured only in the case of the smaller column).

During fluidization, the entrained "**fines"** were captured by the filter bag and their charge was continuously measured by the top Faraday cup as illustrated in Figure 2.5.

Once the fluidization period was complete, the gas flowrate was gradually decreased to zero. In experiments in the larger column with pressure above atmospheric, the system was then gradually depressurized before the manway was opened. The top Faraday cup and the filter bag were removed, after the manway was opened in the case of the larger column. The mass of the filter bag, including the entrained particles, was then measured. Using this mass and the mass of the filter bag before fluidization, the mass of entrained fines was determined. A sample of these fines was collected, whenever possible, for PSD analysis. In some cases, the mass of the fines was too small to be useful for PSD analysis.

The bottom Faraday cup was then connected to the electrometer. A background measurement of half a minute was recorded before the knife-gate valve was opened, dropping the "**bulk**" of the particles into the bottom Faraday cup to measure their net charge. The bottom Faraday cup was then removed, and in the case of the larger unit this required first opening the bottom manway. Since the mass of the empty Faraday cup was known, the mass of the bulk particles was determined. A sample was collected from these particles for PSD analysis.

In all trials a layer of particles remained adhered on the wall of the column after the bulk particles were removed. Photographic images of this layer were taken from the bottom of the column, as example of which is shown in Figure 2.6. This provided a qualitative measurement of the degree and location of wall fouling. The bottom Faraday cup was then cleaned and returned to the bottom of the column. A 0.00635 m (¼") plastic tube in the case of the smaller column, and a 0.00635 m (¼") stainless steel tube in the case of the larger column, was inserted into the column from the top to remove these particles by flowing compressed air across them. Inserting the tube and holding it in the middle of the column removed some of the particles and applying compressed air near the column wall removed particles more strongly attached to the wall. The "**wall**" particles dropped into the bottom Faraday cup where their net charge was measured. Similarly to bulk particles, the particles mass was measured and a sample for PSD analysis was collected. It was observed in some cases that some particles still remained adhered to the wall. In such cases, a larger flowrate of gas was used to detach them from the wall. The charge of these

particles was measured, as well as their mass and PSD in the same manner as described for the bulk and wall particles.

After the removal of these particles, the column wall was thoroughly cleaned in preparation for future trials. A wet towel was inserted followed by a dry towel to remove very fine particles that might have remained adhered to the column wall. The ports and the distributer plate were then vacuumed.

For all experimental runs, the whole fluidization column was grounded and fresh batch of particles were used per trial.

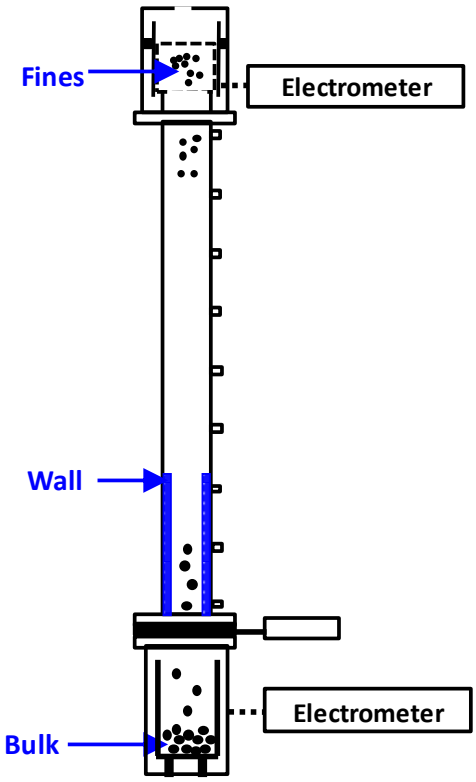

Figure 2.5: Measurement regions of the fluidized bed.

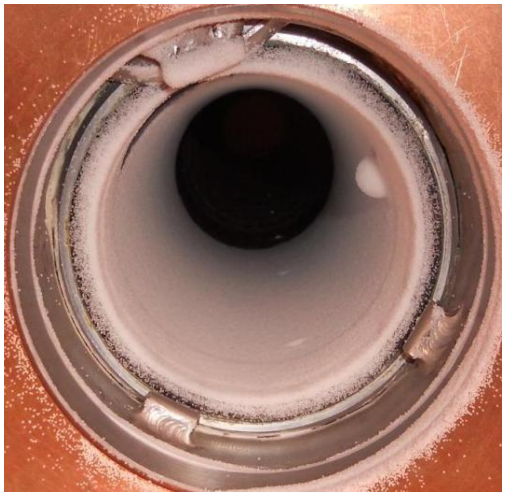

Figure 2.6: A typical picture of wall layer, taken from the bottom of the column.

2.2.3 Operating Conditions

Although the fluidization system was designed to be operated at pressures and temperatures up to 2 600 kPa and 100°C and the pressurized gas to be supplied by gas cylinders, the preliminary experiments presented in this thesis were only conducted with compressed building air. The temperature and relative humidity were on average those of the inlet gas as mentioned previously, i.e. respectively 9.3% and 21.0°C. The operating pressures were either atmospheric at 101 kPa or elevated at 401 kPa. Building air was supplied at a pressure of approximately 791 kPa limiting the maximum operating pressure in the larger column to approximately 451 kPa. A pressure of 401 kPa was chosen for convenience.

The static bed height in the smaller column was chosen based on a height/diameter (L/D) ratio of 4. This required mass of 1.1 kg of particles per experiment. If an L/D ratio of 4 was used for the larger unit as well, the required particles mass would be 5.8 kg per experiment with a volume of 0.011 m^3. This volume is in excess of the volume of the bottom inner Faraday cup. This consideration limited the mass of particles to be fluidized and therefore the bed height. The bed height for the larger unit was chosen to be 0.34 m, the same as the smaller unit, corresponding to an L/D ratio of 2.2 and requiring 3.2 kg of particles to be fluidized.

For the larger column operated at higher pressures, greater mass flowrates of the gas were required to achieve the same superficial gas velocity as during atmospheric operation because the gas density was higher. At 401 kPa, the maximum achievable gas velocity was 1.25 u_{mf}. For consistency, all experiments presented in this thesis were performed at 1.25 u_{mf}.

2.2.4 Charged Particles Separator (CPS)

It has been commonly observed by many researchers that although a batch of particles might have a net charge, there could be significant variation in the underlying charges and the charge polarity (Lacks & Mohan Sankaran, 2011). The particle charge measurement technique used in this research involved Faraday cups which provide particles net charge in different regions of the fluidized bed. To investigate the variation of charge within a region, a charge particles separator device, shown in Figure 2.7 and also described elsewhere (Salama et al., 2013), was used.

The device consisted of two inclined copper plates, each 0.457 m in length and 0.305 m wide, separated by a distance of 0.203 m at the top and 0.686 m at the bottom. Each plate was at an angle of 58.2°. Four Faraday cups (abbreviated as FC), numbered 1 to 4, were located at the bottom of the apparatus and each was connected to an electrometer using a triaxial cable to measure the charge of particles collected inside the Faraday cup. The plates and Faraday cups were located inside an insulating box made of PVC. Electric potential, typically between 15 and 40 kV provided by a high voltage power source, was applied to one of the plates while the other was used as ground. The power source was an Ultravolt HV-Rack-250-00265. The first plate became positively charged and the other negatively charged. Particles were slowly introduced at the top of the apparatus. As particles fell through the apparatus, negatively charged particles were attracted to the positive plate, and therefore tended to fall in FC1 and FC2, and positively charged particles were attracted to the negative plate, and therefore tended to fell in FC3 and FC4. Most particles fell in FC2 and FC3. Particles in FC1 and FC4 were typically more highly charged and had smaller particle diameters than particles in FC2 and FC3.

This unit was designed such that it could be fitted under both fluidization columns. This allowed the measurement of the charge distribution in the particles accumulated on the column wall after fluidization. For the smaller column, the bottom Faraday cup including the windbox was removed allowing the CPS to fit directly under the fluidization column with a small gap between the bottom of the column and the top of the separator. For the larger column, the CPS could not be raised to below the column since the windbox could not be removed. Therefore, a cardbord tube was used to connect the bottom of the column to the CPS as shown in Figure 2.8. The effect of the addition of this tube to the apparatus on particle charge was tested and the effect of pouring particles through the tube on particle charge was found to be insignificant.

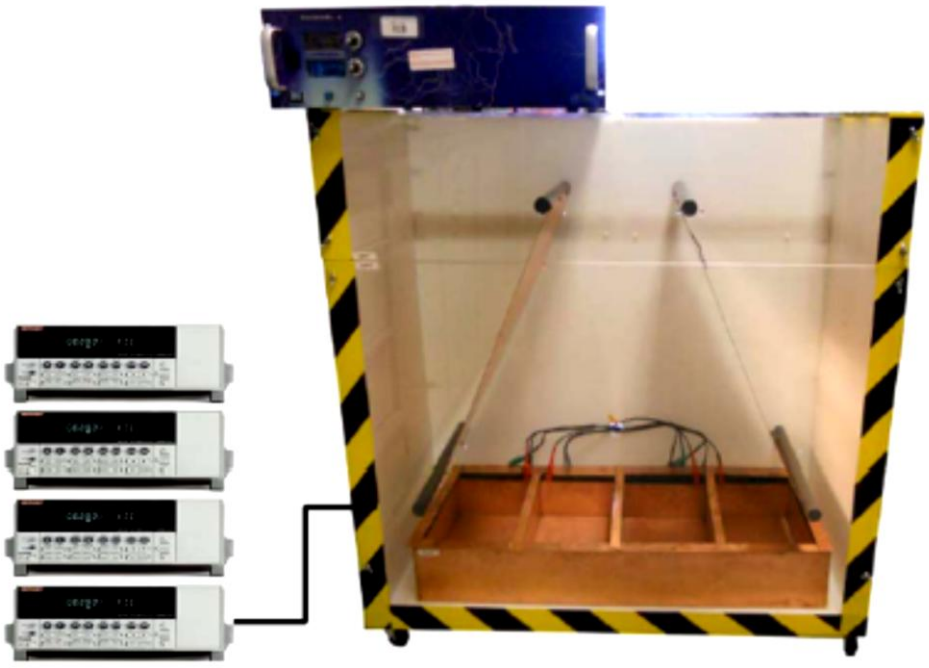

(a)

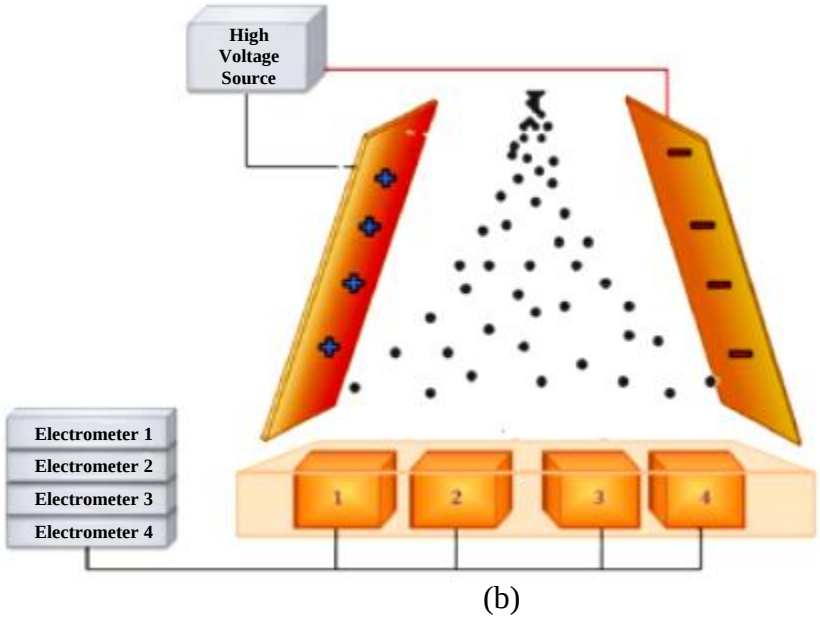

(b)

Figure 2.7: Charged particle separator (a) picture and (b) schematic.

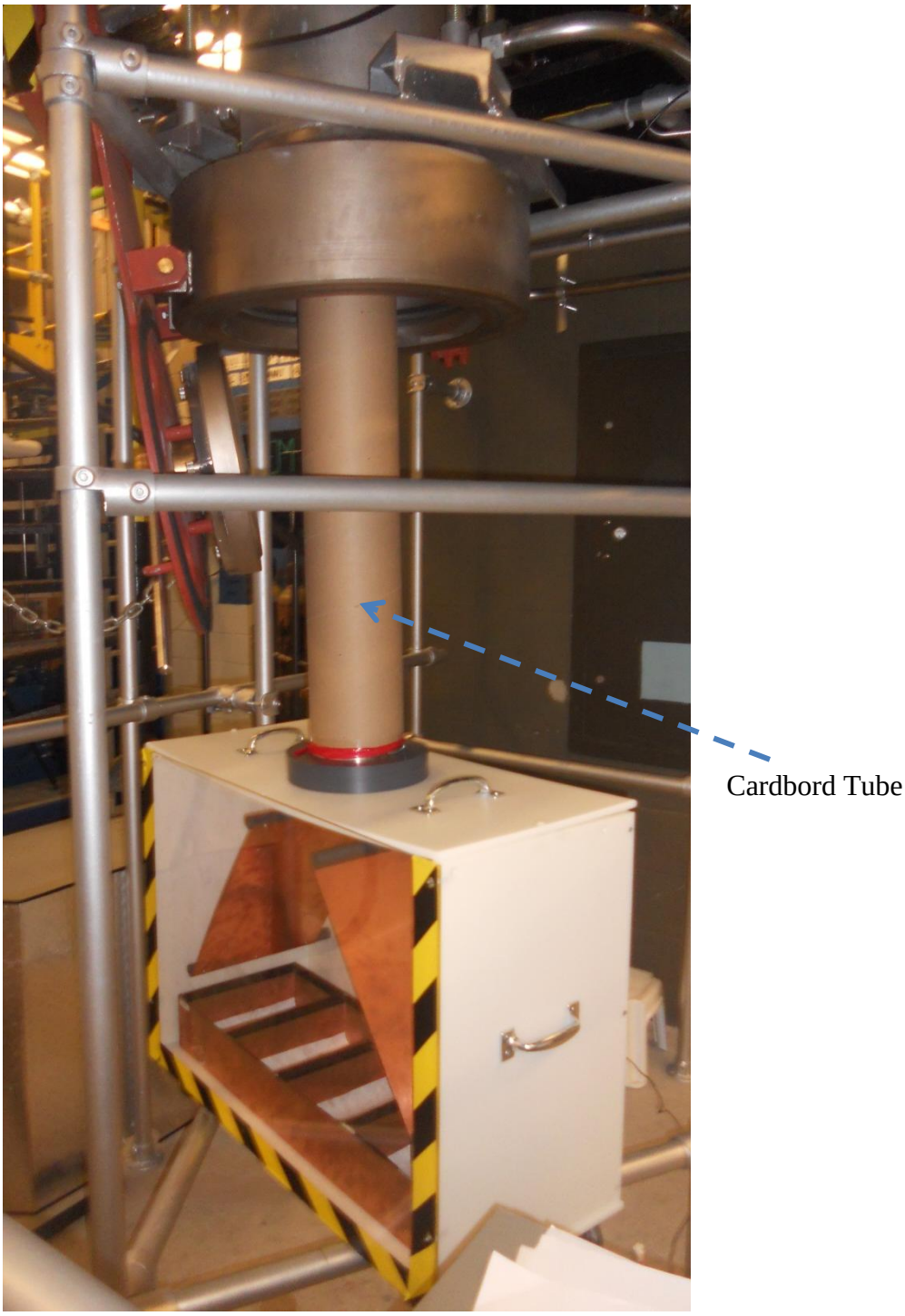

Figure 2.8: Picture of the CPS when placed under the larger column showing the cardboard tube used to direct particles into CPS.

2.3 Bench-Scale Charging Experiments

To measure the effect of particle charging in a more controlled environment than a fluidized bed, bench-scale tests were performed where small samples of particles were shaken in a stainless steel tube of 0.0325 m internal diameter and 0.155 m length. The ends of the tube were sealed with aluminum foil. The tube was clamped to a Ce Tyler model RX-24 portable sieve shaker and shaken for 5 minutes. In each case, a mass of 10 g of particles were used. First, the particles charge was measured using the bench-scale Faraday cup. They were then poured into the tube, with only one of ends capped, with the help of a paper funnel. The other end of the tube was then capped and the tube was shaken as described above. Following 5 minutes of shaking, one of the caps of the tube was removed and the particles adhered to it poured into the bench-scale Faraday cup to measure their charge. First, gentle shaking was used to remove adhered particles and then a stream of compressed air was used to detach any remaining particles in the cap. The particles in the tube were similarly poured into the Faraday cup, and gentle shaking and compressed air were also used to remove any remaining particles. Prior to each trial, the tube was cleaned with ethanol and then dried. New aluminum foil caps were used for each trial.

In some cases, the particles were poured into the CPS apparatus instead of the bench-scale Faraday cup to measure their charge distribution. All other steps of the procedure were the same as described above.

Chapter 3. Results and Discussion

The on-line charge measurement technique previously developed in this research group and implemented in an atmospheric gas-solid fluidization unit was scaled up in this work to a pilot-scale fluidization system with a column of 0.154 m diameter. The fluidization system was designed to operate at pressures and temperatures relevant to polyethylene industrial gas-solid fluidized bed reactors (pressures of up to 2 600 kPa and temperatures of up to 100°C). The measurement technique described in Chapter 2 was used to measure the net charges generated in various regions of the fluidized bed (fines, bulk, and wall), as well as to investigate the degree of reactor wall fouling.

Upon the assembly and commissioning of the high pressure fluidization system, this system was first operated to obtain preliminary data by investigating the effect of operating pressure (up to 401 kPa). The effect of particle size distribution was also examined in the larger column but only under atmospheric condition. And finally, charge generation in the new larger column and smaller column were compared with respect to the column diameter. Before the effects of operating pressure, particle size distribution and column diameter on electrostatics are discussed, the properties of the initial particles and the average results around which results in subsequent sections varied are presented.

3.1 Initial Particles

For all experimental trials, several properties of the fluidizing particles were determined prior to their fluidization including the particles net charge-to-mass ratio and mean particle diameter. In this section, the initial particles net charge, particle size and charge distributions are discussed.

3.1.1 Initial Particles Net Charge-to-mass Ratio (q/m)

A major objective of this work was to study electrostatic charge generation. The final charge on particles after their fluidization was measured. To determine the amount of charge generation due to fluidization, which is the difference between the initial and final charges, measuring the

particles initial charge was required. The initial charge of particles in each trial was measured by an external Faraday cup. The specific charge was found to be relatively small at –0.01 ± 0.03 μC/kg when compared to the specific charge of the bulk particles after fluidization which on average was 0.47 ± 0.19 μC/kg. Therefore, the net charges measured on particles after fluidization were assumed to be equal to the generated charges.

3.1.2 Initial Particles Size Distribution

To determine the size distribution of the initial particles, samples were sieved in a W.S. Tyler Ro-Tap Model RX-29 sieve shaker (W.S. Tyler, Ohio, USA). Samples of 60 g were shaken for 15 minutes after which the mass of particles in each tray was measured. This process was repeated 5 times and the average results were presented in Table 2.1. The particles were fairly widely distributed with 8% of particles in the <250μm size range, 34% in the 250-500μm range, 55% in the 500-1000 μm range, and 8% in the >1000μm range. The presence of a wide distribution of particle sizes generates more electrostatic charges and results in bipolar charging (Lacks & Mohan Sankaran, 2011; Sowinski et al., 2012).

3.1.3 Initial Particles Charge-to-Mass Distribution

The presence of a distribution of charges on polyethylene particles was previously reported by our group (Salama et al., 2013). Using the charged particle separator (CPS) apparatus described in section 2.2.4, the distribution of charges on the initial particles was determined. A potential difference of 30 kV between the plates was used and samples of 50 g of particles were slowly poured into the CPS. This experiment was repeated 4 times. The resulting distribution of mass, charge and particle size across the CPS are shown in Figure 3.1. The particles in FC1 and FC4 were more highly charged and smaller than the particles in the middle cups. The majority of particles dropped into FC2 and FC3, as these particles are the least charged. The majority of particles were positively charged since they dropped into FC3 and FC4. Interestingly, the specific charges of particles in all cups were relatively high, on the order of ±10 μC/kg or higher, compared to the net initial charge of -0.01 μC/kg. This shows that the initial particles were highly charged although the negative and positive portions were almost equal such that in net terms the charge was relatively small. Comparing the mean diameters of particles in FC2 and FC3, and in FC1 and FC4, there was no significant difference in diameter between positively and

negatively charged particles. Therefore, no bipolar charging (defined as a size-dependent polarity correlation) was detected in this case.

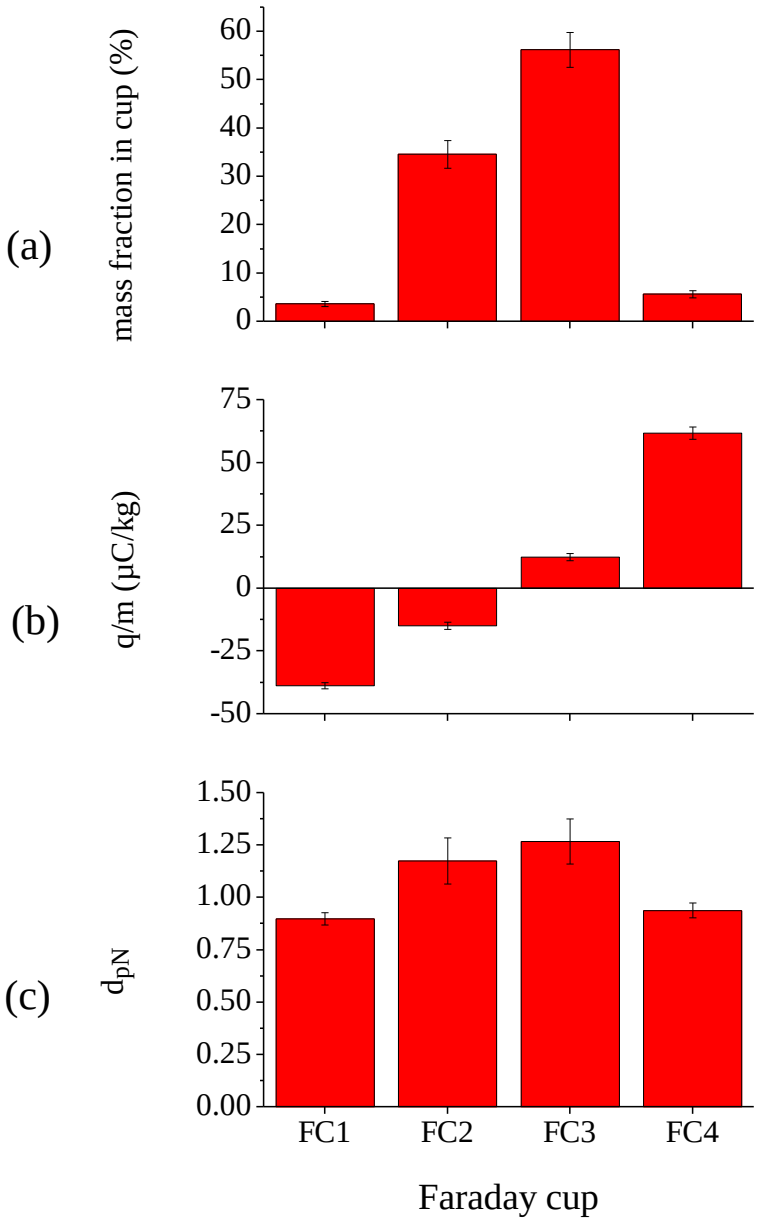

Figure 3.1: Results of initial particles in the CPS showing (a) the mass distribution, (b) the specific charge distribution and (c) the normalized mean particle diameters.

3.2 Bench-Scale Charging Experiments

Polyethylene resin was contacted with a stainless steel pipe using the procedure described in section 2.3. The initial specific charge of the particles was 0.3 ± 0.1 µC/kg. The net specific charge of the particles after shaking in the pipe was 7.3 ± 1.6 µC/kg. This result clearly shows that for the resin used, polyethylene-steel contacts generated more of a positive charge on the polyethylene and therefore a negative charge on the steel.

The charge distribution of the particles upon shaking was examined by introducing the particles into the CPS. The resulting distributions, presented in Figure 3.2, show that the majority of particles were charged positively (due to both particle-tube wall and particle-particle contacts) and a minority were negatively charged (due to particle-particle contacts). This confirms the conclusion that for the particle resin used in this study, polyethylene-steel contacts caused polyethylene to charge more positively and steel negatively.

Bench-scale charging experiment was also performed with sieved particles with diameters of less than 300 µm. The generated net specific charge was 3.6 ± 0.8 µC/kg, which is lower than the charge generated on non-sieved particles reported above. This could imply that the magnitude of particles charging depends on their size.

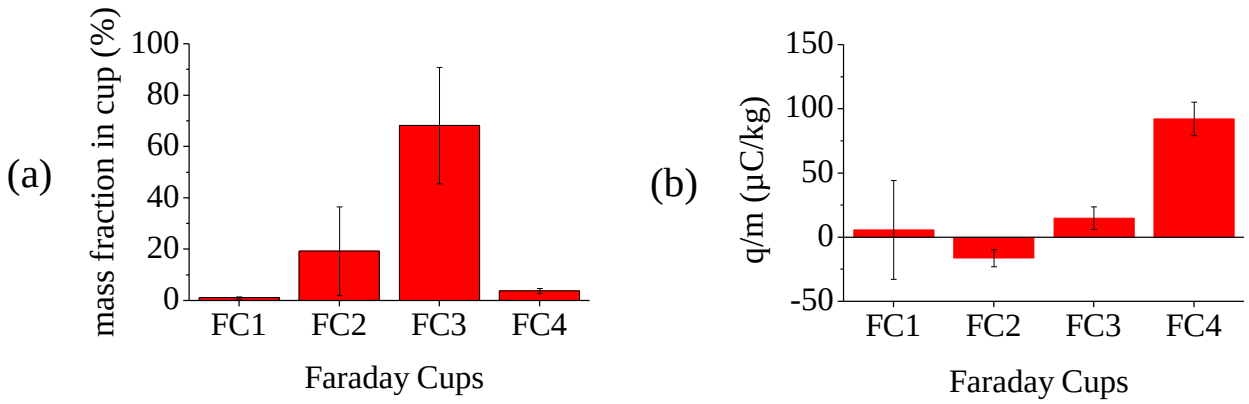

Figure 3.2: (a) Mass and (b) specific charge distributions of particles charged in bench-scale shaking tests.

3.3 Average Results from Fluidization Experiments

In this study, the effects of several variables, specifically the operating pressure, particle size distribution and fluidization column diameter on electrostatic charge generation and wall fouling were studied. In this section, the average or baseline results, summarized in Table 3.1, are presented. In the later sections, the variations around this average will be discussed.

Table 3.1: Average properties of particles after fluidization.

Region	Mass fraction of the initial (m%)	Net specific charge (q/m) (μC/kg)	Normalized mean particle diameter	Mean particle diameter (μm)
Initial	100 ± 0%	-0.01 ± 0.03	1.01 ± 0.11	571 ± 64
Bulk	95.3 ± 1.3%	0.47 ± 0.19	1.01 ± 0.05	575 ± 26
Wall	3.9 ± 1.4%	51.6 ± 30.3	0.63 ± 0.08	358 ± 48
Fines	0.04 ± 0.03%	-69.6 ± 47.2	0.16 ± 0.03	91 ± 16
Lost	0.8 ± 0.4%	-	-	-

3.3.1 Mass distribution

The average mass distribution of particles in various regions of the bed after fluidization is presented in Figure 3.3 and Table 3.1 the initial particles, approximately 95.3 ± 1.3% ended up in the bulk particles, 3.9 ± 1.4% in the wall layer and 0.04 ± 0.03% in the entrained fines. The corresponding masses for the smaller and larger units are shown in Table 3.2.

The wall layer particles were those adhered to the column wall due to their high electrostatic charge. The fines were those elutriated due to their small size. The bulk of the bed was composed of particles which were not sufficiently small to be elutriated and were not sufficiently charged to adhere to the column wall.

The remaining 0.8 ± 0.4% of the particles were lost in several places. Some of the particles adhered to the containers used for handing prior to the introduction of particles into the fluidization column, such as the bench-scale Faraday cup. Some of the particles, due to their small size or very high specific charge, remained adhered to the column wall even after the

application of pressurized air. Some particles remained in the ports along the column wall. Others remained on the distributor plate, particularly in the larger column. This lost mass of particles did not likely affect the resulting mass, charge or size distributions for several reasons. First, the lost mass was relatively small compared to the bulk and wall particles. Second, the amount of particles lost in the smaller column was only 0.3 ± 0.2% corresponding to a mass of 2.9 ± 2.5 g, which is even smaller. Third, the amount of particles lost in the larger column was 1.0 ± 0.2% corresponding to a mass of 31 ± 5 g, which was higher than that in the smaller column. In order to seal the distributor plate of this column, a Teflon gasket was used. The gasket was elevated above the level of the plate. Therefore, when the knife-gate valve was opened and the distributor plate was retracted, a layer of particles remained on the plate which its height equaled to the gasket thickness. Approximately 25 g, or 0.8% of the initial particles, were lost in this way. These particles were similar to bulk particles with large nominal diameters and small net specific charges. Comparing their mass to the bulk particles, it is clear that they are negligible. The remaining 0.2% of particles lost in the larger unit is a very small amount and is therefore insignificant.

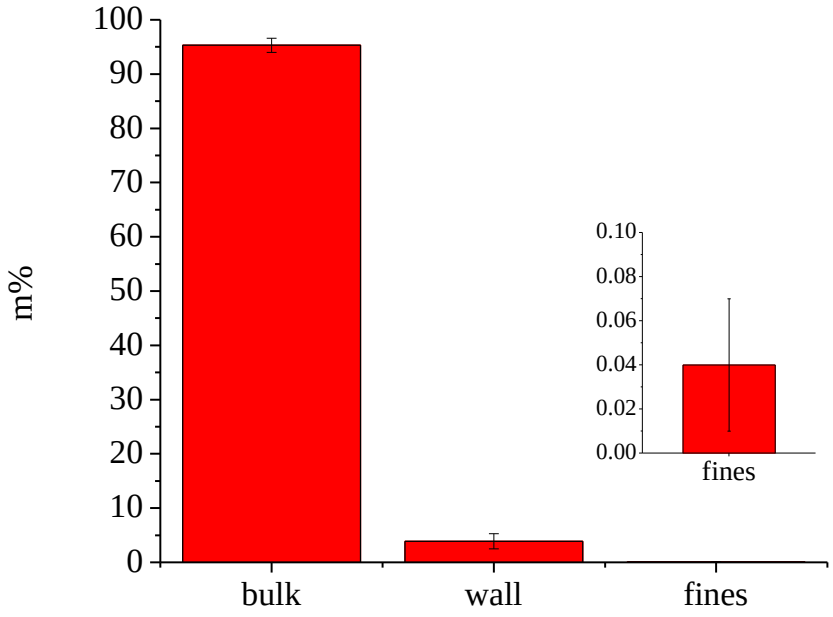

Figure 3.3: Average mass distribution of particles after fluidization in different regions of the bed as a fraction of the initial particles.

Table 3.2: Comparison of the average masses (in g) of particles in the smaller and larger columns.

Region	Smaller Column	Larger Column
Initial	1114	3176
Bulk	1060 ± 10	3030 ± 40
Wall	43 ± 16	124 ± 44
Fines	0.4 ± 0.3	1.3 ± 1

3.3.2 Specific Charge

Average charges of particles in different regions are shown in Figure 3.4. The bulk particles were charged slightly positively, the wall particles highly positively and the fine particles highly negatively at respectively 0.47 ± 0.19 µC/kg, 51.6 ± 30.3 µc/kg and -69.6 ± 47.2 µC/kg.

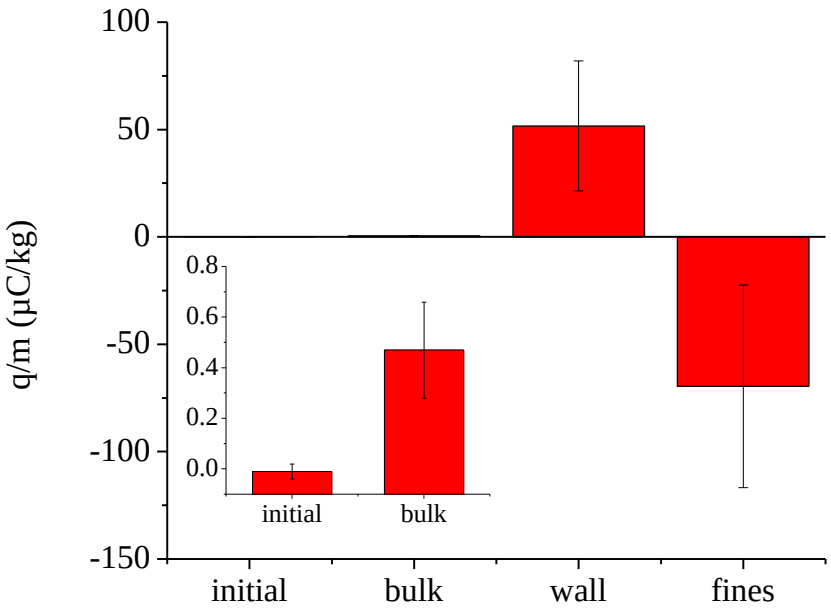

Figure 3.4: Average net specific charge of particles after fluidization in different regions.

Charging in fluidized beds could have been due to either particle-particle contacts or particle-wall contacts. Net charge generation could only occur as a result of particle-wall contact because in particle-particle contacts two particles with equal but opposite charges remain within the bed,

assuming the net charge of the entrained particles is negligible. Therefore, the net charge within the bed would not change.

Particle-particle contacts could only affect charge within the bed if one of the particles was preferentially removed from one region to another. For example, assuming that bipolar charging occurred such that smaller particles were preferentially charged negatively and larger particles positively then the elutriation of these small negatively charged particles would leave behind a net positive charge in the bed. Bipolar charging is a reasonable hypothesis to explain why the entrained fines were negatively charged. However, their net charge was relatively small. As shown in Table 3.3, the net charge of the fines was much smaller than that of the bulk and is therefore a negligible factor when analyzing the net charge on bulk or wall particles.

The charge generated on the wall and bulk particles was mostly not a result of particle-particle contacts but particle-wall contacts. The charge within both regions was positive implying that particle-wall contacts, between polyethylene particles and the stainless steel column wall, produced a net positive charge on the polyethylene particles and a corresponding negative charge on the stainless steel wall. This is only valid for the polyethylene particles used in this study since the opposite result was reported for other polyethylene resins (Sowinski et al., 2010).

Table 3.3: Net charges generated (in μC) of particles in the smaller and larger columns.

Region	Smaller Column	Larger Column
Initial	-0.06 ± 0.07	-0.01 ± 0.03
Bulk	0.91 ± 0.22	0.67 ± 0.08
Wall	5.15 ± 1.65	2.57 ± 2.36
Fines	-0.04 ± 0.04	-0.05 ± 0.04

3.3.3 Particle Size Distribution

Average normalized mean diameters of particles in different regions are shown in Figure 3.5 and Table 3.1. The initial and bulk particles had similar mean diameters. Since approximately 95% of the initial particles ended up in the bulk, a significant change in the mean particle diameter was not expected and was not observed. Note that since the sample of the bulk for particle size measurement was always obtained from the top of the bed, this result also implies that there was no significant vertical segregation in the bed. The normalized mean particle diameter of the wall layer particle was 0.63 ± 0.08. These particles were both more highly charged and smaller than the bulk particles and therefore adhered to the column wall. The elutriated fines had relatively small normalized mean diameters of 0.16 ± 0.03.

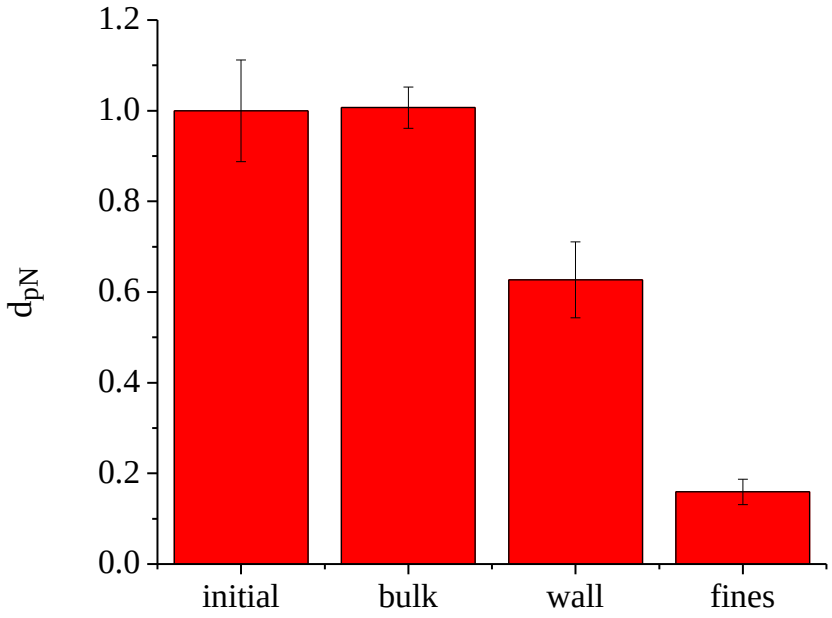

Figure 3.5: Average normalized mean diameters of particles after fluidization in different regions.

3.3.4 Mechanisms of Electrostatic Charge Generation in Fluidized Beds

Relating fluid bed hydrodynamics to electrostatic charge generation is rather difficult because the two phenomena operate on the marcoscale and microscale, respectively. An accurate theoretical description of electrostatics in gas-solid fluidized beds is not possible without the use of discrete particle modeling (DPM). However, the major difficulty in introducing electrostatic phenomena in DPM models is the lack of suitable models for charge generation in insulators which represents most of use-cases, including particles used in this study.

In the absence of theoretical models to explain electrostatics in fluidized beds, proximate descriptions must suffice. In this work, an assumption will be made that the number, frequency and energy of collisions between particles and between particles and the column wall correlate directly to electrostatic charge generation. This is a common assumption by studies of electrostatics in fluidized beds and in electrostatics in general (Lacks & Mohan Sankaran, 2011).

Since collisions were not measured directly in this study, a brief review of proximate methods used in the literature to describe the number or frequency of particle collisions is presented next.

The first method is granular temperature. Granular temperature, which is analogous to temperature in the kinetic theory of gases, is proportional to the root mean square of individual particle velocities (Goldhirsch, 2008). Collision frequency is in turn proportional to the granular temperature (Nilpawar et al., 2006).

The second method is particle pressure. Buffière and Moletta (2000) characterized the collisions of a bed of polyethylene particles with the column wall. They noted that collision frequency is difficult to estimate by literature correlation and an accurate description requires experimental measurement. To measure the collision frequency, a high-frequency-response hydrophone was flush-mounted to the wall of the reactor. The particle pressure, which is proportional to collision frequency, was reported. The authors concluded that particle pressure was proportional to gas velocity. However, increasing gas velocity did not increase the collision velocity but simply increased the number of collisions. Hamidipour et al. (2005) reported differing results. The contact frequency of a bed of sand particles was measured using radioactive tracers. It was concluded that collision frequency decreased with increasing gas velocity in the bubbling regime, reached a minimum at the onset of turbulent fluidization and increasing thereafter.

The last method is qualitative descriptions of mixing within a fluidized bed. It is well known that particle mixing in a gas-solid fluidized bed is entirely induced by the passage of bubbles (Yang, 2003). It would be reasonable to assume that more vigorous bubbling would increase particle-particle and particle-wall contacts, and therefore electrostatic charging. Indeed, a number of studies correlated the presence and velocity of gas bubbles with electrostatic charge generation. Boland and Geldart (1972) measured static electrification around bubbles and concluded that the amount of generated charge increased as the bubble size and bubble rise velocity increased. Park et al. (2002) concluded that signal induced on a potential probe is almost entirely due to the passing of bubbles. Therefore it is possible to state that more rigorous bubbling would generally result in more electrostatic charge generation.

As mentioned above, electrostatic charge generation in a fluidized bed can be due to either particle-particle or particle-wall contacts. Particle-particle contacts do not generate a net charge within the bed because both particles and therefore both equal but positive charges remain in the bed. Particle-wall contacts do however generate a net charge within the bed. Taking the average results found in this study presented above for the specific charge, note that both bulk and wall particles possess a net positive charge (fine particles can be ignored in this analysis because they contribute very little to net charge due to their very small mass). By the law of charge conservation, this indicates that there was a negative charge somewhere else in the system. This charge can only be on the column wall. Therefore contacts between the particles and the column wall generated a net positive charge on the particles.

In this thesis, only charge generation was examined and charge dissipation was neglected since polyethylene is both highly insulating and hydrophobic (Peacock, 2000). For these two reasons it respectively resists the dissipation of charge through it and along its surface (through a surface water layer). In addition, it is reported that at low relative humidities, only less than 10% of the charge is dissipated in 1 day (Burgo et al., 2011). Therefore, for the timescales of the experiments conducted in this research (1 hour of fluidization) charge dissipation is negligible.

3.3.5 Mechanisms of wall layer formation

The formation of a layer of particles on the column wall was previously mentioned to be due to the particles electrostatic charge. In this section, this notion is illustrated in more detail.

The adherence of particles to the column wall is due to their electrostatic charge. This can be illustrated using a simple force balance on a charged particle adhered to a conductive wall of a fluidized bed as presented in Figure 3.6. Based on average results obtained in this research, the particle charge is assumed to be positive. Gravitational and drag forces act on the particle in the vertical direction. The positively charged particle induces an oppositely charged image on the conductive wall. The electrostatic force attracts the particle to the wall but the compression force counteracts it after the particle contacts the wall. Note that it was necessary to assume that the image force was at a higher elevation than the particle for the following reason. If the particle in contact with the wall is under a thick fouling layer, which is the case in this study, the drag force is minimal. The drag force is also generally minimal near the column wall even for non-adhered particles (Fujino et al., 1985). Therefore, another vertical force is required to counteract gravity which in this case must be the electrostatic force.

This simple model makes a number of assumptions. It only considers one particle and does not take into account the charges of the particles surrounding it. It also makes the assumption that particles are static once adhered to the wall. However, these assumptions do not affect the model for the following reasons.

First, other charges within the bed in addition to that of a single particle will be considered. Consider a particle that is exactly at the middle of the bed. Assuming a relatively uniform charge distribution in the vertical direction, electrostatic charges of other particles do not affect the vertical force balance since the forces exerted by the bottom and top half of the bed act are equal but act in opposite direction (assuming it a repulsion force, its direction would be respectively upwards and downwards). Now consider the horizontal direction. The electrostatic force in that direction can either repel the charged particle, reinforcing its adherence to the wall, or attract it, reducing adherence. In either case, only the magnitude of the force and therefore the likelihood of adherence would be modified but the force balance would still be applicable.

Second, it is likely true that generally particles are not statically adhered to the wall. That this is the case can be illustrated by considering the specific charge of the bulk particles. The positive charge of these particles can only be a result of contact with the column wall. Therefore, they clearly contain particles that were at some point in contact with or adhered to the wall. Discussion of the migration of particles between the wall layer and bulk particles will be further discussed in subsequent sections. It does not, however, affect the underlying electrostatic basis of particle-wall fouling.

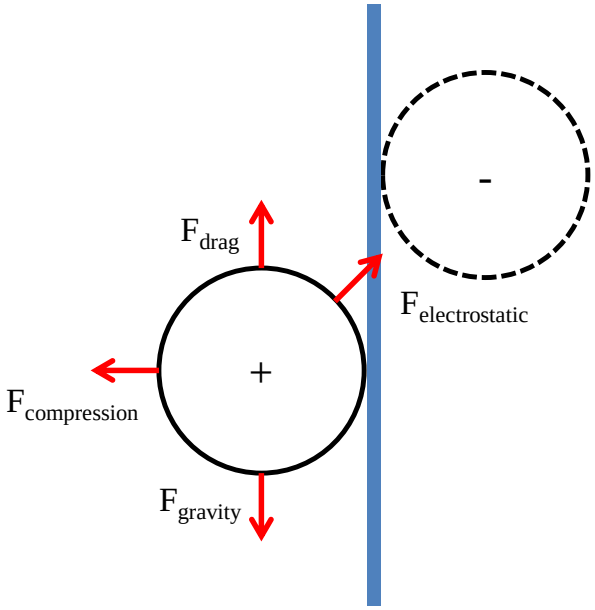

Figure 3.6: A simplified force balance model on a particle adhered to a conductive wall.

The model presented above illustrates the adherence of a single charged particle to the column wall. In the following paragraphs, the adherence of a layer of particles will be examined.

Recall that in section 3.3.4 it was concluded that due to particle-wall contacts a net positive charge developed on the polyethylene bed particles. It is possible to conclude that this net positive charge was responsible for the adherence of a layer of particles to the wall using the following reasoning. For the purposes of this discussion, it will be assumed that the charge is evenly and continuously distributed throughout the bed such that there are no discrete negative charges within it (a topic which will be examined afterwards). This is illustrated in Figure 3.7. First, it is necessary to determine the net image charge on the conductive column wall. Assuming

that the column forms a Faraday cage[2], the net charge enclosed within it is zero and the charge on the inner wall is equal but opposite to the net charge of the bed of particles. In this case the inner wall is negatively charged, since particles had a net positive charge. Considering only horizontal forces, particles next to the wall (point A in the figure) are clearly attracted to the wall since they are positively charged and the wall is negatively charged, and are repulsed by particles further away from the wall which are positively charged. In this case both forces are acting in the same direction and the particle adheres to the wall. Now consider particles further away from the wall (point B in the figure). They are attracted by the wall's image charge but are repulsed by the particles nearer than it to the wall. They are also repulsed by particles further away from the wall than it. However, particles near the wall possess higher charge due to greater interaction with the wall, and hence more particle-wall contacts. The image forces attracting particles to the wall decay according to Coulomb's law for two reasons. First, the distance (r) between the particle and the wall increases. Second, the dielectric constant increases due to the presence of a layer of particles between the particle and the wall[3]. At some distance away from the column wall, the forces balance such that there is no attraction to either direction. Particles further away from that point would therefore not be included in the wall layer since there is no electrostatic force attracting them to the column wall.

The above reasoning assumed that there were no discrete negative charges within the bed of particles. But as will be shown later negatively charged particles also exist within the bed. Indeed, the presence of these particles might have also accounted for the formation of the wall layer. Sowinski et al. (2010) presented a hypothesis whereby particles form succeeding layers of opposing charge. A positive particle adhered to the wall would attract a negative particle, which in turn would attract another positive particle and so forth.

It is not imperative that only one of the two mechanisms presented here operated exclusively. They likely both contributed to wall layer formation. The relative significance of each

[2] In this case the column is grounded. A grounded metal conductor enclosing a volume forms a Faraday cage (also known as a Faraday shield) as described in section 1.2.1. The distributor plate is electrically connected to the column so the bed is shielded from the bottom and the sides. Even though the column does not fully enclose the bed, the height above the bed is sufficiently high such that for the column can be practically assumed to be a full Faraday cage.

[3] For the first layer of particles next to the wall, the dielectric constant is at a minimum (equal to that of the atmosphere) and it increases further away from the wall due to the presence of polyethylene particles between it and the column wall.

mechanism requires further study. For the purposes of future discussion, the two mechanisms will be referred to as the force balance and the layering mechanisms, respectively.

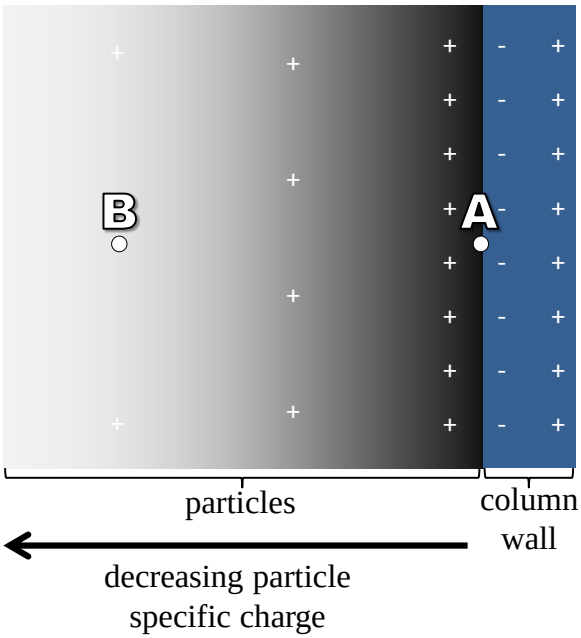

Figure 3.7: An illustration of a proposed wall layer formation mechanism. The column wall is shown in blue and the specific charge of the particles in grey. The darker grey colour (closer to the wall) indicates higher specific charge. Points (A) closer to the wall and point (B) away from the wall are labelled.

As mentioned above, the wall layer was likely not stationary and there was particle exchange between the wall layer and the bulk. Indeed, there is continuous and vigorous particle mixing in a bubbling fluidized bed mainly due to the movement of the bubbles which affects electrostatics in fluidized bed in addition to generating charge as mentioned above. As a bubble rises upwards, it carries solids within its wake which are continuously exchanged with the emulsion in a phenomenon called wake shedding. Solids also move out of the way of the rising bubble and the bubble also draws up a sprout of the particles to produce an upward drift of particles. To balance this upward movement of particles at the center of the bed, there is a downward movement at the bubbles regions near the column walls. This movement of particles redistributes wall particles to some extent but also contributes to charge generation and further growth of the layer of particles on the column wall.

3.4 Effect of Operating Pressure

The experimental conditions under which experiments performed to investigate the effect of operating pressure on the degree of bed electrification and reactor fouling are summarized in Table 3.4.

Table 3.4: Experimental conditions used for testing the effect of operating pressure.

Parameter	**Value**
Fluidizing Particles	
Size Range	20-1500 μm
Fluidizing Gas	
Velocity	1.25 u_{mf}
Fluidization Column	
Diameter	0.154 m
Fluidization Conditions	
Operating Pressure	**101-401 kPa**

3.4.1 Results and Discussion

The obtained mass distributions, net specific charges and normalized mean particle diameters are shown in Figure 3.8. Representative images of wall fouling are shown in Figure 3.9. As shown in Figure 3.8, the specific charges and mean diameters of the initial particles were comparable for experiments conducted at 101 kPa and 401 kPa. Therefore, these sets of experiments can be compared.

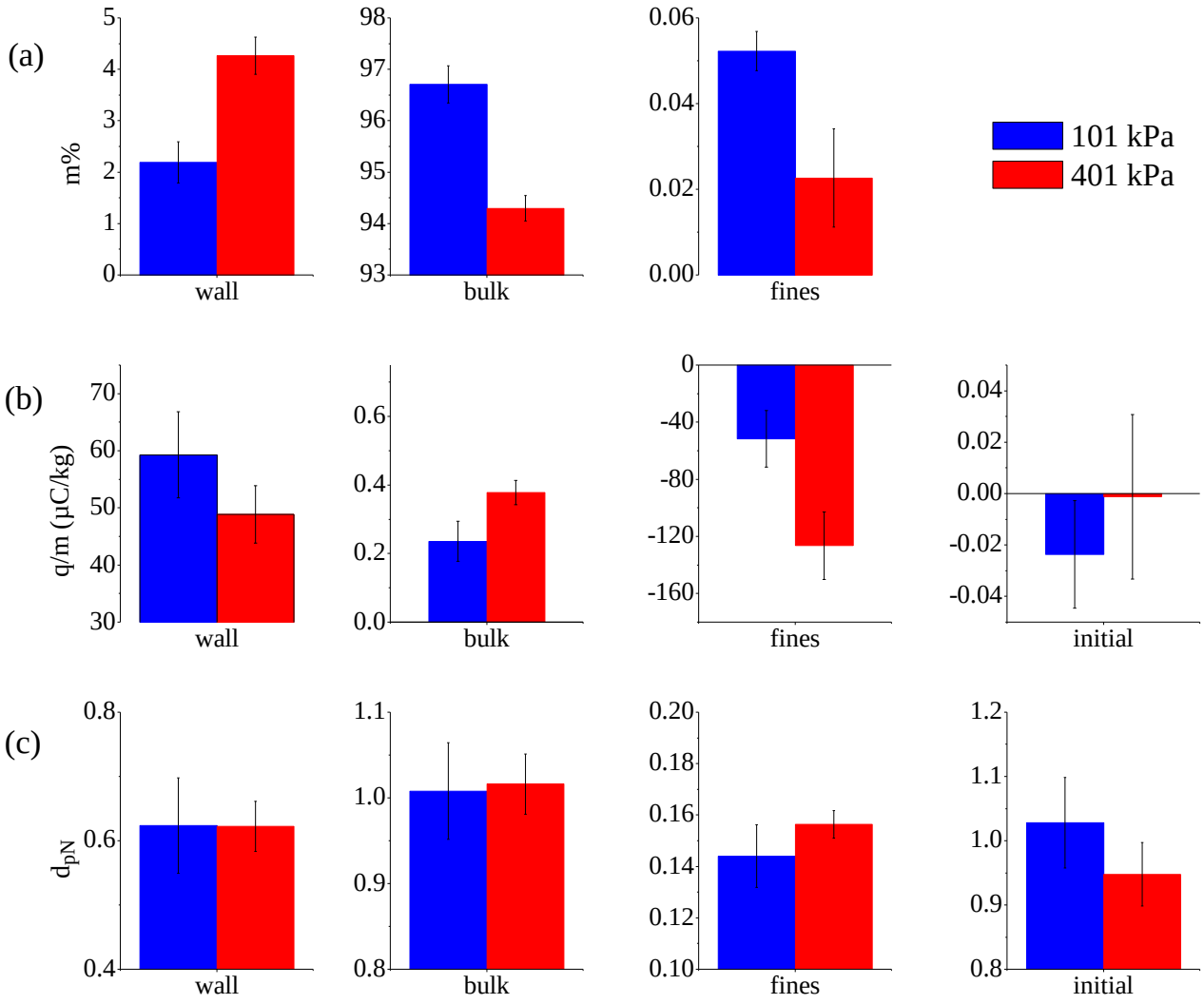

Figure 3.8: Comparing (a) the mass distribution, (b) net specific charge, and (c) normalized mean particle diameters of particles in the wall, bulk, fine and initial regions due to fluidization at 101 kPa and 401 kPa.

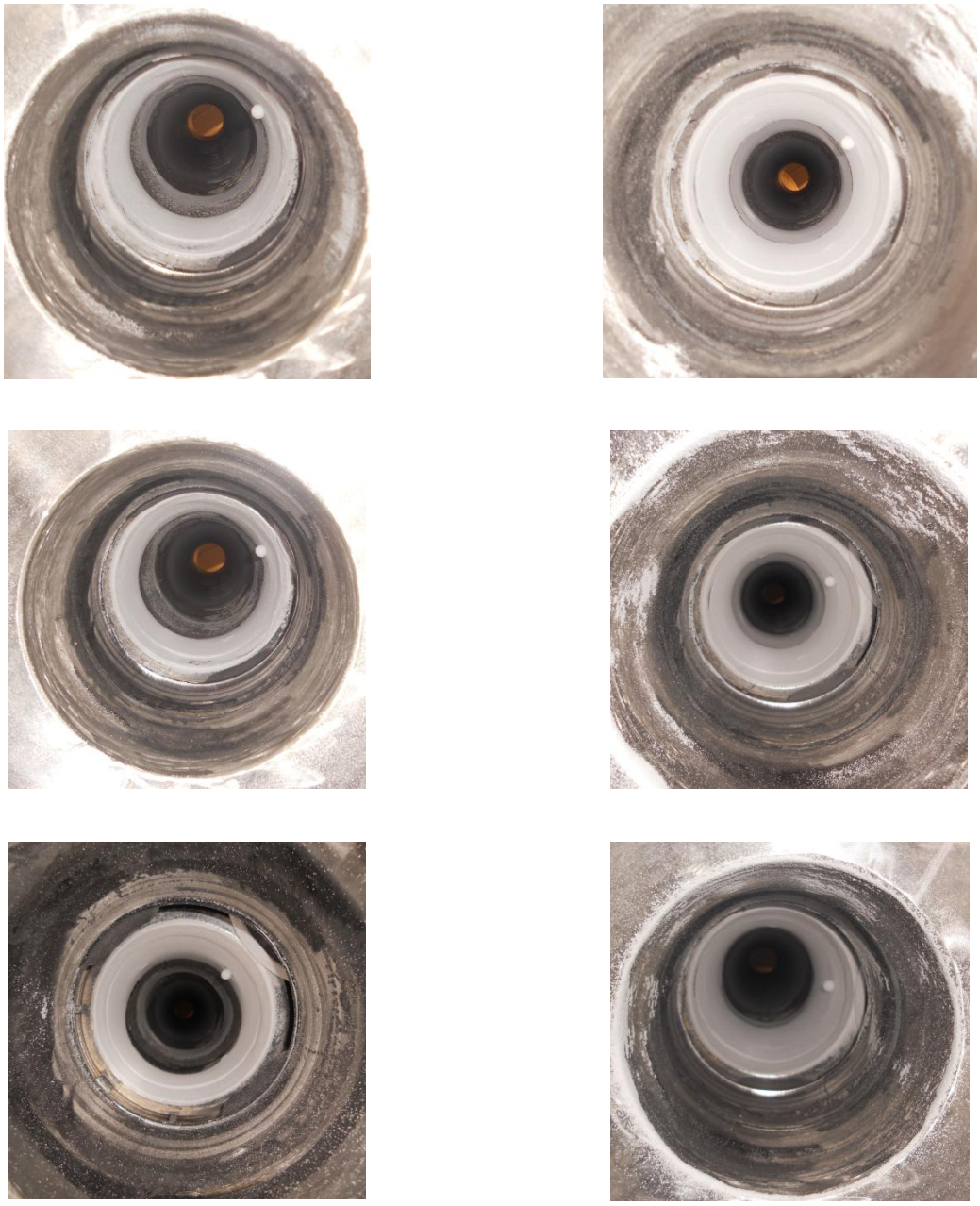

(a) (b)

Figure 3.9: Images of wall fouling after fluidization and the removal of bulk particles showing several repeated trials at (a) 101 kPa and (b) 401 kPa.

As shown in Figure 3.8, the amount of wall fouling almost doubled from approximately 2.2% to 4.3% when the operating pressure was increased. There was no significant difference in either the net specific charge or the mean particle diameter of the wall particles. The increase in the amount of wall fouling indicates an increase in electrostatic charge generation, which can be attributed to changes in bed hydrodynamics due to the increase in operating pressure.

In this study, Geldart group B particles were fluidized at pressure up to 401 kPa. From the studies of Brouwer et al. (2012) and Hoffman and Yates (1986), reviewed in section 1.1.2, it is possible to conclude that increasing pressure will increase bubble size and bubble rise velocity for Geldart group B particles, such as those used in this study, and for a relatively small increase in operating pressure such as the increase from 101 kPa to 401 kPa used in this study[4]. Higher bubble rise velocities enhance the movement and mixing of particles within the bed (see section 3.3.4), and therefore increase particle contacts with other particles and also with the column wall. In addition, Godlieb et al. (2008) calculated the granular temperature of a bed of polyethylene particles modeled using DEM and reported that the granular temperature increases with increasing pressure. Since granular temperature corresponds to particle contacts, increasing the pressure increases contacts. As discussed in section 3.3.4, electrostatic charge generation is proportional to particle-particle and particle-wall contacts. Therefore, the higher bubble velocity and the higher granular temperature account for the increase in electrostatic charge generation. And as discussed in section 3.3.5, wall fouling is due to the particles electrostatic charge. Therefore, the increased charge explains the higher amount of wall fouling observed.

Despite the increase in bed electrification, the net specific charge of the wall particles did not change. This could be due to one of several reasons. First, the wall layer particles might have reached charge saturation. However, this was not the case since the surface charge density of the wall particles, 2.50 ± 1.45 μC/m^2, was an order of magnitude below the breakdown limit of air which is 26.4 μC/ m^2 (Cross, 1987). Second, increased charge generation caused the adhesion of more particles to the wall. Particles furthest away from the wall were likely the least changed because net change results from contact with the wall. Therefore, the increase in wall fouling caused an increase in these particles (i.e., the mass collected from the wall), which decreased the

[4] As previously noted, for other experimental conditions such as the fluidization Geldart group A particles or group B particles at higher pressures, increasing pressure decreases bubble size. These conclusions are not relevant to the operating conditions of this current study.

net specific change. Thirdly, as will be shown later, there was an increase in the amount of both positively and negatively charged particles resulting in no change in the net charge. Finally, more rigorous mixing due to the higher bubble rise velocities might have increased particle migration between the wall to the bulk regions, removing some of the highly charged wall particles into the bulk and adding some of the less charged bulk particles to the wall layer. This would decrease the net charge remaining in the wall layer.

The increase amount of wall fouling resulted in a corresponding decrease in the amount of bulk particles at the higher pressure as shown in Figure 3.8(a). A higher net specific charge was observed for the bulk particles at the higher pressure. This is due to the enhanced electrostatic charge generation discussed above and can be explained with the same reasoning. The higher pressure increased bubble rise velocity and particle contacts which in turn caused higher electrostatic charge generation, hence the higher specific charge of the bulk particles. In addition, more vigorous mixing resulting in increased migration between particles in the wall layer and the bulk might have increased the charge in the bulk. There was no effect of pressure on the bulk particles mean normalized diameters.

Finally, there was a decrease in the amount of elutriated fines and an increase in their net specific charge at elevated pressure. This result is not significant because the fluidization column overhead is very long (over 2 meters) and the mass of the fines collected is very small (<0.05% of initial particles). The elutriated fines do not affect the overall charge balance in the bed.

3.4.1.1 Visual Observations

Representative images showing wall fouling at 101 kPa and 401 kPa are shown in Figure 3.9. The majority of the fouling was located near the bottom of the bed with the top of this layer located at approximately the height of the electrostatic probe or slightly higher. The probe was located at 0.165 m above the distributor plate, at approximately half the static bed height. This indicates that the majority of fouling occurred in the bottom half of the bed. At 101 kPa, there was a gap in fouling above this level followed by a short layer of fouling at approximately static bed level. However, at 401 kPa, there was no clear gap in fouling layer but there was relatively more fouling at bed level.

Bubbles agglomerate, increasing in diameter, as they rise upwards in a fluidized bed. Sowinski et al. (2010) found that the wall fouling decreases in the slugging fluidization regime. In this study, at 1.25 u_{mf} and at atmospheric pressure, larger bubbles were observed to burst at the bed surface. Although not slugging, this bubble diameter might have been sufficiently large to remove particles near the top of the bed. This might explain the gap in fouling observed.

Fouling at or above the static bed level was likely due to the deposition of particles carried by bursting bubbles.

3.4.1.2 Charge Distribution

The net specific charge of wall particles was found to be positive at both operating pressures but further study was required to investigate the effect of pressure on charge distribution within the wall fouling layer. The charged particle separator unit described in section 2.2.4 was used. For the purpose of this analysis, the masses and charges of wall particles collected in the negative Faraday cups (FC1 and FC2) were summed, as were the masses and charges of particles collected in the positive cups (FC3 and FC4).

As shown in Figure 3.10, fluidization at 401 kPa resulted in both more negatively and more positively charged particles. In each case, there were approximately 40% more particles at 401 kPa than what resulted after fluidization at 101 kPa. The distribution of particles did not change with approximately 60% of the particles being positively and 40% negatively charged. Corresponding to the higher mass collected at 401 kPa, higher net positive and negative charges were recorded.

While majority of the net specific charges discussed in the beginning of section 3.4.1 were the result of particle-wall contacts, for the charges presented in this section both particle-particle and particle-wall contacts contributed to charge generation. This can be illustrated by noting that negative charges are reported here since the polyethylene resin used charged positively upon contact with stainless steel wall. Therefore polyethylene-column wall contacts caused polyethylene to charge positively, the negative charges can only be the result of particle-particle contacts (i.e., biopolar charging). For both pressures, the negatively charged particles (in FC1 and FC2) were smaller than the positively charged particles. This indicates that particle-particle contacts caused the smaller particles to charge negatively and the larger particles positively. This

explains the negatively charged elutriated fines in Figure 3.8. Since the fines are smaller than the bulk particles, they charged negatively when contacting larger particles.

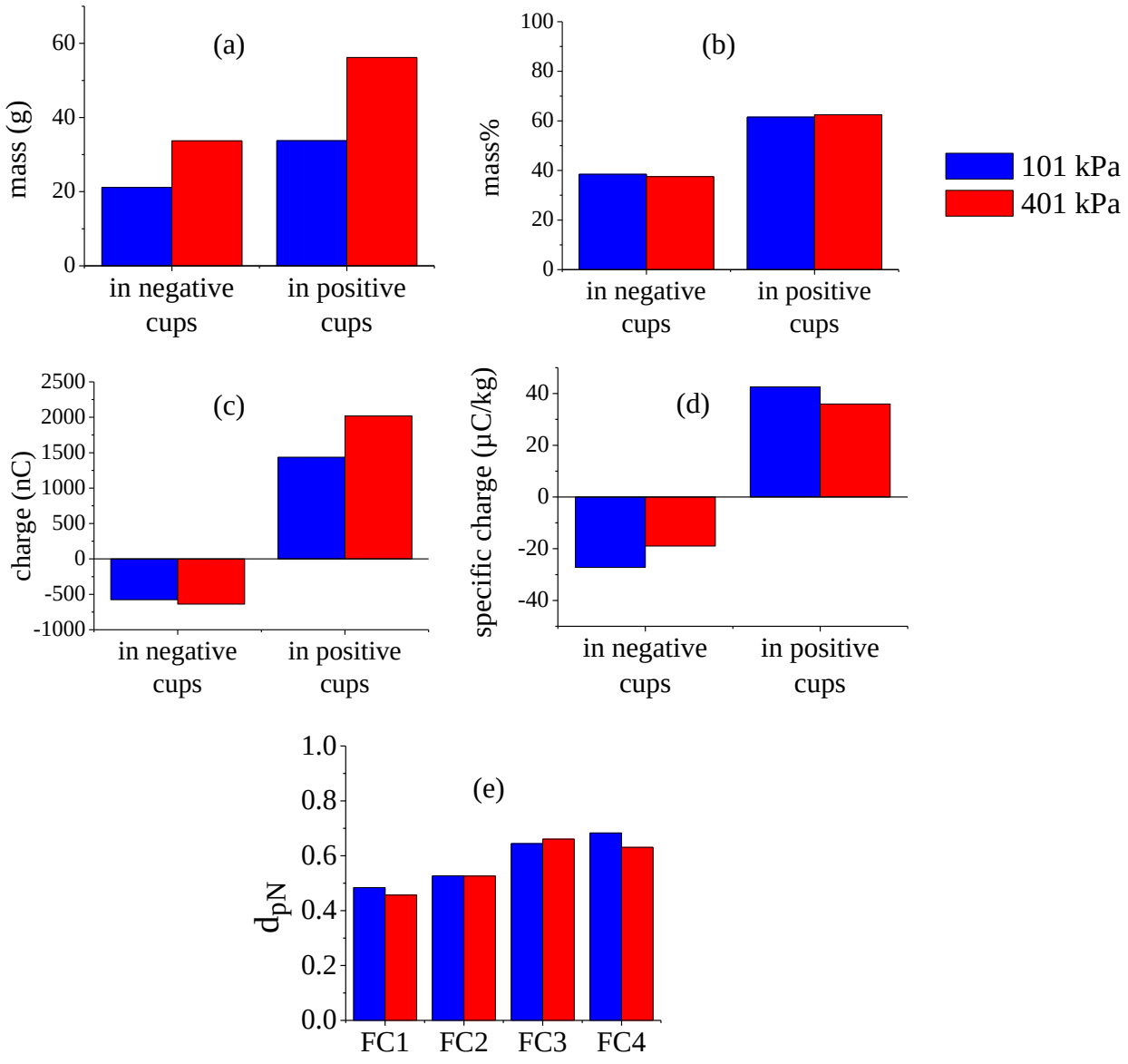

Figure 3.10: Mass and charge distribution of particles in the charged particles separator after fluidization at 101 kPa and 401 kPa including (a) the resulting masses in negative and positive Faraday cups, (b) the mass distributions particles as a percentage of the total mass of particles collected, (c) the recorded charges in the negative and positive cups, (d) the specific net charges and (e) the normalized mean particle diameters in each of the cups.

The presence of both more negatively and positively charged particles indicated the operation of the layering mechanism of wall fouling formation discussed in section 3.3.5. Increase particle-wall contacts caused an increase in particles positive charge generation. The resulting positively charged particles attracted more negatively charged particles which increased the amount of wall fouling. The fact that the ratio of positive to negative particles did not vary supports this hypothesis. The specific charges were 20-40% smaller at the higher pressure which can be attributed to the same reasons discussed in the beginning of section 3.4.1 for the decrease in the net specific charge. The negative charges also could have simply been the charges existed on the initial particles. For initial particles, the average net charge of the negative particles (in FC1 and FC2) was -17.2 μC/kg and for the positive particles (in FC3 and FC4) was 16.9 μC/kg. In the wall particles presented above, the charge of the negative particles was -27.2 μC/kg at 101 kPa and -19.0 μC/kg at 401 kPa. Therefore, the majority of negative charges were present in the initial particles and the remainder generated during particle-particle contacts during fluidization. There was a significant increase in positive charges due to particle-wall contacts during fluidization.

The variation in the particle diameter was found to be relatively small.

3.4.2 Conclusions

Increasing operating pressure from 101 kPa to 401 kPa increased the bubble rise velocity. This in turn increased the frequency of particle-wall contacts resulting in more net charge generation. The higher electrostatic charge caused more wall fouling.

3.5 The Effect of Particle Size Distribution

It was observed in section 3.4.1.2 that smaller particles had a tendency to be negatively charged. The negatively charged particles were also found to be one of the factors causing the wall layering effect. Therefore, the effect of particle size distribution was examined next. Experiments were conducted in which bulk particles collected from fluidization experiments with fresh full samples were fluidized again. These particles were referred to as "used" particles. The experimental conditions under which experiments performed to investigate the effect of particle size distribution on the degree of bed electrification and reactor fouling are summarized in Table 3.5.

Table 3.5: Experimental conditions used for testing the effect of particle size distribution

Parameter	Value
Fluidizing Particles	
Size Range	**Full sample: 20-1500 µm**
	Used: 250-1500 µm
Fluidizing Gas	
Velocity	1.25 u_{mf}
Fluidization Column	
Diameter	0.154 m
Fluidization Conditions	
Operating Pressure	101 kPa

3.5.1 Results and Discussion

The obtained mass distributions, net specific charges and normalized mean particle diameters are shown in Figure 3.11. Representative images of wall fouling are shown in Figure 3.12.

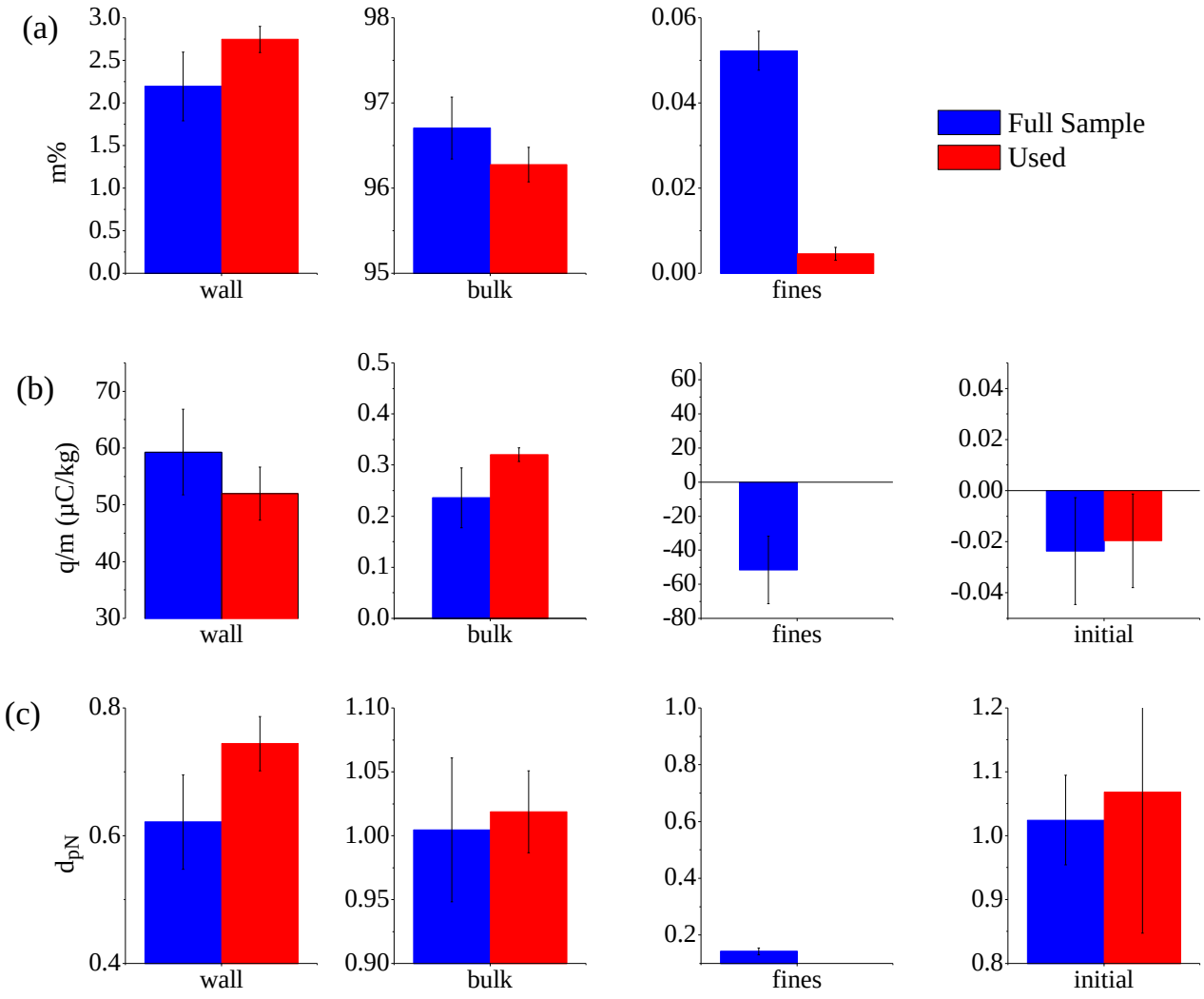

Figure 3.11: Comparing (a) the mass distribution, (b) net specific charge, and (c) normalized mean diameters of particles after the fluidization of full sample and used particles in the wall, bulk, fine and initial regions of the bed of the larger column.

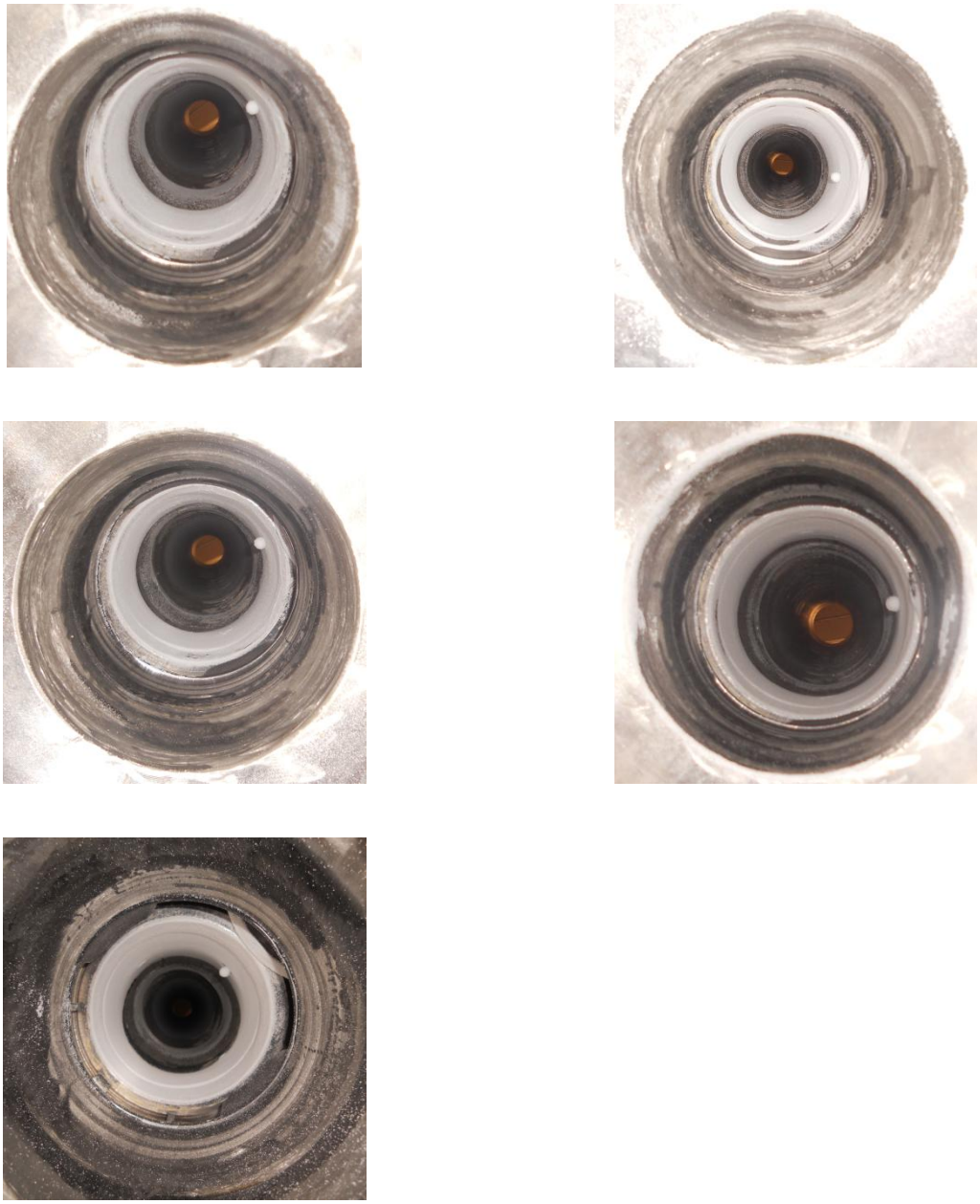

(a) (b)

Figure 3.12: Images of wall fouling upon the removal of bulk particles for repeated trials after fluidizing (a) full sample and (b) used particles in the larger column at atmospheric condition.

As shown in Figure 3.11, the mass percentage of the wall particles was higher and their specific charge was lower when the used particles were fluidized although the difference was not significant. The normalized mean particle diameter for the wall layer was larger for the used particles.

Sowinski et al. (2012) fluidized various sizes of particles and found that there was no significant difference in fouling when particle size was below 600 μm but there was a significant drop in fouling if the particle diameter was above that threshold. In the current study, particles which formed the wall layer (on average 358 μm in diameter) as well as entrained fines (on average 91 μm in diameter) were removed in the used particles. Almost all particles less than 250 μm were removed but there was a sufficient proportion of particles in the 250-600 μm range. Therefore, no decrease in fouling was found although the mean particle diameter increased because of the removal of the smaller particles. This also implies that the bulk particles found in the fluidization of full samples were not charged due to not having much chance to contact the wall and become tribocharged. However, when just these particles were fluidized again, they were charged by wall contacts and contributed to the wall layer formation.

There was no significant difference in the amount of bulk particles. The specific charge of the bulk particles was slightly higher when used particles were fluidized. This was likely due to the increased charge generation in particle-wall contacts resulting from the larger particle diameter. As discussed in section 3.2, smaller particles charge less when contacted with stainless steel. Therefore, removing these particles would increase the generated charge.

Since the used particles contained a much reduced amount of smaller particles, a very small amount of fines was collected. Thus, the mass and particle diameter of these particles could not be measured accurately. And hence, the specific charges and normalized mean particles diameter were not reported.

3.5.1.1 Visual Observations

Images of fouling after the removal of the bulk particles are shown in Figure 3.12. In both cases, a layer of fouling was observed up to a height of half the static bed level. A gap in fouling separated this layer from another thin layer located at approximately bed height. There was no observed difference in fouling between the two cases.

3.5.2 Conclusions

The removal of particles with diameters of less than 250μm did not affect the amount or the specific charge of the wall layer.

3.6 The Effect of Column Diameter

Experiments were performed with operating conditions shown in Table 3.6 to investigate the effect of fluidization column diameter.

The effect of column diameter was previously studied by Rojo et al. (1986), reviewed in section 1.3.3.4. The conclusions of this work, while valuable, are not necessarily applicable to the experimental conditions used in this thesis. First, the particles used were relatively more conductive than polyethylene. Therefore, charge dissipation was more significant. As mentioned above, charge dissipation was used by the author to explain some of the experimental results. Charge dissipation in polyethylene particles is insignificant within the time frame of minutes or hours (Burgo et al., 2011). Second, the material of the column wall was Perspex which is more insulating than the stainless steel columns used in this thesis. The mechanism of image charging used in this thesis to explain wall fouling would not be applicable to Perspex columns. Finally, the charges generated due to insulator-insulator contacts would be different in polarity and magnitude distributions from that generated resulting from insulator-metal contacts.

Table 3.6: Experimental conditions used for testing the effect of column diameter.

Parameter	Value
Fluidizing Particles	
Size Range	20-1500 µm
Fluidizing Gas	
Velocity	1.25 u_{mf}
Fluidization Column	
Diameter	**0.102, 0.154 m**
Fluidization Conditions	
Operating Pressure	101 kPa

3.6.1 Results and Discussion

The obtained mass distributions, net specific charges and normalized mean particle diameters are shown in Figure 3.13. Representative images of wall fouling are shown in Figure 3.14. As shown in Figure 3.13, the specific charges and mean diameters of the initial particles were comparable for experiments conducted at smaller and larger columns. Therefore, these sets of experiments can be compared.

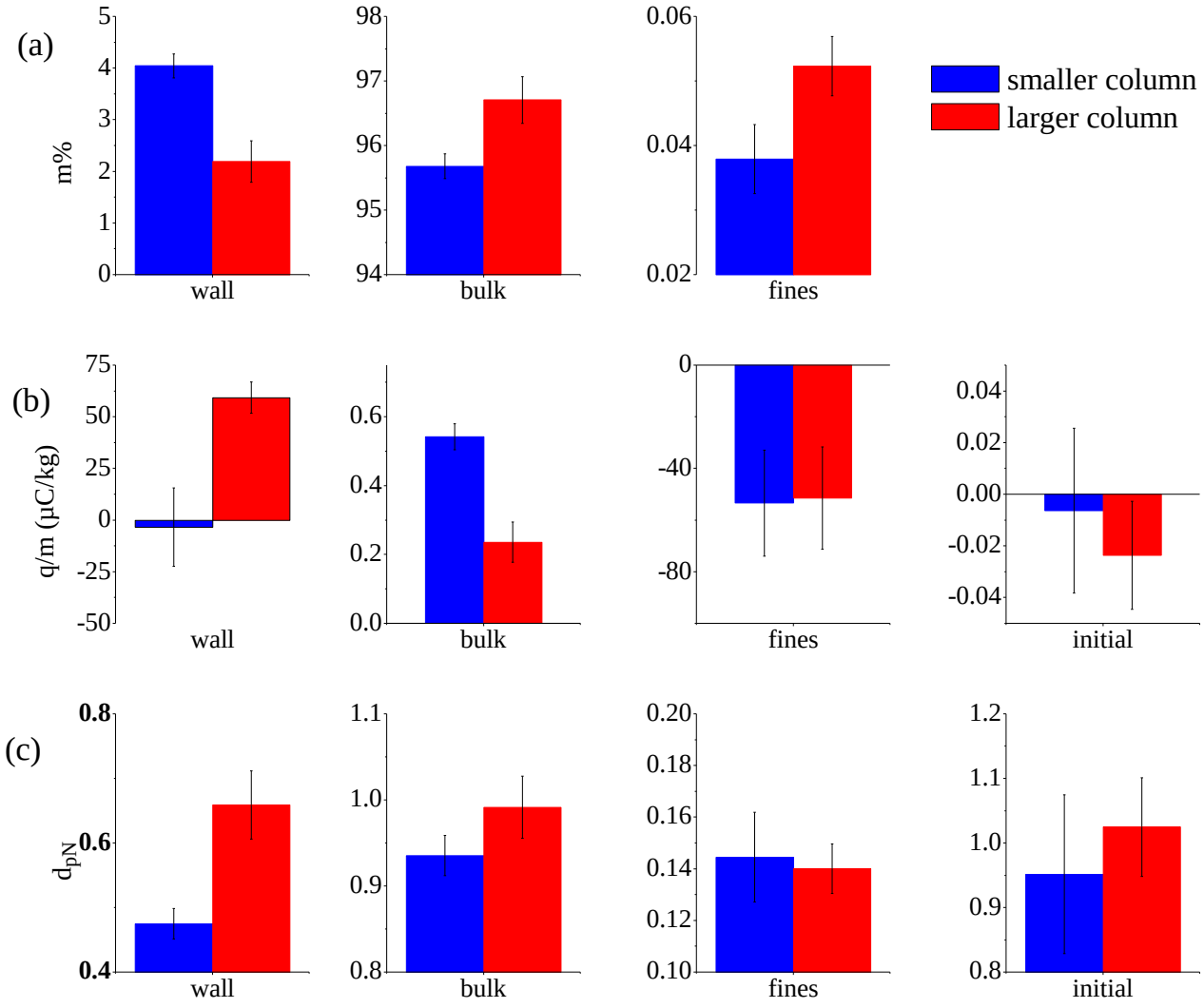

Figure 3.13: Comparing (a) the mass distribution, (b) net specific charge, and (c) normalized mean diameters of particles due to fluidization in the smaller and larger columns in the wall, bulk, fine and initial regions of the bed.

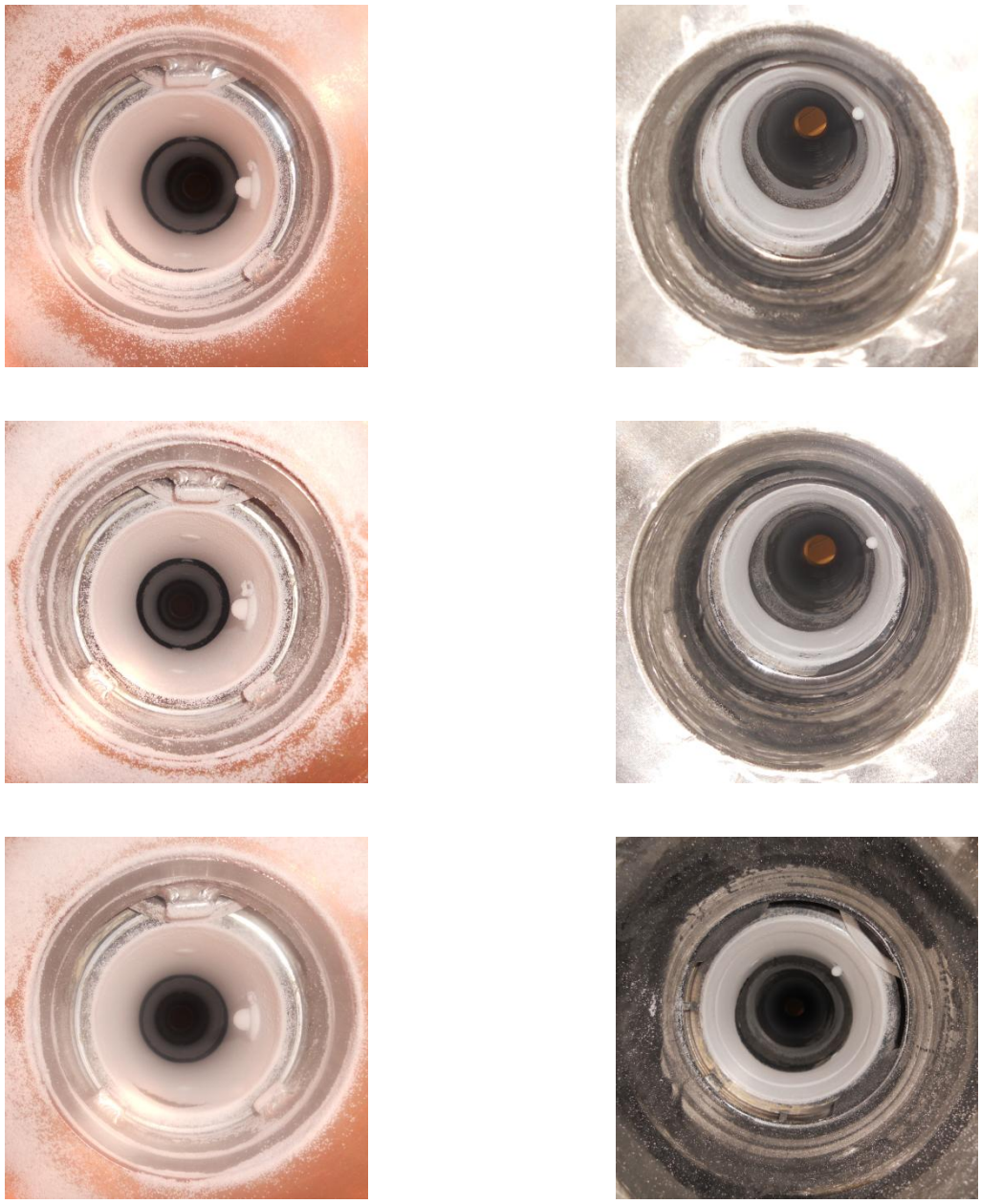

(a) (b)

Figure 3.14: Images of wall fouling after fluidization and removal of bulk particles for three repeated trials in the (a) smaller and (b) larger columns.

As shown in Figure 3.13, the wall layer as a percentage of the initial particles was larger in the smaller column (4% ± 0.2 vs. 2.2% ± 0.4). Interestingly, the net specific charge of the wall particles in the smaller column was almost zero on average (-3.4 ± 19 μC/kg) while the wall particles in the larger column had a significant positive charge (59.3 ± 7.6 μC/kg). Finally, the wall particles in the smaller column had smaller normalized mean diameters (0.48 ± 0.02 vs. 0.66 ± 0.05). To explain the specific charge, further experimentation was required. The obtained results are analyzed in section 3.6.1.2.

The static bed heights were kept the same in the two columns in order to isolate the effect of column diameter for two reasons. First, significantly less mass of particles in the larger column would be needed. Since there is significant variation in the electrostatic properties within and between batches of polyethylene resin even if they are produced using the same process, the less mass is used, the less variation there is between particles used in different trials of the same experiment. Second, if the H/D ratio was kept constant several aspects of bed hydrodynamics would have been changed for the larger column. Bubble sizes would grow to larger diameters in the larger column causing more electrostatic charge generation.

The increase in wall fouling might have been due to the increase in column wall area per mass of particles. This value was 0.11 m^2/kg for the smaller column and 0.05 m^2/kg for the larger column. As discussed in previous sections, net charge generation within the bed can only be due to particle-wall contacts (assuming negligible particle entrainment and thus effect of biopolar charging due to particle-particle contacts). The increase in column area per mass of particles would imply more charge generated per mass of particles (i.e. specific charge), which would result in more wall fouling as was observed.

The wall particles had a significantly smaller mean diameter in the smaller column. This might have been due to greater particle mixing in the smaller column due to the smaller distance between the bulk and the column wall. Smaller particles preferentially adhered to surfaces due to their higher charge-to-mass ratio. This is due to their higher specific surface area. Since the electrostatic phenomenon is a surface phenomenon, higher surface to volume ratios (or to mass assuming constant particle density) would result in higher charge-to-mass ratios.

The difference in distributor plate hole sizes likely did not have an impact on the results. The larger column had a top distributor plate hole size of 3 mm while the smaller one had a size of 2 mm. The size of bubbles formed at the distributor plate is primarily a function of the excess gas velocity and the number of holes per unit area, not the hole size. Since the columns were operated at the same superficial gas velocity and the numbers of holes per unit area were equivalent, the distributor plate would not affect bubble size and therefore electrostatic charging.

The smaller bulk particles mass percentage in the smaller column corresponded to the larger percentage of wall fouling. The bulk particles specific charge was significantly larger in the smaller column. The smaller column size would also lower the distance between the bulk of the bed and the column wall. This might have resulted in increased migration of particles from the bulk to the wall layer and reverse migration from the wall layer to the bulk. This migration would explain the increased bulk specific charge.

The bulk particles mean diameter was slightly larger in the larger column. This result is not significant because the majority of the initial particles ended up in the bulk and the majority of the remainder ended up in the wall layer. If the wall layer mean diameter was smaller in the smaller column, then the bulk particles mean diameter would be expected to be larger. However, the opposite of this was observed. This might be due to slightly different sampling techniques for the particles. Unlike in the smaller column, in the larger column upon opening the distributor plate to drop the bulk particles into the bottom Faraday cup some particles remained within the distributor plate, possibly altering the size distribution. Moreover, there were more and larger ports along the larger column wall which can be filled with particles, again altering the size distribution. Finally, the distance between the bed and the bottom Faraday cup is larger in the larger column. Therefore in the larger column there is a greater possibility that the falling particles are trapped in openings on the wall along this path.

Finally, the mass percentage of elutriated fines was larger in the larger column. The specific charges and mean diameters of the fines were similar in the two columns. The amounts of fines collected in both cases were very small. The lower percentage of fines collected in the smaller column might have been due to the increase of wall fouling, attracting the negatively charged smaller particles and decreasing elutriation.

3.6.1.1 Visual Observations

Representative images showing wall fouling in the smaller and larger columns are shown in Figure 3.14. In both cases, the wall layer consisted of two sections. In the smaller column, the electrostatic probe, which was at a height of 0.076 m above the distributor plate, approximately bisected the bottom layer. Therefore, the bottom layer was up to about 0.15 m which is slightly lower than half the bed height of 0.34 m. In the larger column, the top of the bottom layer was approximately at the level of the electrostatic probe, 0.165 m above the distributor plate, which was again approximately half the bed height. Therefore, in both cases, the bottom fouling layer was located at the bottom half of the bed. The occurrence of the two layers at roughly the same height indicates that the bubble hydrodynamics in the two layers are equivalent at the bottom of the column. This supports the decision made to compare the two columns using the same static bed height.

Above the bottom layer, there was a gap with little or no fouling above which there was another layer of fouling. This layer was approximately located at bed level. As discussed previously, this layer is likely the result of bubble bursting at the top of the fluidized bed.

3.6.1.2 Incremental Wall Layer Removal

To investigate the anomalous result shown in Figure 3.13(b) whereby the specific net charge of particles fluidized in the smaller column was almost zero, additional experiments were performed where the wall layer was incrementally sampled. Compressed air was used to remove particles and the air velocity was increased incrementally to remove successive portions. Their masses, specific net charges and normalized particle diameters are shown in Figure 3.15. Picture taken before the removal of each portion are shown in Figure 3.16.

As Figure 3.15(c) shows, the net specific charge of the entire wall layer was still relatively small. The first portion was removed first, the second portion second and the third portion last. There was a distribution of charge on the particles. The first portion was positively charged likely due to charge generated from particle-wall contacts. The succeeding portions were negatively charged. It is important to note that these portions required a higher gas velocity for their removal because their higher specific charge due to which they were more strongly adhered to the column wall. The charge generated within this portion must have been a result of particle-particle contact causing some particles to be positively charged and others negatively or were

initially negative charged as discussed in section 3.1.3, because the initial particles had significant positive and negative portions. The migration of these negative particles from the bulk leaving their positively charged counterparts behind in the bulk resulted in a positive charge on the bulk particles. Beside the mechanism discussed above whereby particles that charge positive after contact with the wall migrate to the bulk, this is a second mechanism that can cause a net positive charge on the bulk particles. The mean diameter of the second layer is slightly smaller than the first, possibly indicating bipolar charging where smaller particles charged negatively and larger ones positively. However, the diameter of the third portion which is also negatively charged was larger than the first positively charged portion.

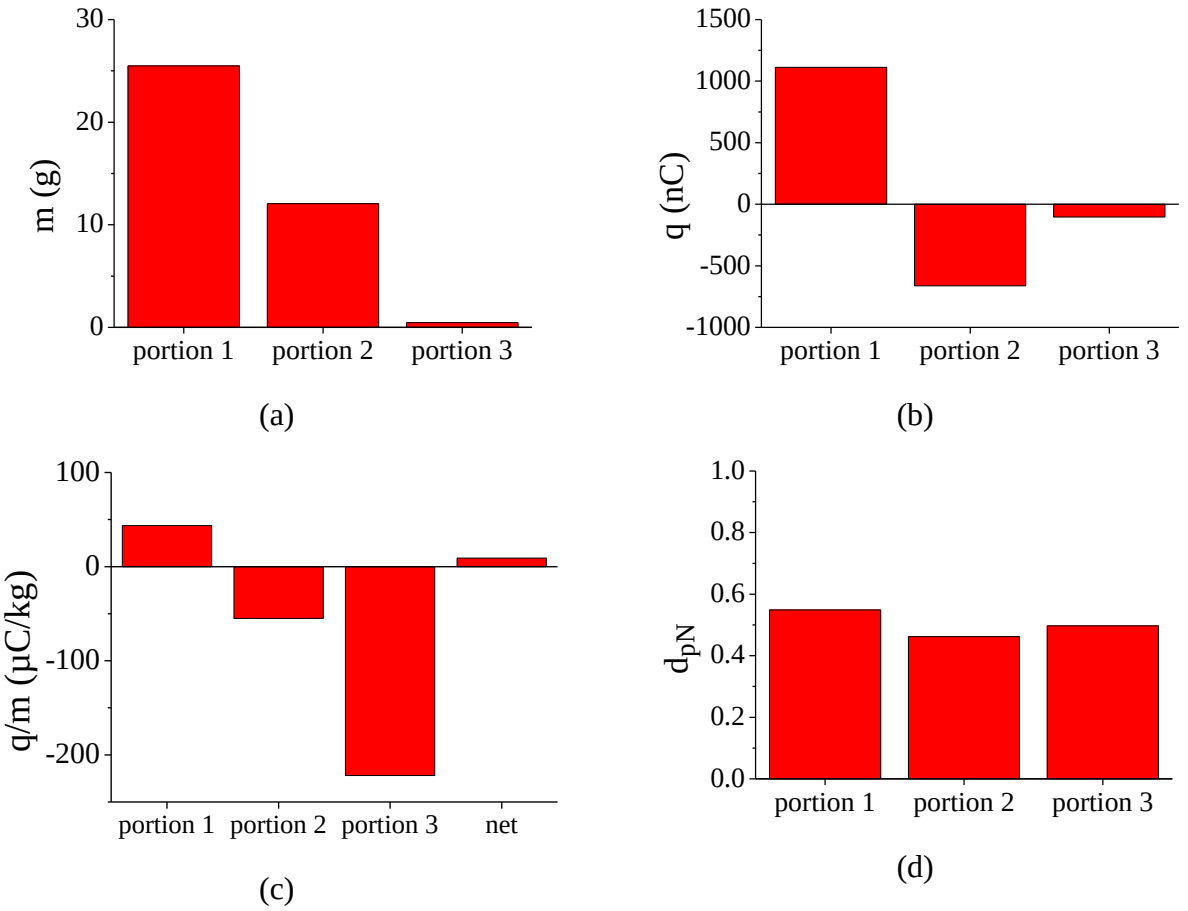

Figure 3.15: Sampling successive layers of wall particles in the smaller column. Shown are the particle (a) masses, (b) net charges, (c) net specific charges including the total net specific of the whole wall layer, and (b) normalized mean particle diameters.

Regardless of the mechanisms, the observed result is interesting and has a larger significance. Most studies on electrostatics so far have assumed that charge can be directly correlated to wall fouling. However, as this result shows, this is not necessarily the case. Although the net charge might be very small or even zero, the presence of significant underlying charges can also cause wall fouling. This finding also indicates that charge measurement techniques such as electrostatic probes which provide information on the net charge of particles but not their distribution might not be accurate methods of studying fluidized bed electrification.

(a)

(b)

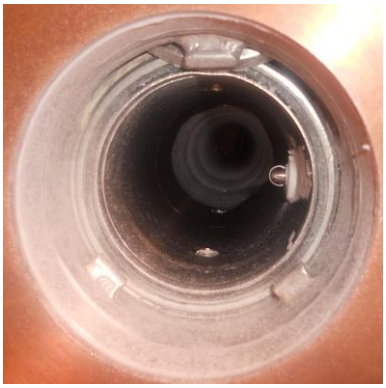

(c)

Figure 3.16: Images of successive sampling of the wall particles in the smaller column showing it (a) before the removal of portion 1, (b) after the removal of portion 1 and (c) after the removal of portion 3.

3.6.2 Conclusions

More electrostatic charge generation and wall fouling were observed in a column with a smaller diameter (0.102 m) compared with that of the larger diameter (0.154 m). This was due to the larger surface area per mass of particles in the smaller column. The wall layer was found to consist of both negatively and positively charged particles. The net charge of the wall layer does not necessarily correlate to wall fouling. Fouling can consist of a layer of particles with equal positive and negative portions.

Chapter 4. Conclusions and Recommendations

Electrostatic charge generation in some gas-solid fluidized beds can be a significant nuisance. In the polyolefin industry, the generation of electrostatic charges in polyethylene fluidized bed reactors causes the adhesion of a layer of particles to the reactor wall. The heat released by the exothermic polymerization reaction then causes this layer to melt, forming polymer sheets on the reactor wall. These sheets then detach from the wall, drop onto the distributor plate and block it necessitating reactor shutdown for clean-up which causes significant economic loss. This phenomenon is a major problem in gas-solid fluidized bed polyolefin production reactors. The objective of this thesis was study the mechanisms of electrostatic charge generation and wall layer formation in gas-solid fluidized beds in general and for polyethylene process in particular.

4.1 Conclusions

In this work, a technique to measure the amount and charge of the fluidized bed wall fouling layer which was previously developed by Sowinski et al. (2010) was extended to a larger system, stainless steel column, 0.154 m in diameter and 4.5 m in height, designed to be capable of operating at up to the pressures, temperatures, and gas velocity of industrial reactors of 2 600 kPa, 100°C and 1 m/s, respectively. The system included two Faraday cups located at the top and bottom (forming the windbox) of the fluidization column, and a knife gate valve that acted as the distributor plate. Due to the larger scale and elevated operating pressures of this system, a mechanism was required to to allow convenient access of the two Faraday cups. This was achieved by the placement of two manways, one at the top and another at the bottom of the column. This addition is quite unique for fluidization columns. This system is the only academic unit to include an online electrostatic charge measurement technique capable of providing information on the degree of wall fouling at high pressures and high gas velocities (specifically in the turbulent fluidization regime).

Preliminary tests were performed on the system, including investigation of the effects of operating pressure, particle size distribution and column diameter on degree of bed electrification and wall fouling.

The increase of operating pressure from 101 kPa to 401 kPa was found to double the amount of wall fouling. This was due to the greater bubble rise velocities at the higher pressure which caused more mixing in the bed, increasing particle-column wall and particle-particle contacts and therefore increased the generation of electrostatic charges and wall fouling.

The change in particle size distribution, removing particles with diameters less than 250 μm, was found to not affect the amount particles accumulated on the wall or their net specific charges.

Higher electrostatic charge generation and wall fouling was observed when particles were fluidized in the smaller column. This was due to the higher column wall surface area per mass of particles in the smaller column. In the smaller column, the layer of wall fouling was found to contain both positively and negatively charged particles and therefore had almost zero net charge. This result shows that the measured net charge on particles might not be a good indicator of the degree of wall fouling.

Overall in results of this research indicated that the polyethylene resin used became more positively charged due its contacts with the column wall although both positive and negative particles existed within the bed. This charge polarity was further confirmed by conducting bench-scale shaking tests.

Finally, possible mechanisms underlying the charge generation in the fluidized bed and formation of the wall layer were proposed. Both particle-particle and particle-wall contact charging were found to be present within the fluidized bed. However, in this study in which entrainment was negligible, the net specific charge observed within the bulk of the bed and the wall layer was found to be only due to the particles-wall contacts. The wall layer was found to be formed due to image forces formed by the charged particles inducing an opposite image of their charge on the conductive fluidization column wall which causes the particles to be attracted to the column wall. In addition, the existence of both negatively and positively charged particles confirmed the layering effect in which oppositely charged particles would be attracted to each other.

4.2 Recommendations for Future Work

There are still many unknowns about wall fouling and electrostatic charge generation in fluidized beds. This is partly due to the lack of understanding of fundamental mechanisms underlying electrostatic phenomena in insulators. Having commissioned and tested the new larger high-pressure system the following recommendations are proposed for future work:

a) This thesis showed that by increasing the operating pressure to only 401 kPa the amount of wall fouling doubled. Increasing the pressure with small increments and studying its effects up to 2 600 kPa might yield significant results.

b) Since the system allows operation close to industrial conditions, it is suggested to preform tests at 2 600 kPa and study the effects of gas velocity. Industrial polyethylene reactors operate at turbulent fluidization regime which in this system can be achieved at high pressures. This parameter has not been studied before.

c) The effect of particle size distribution was briefly studied in this thesis. Sowinski et al. (2012) have fluidized sieved particles in various size ranges at atmospheric conditions and found that fouling decreased for particles larger than 600 μm. This experiment could be repeated at higher pressure to examine whether or how this threshold changes.

d) Bench-scale tests showed that particles with diameters of less than 300 μm charged less than the full sample particles. Repeating this experiment with various particle sizes can help explain the reasons for this difference.

e) The static bed height was kept constant between the two columns. The effect of static bed height on the amount, charge and location of wall fouling can be examined in future studies.

f) Finally, the pneumatic transport of elutriated catalyst in the recycle loop of the Unipol process is thought to generate significant electrostatic charges increasing wall fouling inside the bed. The effect of this parameter can be tested in the new system.

Bibliography

Ali, F., Ali, M., Ali, R., & Inculet, I. (1998). Minority charge separation in falling particles with bipolar charge. Journal of Electrostatics, 45(2), 139-155.

Apodaca, M. M., Wesson, P., K.Bishop, J., Ratner, M., & Grzybowski, B. (2010). Contact electrification between identical materials. Angewandte Chemie International Edition, 49, 946-949.

Bafrnec, M., & Bena, J. (1972). Quantitative data on the lowering of electrostatic charge in a fluidized bed. Chemical Engineering Science, 27(5), 1177-1181.

Baytekin, H. T., Baytekin, B., Incorvati, J. T., & Grzybowski, B. A. (2012). Material Transfer and Polarity Reversal in Contact Charging. Angew. Chem. Int. Ed., 51, 4843-4847.

Baytekin, H., Patashinski, A., Branicki, M., Baytekin, B., Soh, S., & Grzybowski, B. (2011). The Mosaic of Surface Charge in Contact Electrification. Science, 333, 308-312.

Boland, D., & Geldart, D. (1972). Electrostatic charging in gas fluidised beds. Powder Technology, 5(5), 289-297.

Brouwer, G., Wagner, E., van Ommen, J., & Mudde, R. (2012). Effects of pressure and fines content on bubble diameter in a fluidized bed studied using fast X-ray tomography. Chemical Engineering Journal, 207-208, 711-717.

Buffière, P., & Moletta, R. (2000). Collision frequency and collisional particle pressure in three-phase fluidized beds. Chemical Engineering Science, 55(22), 5555-5563.

Burgo, T. A., Ducati, T. R., Francisco, K. R., Clinckspoor, K. J., Galembeck, F., & Galembeck, S. E. (2012). Triboelectricity: Macroscopic Charge Patterns Formed by Self-Arraying Ions on Polymer Surfaces. Langmuir, 28, 7407−7416.

Burgo, T., Rezende, C., Bertazzo, S., Galembeck, A., & Galembeck, F. (2011). Electric potential decay on polyethylene: Role of atmospheric water on electric charge build-up and dissipation. Journal of electrostatics, 69(4), 401 -409.

Cai, X. (2013). Triboelectric charge distribution in insulative granular systems.

Cartwright, P., Singh, S., Bailey, A. G., & Rose, L. (1985). Electrostatic charging characteristics of polyethylene powder during pneumatic conveying. IEEE Transactions on Industry Applications, IA-21(2), 541-546.

Ciborowski, J., & Wlodarski, A. (1962). On electrostatic effects in fluidized beds. Chemical Engineering Science, 17(1), 23-32.

Cross, J. (1987). Electrostatics: Principles, Problems and Applications. Bristol: Adam Hilger.

Fasso, L., Chao, B., & Soo, S. (1982). Measurement of electrostatic charges and concentration of particles in the freeboard of a fluidized bed. Powder Technology, 33(2), 211-221.

Forward, K., Lacks, D., & Sankaran, R. (2009). Triboelectric charging of granular insulator mixtures due solely to particle - Particle interactions. Industrial and Engineering Chemistry Research, 48(5), 2309-2314.

Fujino, M., Ogata, S., & Shinohara, H. (1985). The electric potential distribution profile in a naturally charged fluidized bed and its effects. Int. Chem. Eng., 25, 149-159.

Fulks, B., Sawin, S., Aikman, C., & Jenkins, J. (1985). Patent No. 4532311. United States.

Geldart, D. (1973). Types of gas fluidization. Powder Technology, 7(5), 285-292.

Giffin, A., & Mehrani, P. (2010). Comparison of influence of fluidization time on electrostatic charge build-up in the bubbling vs. slugging flow regimes in gas-solid fluidized beds. Journal of Electrostatics, 68(6), 492-502.

Giffin, A., & Mehrani, P. (2013). Effect of gas relative humidity on reactor wall fouling generated due to bed electrification in gas-solid fluidized beds. Powder Technology, 235, 368-375.

Godlieb, W., Deen, N., & Kuipers, J. (2008). On the relationship between operating pressure and granular temperature: A discrete particle simulation study. Powder Technology, 182(2), 250-256.

Goldhirsch, I. (2008). Introduction to granular temperature. Powder Technology, 182(2), 130-136.

Guardiola, J., Rojo, V., & Ramos, G. (1996). Influence of particle size, fluidization velocity and relative humidity on fluidized bed electrostatics. Journal of Electrostatics, 37(1), 1-20.

Hagerty, R. O., Muhle, M. E., Agapiou, A. K., Kuo, C.-T., Goode, M. G., Hussein, F. D., Pannell, R. B., Szul, J. F. (2005). Patent No. 20050148742 A1. US.

Ham, R., Galtier, P., & Bergougnou, M. (1992). Electrostatics in an air/catalyst fluidized bed at ambient temperature and pressure. In O. Potter, & D. Nicklin (Ed.), Fluidization VII (pp. 611-620). Brisbane: Engineering Foundation.

Hamidipour, M., Mostoufi, N., Sotudeh-Gharebagh, R., & Chaouki, J. (2005). Experimental investigation of particle contact time at the wall of gas fluidized beds. Chemical Engineering Science, 60(15), 4349-4357.

Harper, W. R. (1967). Contact and Frictional Electrification. Oxford: Oxford University Press.

Hendrickson, G. (2006). Electrostatics and gas phase fluidized bed polymerization reactorwall sheeting. Chemical Engineering Science, 61, 1041-1064.

Hoffman, A., & Yates, J. (1986). Experimental observations of fluidized beds at elevated pressures. Chemical Engineering Communications, 41(1-6), 133-149.

Iversen, P., & Lacks, D. (2012). A life of its own: The tenuous connection between Thales of Miletus and the study of electrostatic charging. Journal of Electrostatics, 70(3), 309-311.

Kok, J., & Lacks, D. (2009). Electrification of granular systems of identical insulators. Physical Review E - Statistical, Nonlinear, and Soft Matter Physics, 79(5), art. no. 051304.

Kunii, D., & Levenspiel, O. (1991). Fluidization Engineering (2nd ed.). Newton, MA: Butterworth-Heinemann.

Lacks, D. (2012). The unpredictability of electrostatic charging. Angewandte Chemie - International Edition, 51(28), 6822-6823.

Lacks, D., & Mohan Sankaran, R. (2011). Contact electrification of insulating materials. Journal of Physics D: Applied Physics, 44(45), art. no. 453001.

Lewis, W. K., Gilliland, E. R., & Bauer, W. C. (1949). Characteristics of Fluidized Particles. Industrial & Engineering Chemistry, 41(6), 1104-1117.

Liu, Z., Bi, X., & Grace, J. (2010). Electrostatic charging behaviour of dielectric particles in a pressurized gas-solid fluidized bed. Journal of Electrostatics, 68, 321-327.

Lowell, J., & Rose-Innes, A. (1980). Contact electrification. Advances in Physics, 29, 947-1023.

Lowell, J., & Truscott, W. (1986). Triboelectrification of identical insulators. I. An experimental investigation. Journal of Physics D: Applied Physics, 19(7), 1273-1280.

Mardiguian, M. (2005). Electrostatic discharge: understand, simulate and fix ESD problems. Piscataway, NJ: IEEE Press.

Matsusakaa, S., Maruyamaa, H., Matsuyamab, T., & Ghadiri, M. (2010). Triboelectric charging of powders: A review. Chemical Engineering Science, 65(22), 5781-5807.

McCarty, L. S., & Whitesides, G. M. (2008). Electrostatic Charging Due to Separation of Ions at Interfaces: Contact Electrification of Ionic Electrets. Angew. Chem. Int. Ed., 47, 2188-2207.

Mehrani, P., Bi, H., & Grace, J. (2005). Electrostatic charge generation in gas-solid fluidized beds. Journal of Electrostatics, 63(2), 165-173.

Moughrabiah, W., Grace, J., & Bi, X. (2009). Effects of pressure, temperature, and gas velocity on electrostatics in gas-solid fluidized beds. Industrial and Engineering Chemistry, 48, 320-325.

Mountain, J., Mazumder, M., Sims, R., Wankum, D., Chasser, T., & Pettit, P. J. (2001). Triboelectric charging of polymer powders in fluidization and transport processes. IEEE Transactions on Industry Applications, 37(3), 778-784.

Mun, T. C. (2005). Production of Polyethylene Using Gas Fluidized Bed Reactor . Retrieved 07 30, 2013, from http://www.klmtechgroup.com/PDF/Articles/Fluidized-Bed-Reactor.pdf

Murtomaa, M., Räsänen, E., Rantanen, J., Bailey, A., Laine, E., Mannermaa, J.-P., & Yliruusi, J. (2003). Electrostatic measurements on a miniaturized fluidized bed. Journal of Electrostatics, 57(1), 91-106.

Nilpawar, A., Reynolds, G., Salman, A. D., & Hounslow, M. J. (2006). Estimating aggregation efficiency from observation of flow behaviour in a high shear mixer. AIChE Annual Meeting, Conference Proceedings.

Olowson, P., & Almstedt, A. (1990). Influence of pressure and fluidization velocity on the bubble behaviour and gas flow distribution in a fluidized bed. Chemical Engineering Science, 45(7), 1733-1741.

Park, A.-H., Bi, H., & Grace, J. (2002). Reduction of electrostatic charges in gas-solid fluidized beds. Chemical Engineering Science, 57(1), 153-162.

Peacock, A. (2000). Handbook of Polyethylene: Structures: Properties, and Applications. New York, NY: Marcel Dekker.

Rojo, V., Guardiola, J., & Vian, A. (1986). A capacitor model to interpret the electric behaviour of fluidized beds. Influence of apparatus geometry. Chemical Engineering Science, 41(8), 2171-2181.

Salama, F., Sowinski, A., Atieh, K., & Mehrani, P. (2013). Investigation of electrostatic charge distribution within the reactor wall fouling and bulk regions of a gas-solid fluidized bed. Journal of Electrostatics, 71(1), 21-27.

Sow, M., Lacks, D., & Sankaran, R. (2012). Dependence of contact electrification on the magnitude of strain in polymeric materials. Journal of Applied Physics, 112(8), art. no. 084909.

Sow, M., Lacks, D., & Sankaran, R. (2013). Effects of material strain on triboelectric charging: Influence of material properties. Journal of Electrostatics, 71(3), 396-399.

Sowinski, A., Mayne, A., & Mehrani, P. (2012). Effect of fluidizing particle size on electrostatic charge generation and reactor wall fouling in gas-solid fluidized beds. Chemical Engineering Science, 71, 552-563.

Sowinski, A., Mayne, A., Javed, B., & Mehrani, P. (2011). Comparison of the effect of grounding the column wall in gas-solid fluidized beds on electrostatic charge generation. Journal of Physics: Conference Series, 301(1), art. no. 012068.

Sowinski, A., Miller, L., & Mehrani, P. (2010). Investigation of electrostatic charge distribution in gas-solid fluidized beds. Chemical Engineering Science, 65(9), 2771-2781.

Sowinski, A., Salama, F., & Mehrani, P. (2009). New technique for electrostatic charge measurement in gas-solid fluidized beds. Journal of Electrostatics, 67(4), 568-573.

Tanoue, K., & Masuda, H. (2006). Electrostatic separation. In Powder Technology Handbook (p. 656). Florida: Taylor & Francis Group, LLC.

Tardos, G., & Pfeffer, R. (1980). Method to measure electrostatic charge on a granule in a fluidized bed. Chemical Engineering Communications, 4(6), 665-671.

Wang, F., Wang, J., & Yang, Y. (2008). Distribution of electrostatic potential in a gas-solid fluidized bed and measurement of bed level. Industrial and Engineering Chemistry Research, 47(23), 9517-9526.

Williams, M. W. (2012). Triboelectric charging of insulating polymers–some new perspectives. AIP Advances, 2(1), art. no. 010701.

Yang, W.-C. (2003). Bubbling Fluidized Beds. In W.-C. Yang (Ed.), Handbook of Fluidization and Fluid-Particle Systems (p. 89). New York, NY: Marcel Dekker.

Yao, L., Bi, H., & Park, A.-H. (2002). Characterization of electrostatic charges in freely bubbling fluidized beds with dielectric particles. Journal of Electrostatics, 56(2), 183-197.

Yates, J. G. (1996). Effects of temperature and pressure on gas-solid fluidization. Chemical Engineering Science, 51, 167-205.

Yu, X., Li, W., Xu, Y., Wang, J., Yang, Y., & Xu, N. (2010). Wang, H. Effect of polymer granules on the electrostatic behavior in gas-solid fluidized beds. Industrial and Engineering Chemistry Research, 49(1), 132-139.

Zhao, H., Castle, G., Inculet, I., & Bailey, A. (2000). Bipolar charging in polydisperse polymer powders in industrial processes. Conference Record - IAS Annual Meeting (IEEE Industry Applications Society), 2, 835-841.

Zhao, H., Castle, G., Inculet, I., & Bailey, A. (2003). Bipolar charging of poly-disperse polymer powders in fluidized beds. IEEE Transactions on Industry Applications, 39(3), 612-618.

Appendices

Appendix 1. Additional Literature Figures and Tables

Table A1.1: A selection of experimental conditions for experiments on electrostatics in gas-solid fluidization

Source	Material	Particle diameter (μm)	Material of construction	Method
Ali et al., 1998	Polyamide, Acrylic	98	PVC	Faraday cup
Bafrnec & Bena, 1972	Glass ballotini	170-210	Metal	
Boland & Geldart, 1972	Lead glass ballotini	100-800	Perspex, glass or Protectafilm	Potential probe
Ciborowski & Wlodarski, 1962	Vinylpolyacetate, Polystyrol, Sand	300-750	Rasotherm glass	
Fujino et al., 1985	Glass beads, Neo beds, PMMA	200-540	Acrylic, iron	Potential probes, current probe and Faraday cup
Guardiola et al., 1996	Glass beads	250-420	Perspex	Potential probe
Ham et al., 1992	Fluid cracking catalyst (FCC)	82	Polymethyl methacrylate	Potential probe
Liu et al., 2010	Polyethylene resin	570-640	Carbon steel	Current probe
Moughrabiah et al., 2009	Glass beads, LLDPE	321-600	Carbon steel	Current probe, Faraday cups
Mountain et al., 2001	Acrylic	19-24		Faraday cup
Murtomaa et al., 2003	Microcrystalline cellulose, Lactose monohydrate, Glass beads	180-1130	Glass or acrylic	Potential probe

Source	Material	Particle diameter (μm)	Material of construction	Method
Rojo et al., 1986	Glass ballotini	350-420	Perspex	Capacitance probe
Tardos & Pfeffer, 1980	Porcelain	2000	Plastic	Faraday cup or current probe
Wang et al., 2008	LLDPE	185-1700	Plexiglas	Potential probe
Yao et al., 2002	Polyethylene	318-378	Plexiglas	Ball probe
Yu et al., 2010	Polyethylene	1275	Plexiglas	Potential contacting probe
Zhao et al., 2000	Acrylic	79.5-84.4	Steel	Faraday cups
Zhao et al., 2003	Acrylic	79.5-84.4	Steel	Faraday cups

Appendix 2. Experimental Data

Table A2.2: Summary of experimental data

Tested Parameter	Region	Specific charge - q/m (μC/kg)		Mass distribution - m%		Normalized particle size - d_p	
Operating Pressure		**101 kPa**	**401 kPa**	**101 kPa**	**401 kPa**	**101 kPa**	**401 kPa**
	Initial	-0.02 ± 0.02	0 ± 0.03	100 ± 0	100 ± 0	1.03 ± 0.07	0.95 ± 0.05
	Bulk	0.24 ± 0.06	0.38 ± 0.04	96.71 ± 0.36	94.3 ± 0.25	1.01 ± 0.06	1.02 ± 0.04
	Wall	59.32 ± 7.56	48.91 ± 5.02	2.2 ± 0.4	4.27 ± 0.36	0.62 ± 0.07	0.62 ± 0.04
	Fines	-51.39 ± 19.79	-126.25 ± 23.61	0.05 ± 0	0.02 ± 0.01	0.14 ± 0.01	0.16 ± 0.01
Particle Size Distribution		**Full Sample**	**Used**	**Full Sample**	**Used**	**Full Sample**	**Used**
	Initial	-0.02 ± 0.02	0.02 ± -0.02	100 ± 0	100 ± 0	1.03 ± 0.07	1.07 ± 0.22
	Bulk	0.2 ± 0.1	0.3 ± 0	96.7 ± 0.4	96.3 ± 0.2	1.01 ± 0.06	1.02 ± 0.03
	Wall	59.3 ± 7.6	52 ± 4.7	2.2 ± 0.4	2.7 ± 0.2	0.62 ± 0.07	0.75 ± 0.04
	Fines	-51.4 ± 19.8	2.5 ± 52.2	0.1 ± 0	0 ± 0	0.14 ± 0.01	0.8 ± 0.09
Column Diameter		**Smaller**	**Larger**	**Smaller**	**Larger**	**Smaller**	**Larger**
	Initial	-0.01 ± 0.03	-0.02 ± 0.02	100 ± 0	100 ± 0	0.95 ± 0.12	1.02 ± 0.08
	Bulk	0.54 ± 0.04	0.24 ± 0.06	95.68 ± 0.19	96.71 ± 0.36	0.94 ± 0.02	0.99 ± 0.04
	Wall	-3.36 ± 19.01	59.32 ± 7.56	4.05 ± 0.23	2.2 ± 0.4	0.48 ± 0.02	0.66 ± 0.05
	Fines	-53.36 ± 20.54	-51.39 ± 19.79	0.04 ± 0.01	0.05 ± 0	0.14 ± 0.02	0.14 ± 0.01

Appendix 3. Electrostatic Probe Bench-Scale Tests

A3.1 Purpose

The objective of this study was to aid in the interpretation of data collected from an electrostatic probe inserted in the fluidized bed. When an object approaches or contacts the probe, three mechanisms can contribute to the measured charge on the probe:

1. Transfer: Charge transfer from the object to the probe due to the contact.
2. Generation: Charge generation due to the contact of object with the probe.
3. Induction: Charge induction by the charge of the object on the probe.

Bench-scale experiments were performed to determine the relative significance of these three mechanisms.

A3.2 Experimental Procedure

Experiments were performed with 45 g of polyethylene (PE) resin. Particles charge was simultaneously measured by two probes and a Faraday cup as shown in Figure A3.1. The particles were poured into a funnel and flowed in a plastic tube, after which contacted Electrometer 3 (E3) probe and then dropped into the Faraday Cup (FC). Electrometer 1 (E1) was used to sample charge from the FC while E3 and E4 were connected to the probes as shown in the figure and also sampled charge. Since the E3 probe contacted the particles, it measured the transferred and generated charge. Since the E4 probe did not, it only measured the inducted charge. The same sample of particles used in the previous trial was then removed into a glass beaker and reused for the next trial. This process was repeated for this same sample many times. The results are shown Figure A3.2 and Figure A3.3.

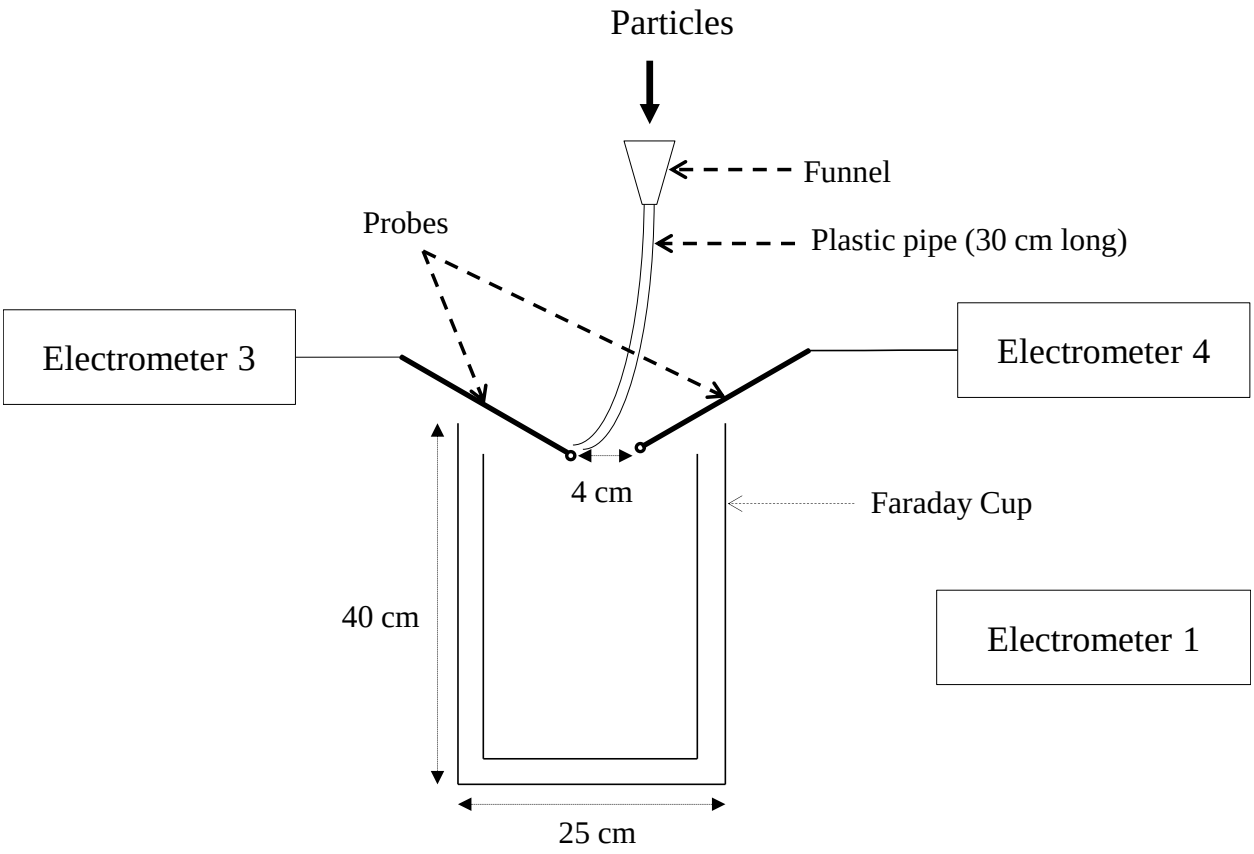

Figure A3.1: Schematic of the apparatus. Particles contact with electrometer 3 probe before falling into the Faraday cup (distances are approximate)

A3.3 Transferred and Generated Charge

Results from E3 are shown in Figure A3.2. Note that at all times, the particles charge measured using the FC was negative and the charge detected by E3 probe was positive. This strongly suggests that charge generation was dominant. Contact between metals and plastics (e.g. stainless steel and polyethylene), generally charges the metal positively and the plastic negatively (Cross, 1987) which was observed for this resin[5]. There was no correlation between the E3 probe charge and the charge measured using the FC, indicating that if a probe contacts polyethylene particles it does not measure their charge. Therefore, charge transfer from the

[5] The resin of particles used in this case is different from the resin used in the main part of the thesis.

polyethylene particles to the probe was negligible and the measured charge consisted of the charge generated due to polyethylene-probe contact.

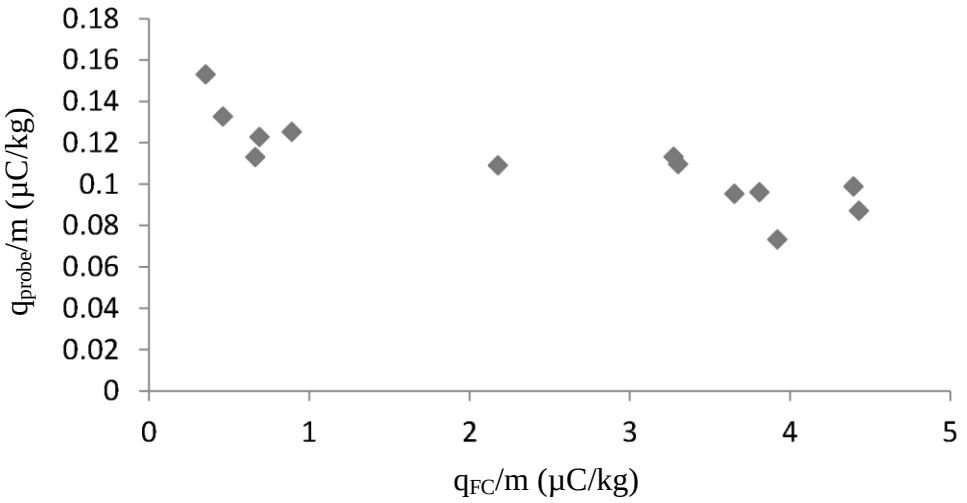

Figure A3.2: Specific charge of particles on probe E3 as a function specific charge measured by the Faraday cup.

A3.4 Induced Charge

Results from E4 as shown in Figure A3.2. There is some correlation between the Faraday cup charge and the probe induced charge indicating that the probe is correctly reading the charge of the particles but the low coefficient of correlation (79%) indicates that there is significant error in the measurement. Note that the induced charge is very small (0 to -0.008 nC/g). This indicates that the induced charge is negligible for probes in contact with particles, as is the case in fluidized beds.

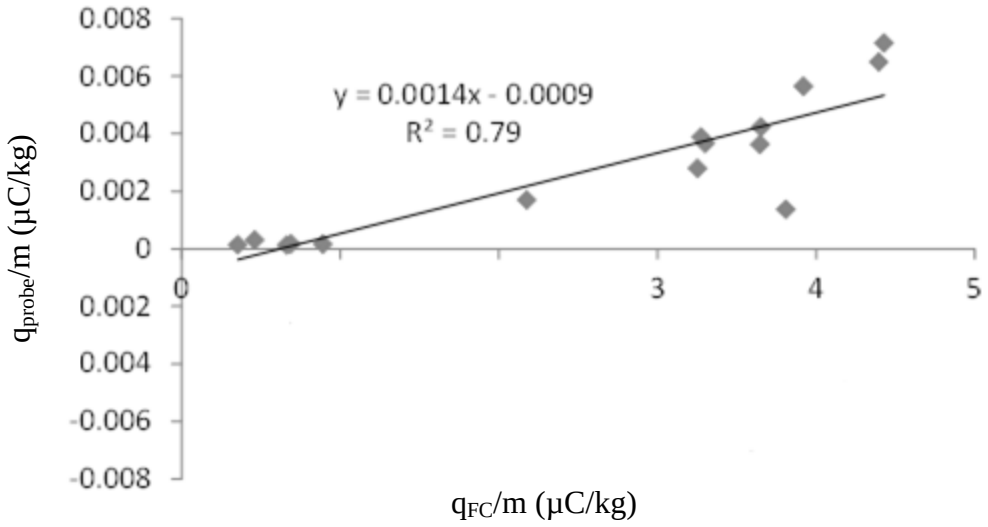

Figure A3.3: Specific charge of particles on probe E4 as a function specific charge measured by the Faraday cup.

A3.5 Summary

The probe charge reading, at least for polyethylene particles, is a measure of charge generation due to particle-probe contacts, not charge induction or transfer. This charge is an estimate of charge generation on particle-wall contacts (Hagerty et al. 2005).